Paleoceanography and Paleoclimatology

RESEARCH ARTICLE
10.1029/2025PA005213

MioVeg1: A Global Middle Miocene Vegetation Reconstruction for Climate Modeling

Catherine D. Bradshaw[1,2], Tamara Fletcher[3], Tammo Reichgelt[4], Funda Akgün[5], David J. Cantrill[6,7], Manuel Casas-Gallego[8], Nela Doláková[9], Boglárka Erdei[10], Mine Sezgül Kayseri-Özer[11], Marianna Kováčová[12], Diana Ochoa[13], Matthew Pound[14], Torsten Utescher[15,16], Jiagang Zhao[17,18], Pierre Sepulchre[19], Sarah J. Feakins[20], Dimiter Ivanov[21], Shufeng Li[17], Yunfa Miao[22], Elżbieta Worobiec[23], Caroline A. E. Strömberg[24], Joseph Novak[25], Nicholas Herold[26], Matthew Huber[27], Amanda Frigola[28,29], Matthias Prange[29], Gregor Knorr[30], Gerrit Lohmann[30], Alexander Farnsworth[31,32], Yousheng Li[31], Daniel J. Lunt[31], Quentin Pillot[33], Yannick Donnadieu[33], R. Paul Acosta[34], and Natalie Burls[34]

[1]The Global Systems Institute, University of Exeter, Exeter, UK, [2]Met Office Hadley Centre, Exeter, UK, [3]School of Physics, Chemistry and Earth Sciences, The University of Adelaide, Adelaide, SA, Australia, [4]Department of Earth Sciences, University of Connecticut, Storrs, CT, USA, [5]Department of Geology Engineering, Dokuz Eylül University, İzmir, Türkiye, [6]Royal Botanic Gardens Victoria, Melbourne, VIC, Australia, [7]School of BioSciences, The University of Melbourne, Melbourne, VIC, Australia, [8]Department of Geodynamics, Stratigraphy and Paleontology, Complutense University of Madrid, Madrid, Spain, [9]Department of Geological Sciences, Masaryk University, Brno, Czech Republic, [10]Botanical Department of the Hungarian Natural History Museum, Hungarian National Museum Public Collection Centre, Budapest, Hungary, [11]Institute of Marine Science and Technology, Dokuz Eylül University, İzmir, Türkiye, [12]Department of Geology and Paleontology, Faculty of Natural Sciences, Comenius University Bratislava, Bratislava, Slovak Republic, [13]Geology Department, Salamanca University, Salamanca, Spain, [14]School of Geography and Natural Sciences, Northumbria University, Newcastle, UK, [15]Senckenberg Research Institute and Natural History Museum Frankfurt/M., Senckenberg Research Station of Quaternary Palaeontology, Weimar, Germany, [16]Geological Department, Institute for Geosciences, Bonn University, Bonn, Germany, [17]State Key Laboratory of Plant Diversity and Specialty Crops, Xishuangbanna Tropical Botanical Garden, Chinese Academy of Sciences, Menglun, China, [18]University of Chinese Academy of Sciences, Beijing, China, [19]Laboratoire des Sciences du Climat et de l'Environnement, LSCE/IPSL, CEA-CNRS-UVSQ, Université Paris-Saclay, Gif-sur-Yvette, France, [20]Department of Earth Sciences, University of Southern California, Los Angeles, CA, USA, [21]Institute of Biodiversity and Ecosystem Research, Bulgarian Academy of Sciences, Sofia, Bulgaria, [22]Key Laboratory of Ecological Safety and Sustainable Development in Arid Lands, Northwest Institute of Eco-Environment and Resources, Chinese Academy of Sciences, Lanzhou, China, [23]W. Szafer Institute of Botany, Polish Academy of Sciences, Kraków, Poland, [24]Department of Biology & Burke Museum of Natural History and Culture, University of Washington, Seattle, WA, USA, [25]Ocean Sciences Department, University of California, Santa Cruz, CA, USA, [26]Applied Climate Science Pty Ltd., Adelaide, SA, Australia, [27]Department of Earth, Atmospheric, and Planetary Sciences, Purdue University, West Lafayette, IN, USA, [28]Barcelona Supercomputing Center, Barcelona, Spain, [29]MARUM —Center for Marine Environmental Sciences, University of Bremen, Bremen, Germany, [30]Alfred Wegener Institute Helmholtz Centre for Polar and Marine Research, Bremerhaven, Germany, [31]School of Geographical Sciences, University of Bristol, Bristol, UK, [32]Tibetan Plateau Earth System, Environment and Resources (TPESER), Institute of Tibetan Plateau Research, Chinese Academy of Sciences, Beijing, China, [33]CEREGE, Aix Marseille University, CNRS, IRD, INRAE, Collège de France, Aix-en-Provence, France, [34]Department of Atmospheric, Oceanic & Earth Sciences, Center for Ocean-Land-Atmosphere Studies, George Mason University, Fairfax, VA, USA

Abstract Climate models require boundary condition information, such as vegetation and soil distributions because they influence the mean state climate, and feedbacks can significantly influence regional climate and climate sensitivity to CO_2 forcing. Information about past distributions comes primarily from the paleobotanical record, which is often supplemented by a vegetation model to fill data gaps. For recent past periods such as the Pliocene, a quantitative suitability assessment of these vegetation model simulations is sufficient. However, the Miocene Climate Optimum spanning 16.9–14.7 Ma was the warmest period on Earth over the last ~25 million years and models struggle to reproduce those conditions for the range of paleogeographies and CO_2 concentrations tested, particularly at high latitudes. Here we bring together the Miocene modeling and data communities to update previous vegetation reconstructions used for climate modeling with a new regional approach that relaxes the requirement for a single model simulation to be used, blending instead simulations forced by different paleogeographies and CO_2 concentrations. This ensures the simulated vegetation is first, and foremost, consistent with the paleorecord and provides a baseline for future comparisons. The reconstruction

Key Points:

- A new approach to data-model syntheses for vegetation reconstruction ensuring consistency with the paleobotanical record is demonstrated
- A new Middle Miocene vegetation and soil reconstruction is provided for climate model boundary conditions
- Middle Miocene vegetation was characterized by extensive forests globally and large Northern Hemisphere grasslands

Supporting Information:

Supporting Information may be found in the online version of this article.

Correspondence to:

C. Bradshaw,
c.bradshaw@exeter.ac.uk

Citation:

Bradshaw, C. D., Fletcher, T., Reichgelt, T., Akgün, F., Cantrill, D. J., Casas-Gallego, M., et al. (2025). MioVeg1: A global Middle Miocene vegetation reconstruction for climate modeling. *Paleoceanography and Paleoclimatology*, *40*, e2025PA005213. https://doi.org/10.1029/2025PA005213

Received 29 MAY 2025
Accepted 10 OCT 2025

Author Contributions:

Conceptualization: Catherine D. Bradshaw, Natalie Burls
Data curation: Catherine D. Bradshaw, Tamara Fletcher, Tammo Reichgelt, Funda Akgün, David J. Cantrill, Manuel Casas-Gallego, Nela Doláková, Boglárka Erdei, Mine Sezgül Kayseri-Özer, Marianna Kováčová, Diana Ochoa, Matthew Pound, Torsten Utescher, Jiagang Zhao, Sarah J. Feakins, Dimiter Ivanov, Shufeng Li, Yunfa Miao, Elżbieta Worobiec, Caroline A. E. Strömberg, Joseph Novak

Formal analysis: Catherine D. Bradshaw, Tamara Fletcher, Tammo Reichgelt, Funda Akgün, David J. Cantrill, Manuel Casas-Gallego, Nela Doláková, Boglárka Erdei, Mine Sezgül Kayseri-Özer, Marianna Kováčová, Diana Ochoa, Matthew Pound, Torsten Utescher, Jiagang Zhao, Pierre Sepulchre, Sarah J. Feakins, Dimiter Ivanov, Shufeng Li, Yunfa Miao, Elżbieta Worobiec, Caroline A. E. Strömberg
Investigation: Catherine D. Bradshaw, Tamara Fletcher, Tammo Reichgelt
Methodology: Catherine D. Bradshaw, Tamara Fletcher, Tammo Reichgelt, Pierre Sepulchre, Matthew Huber, Natalie Burls
Resources: Catherine D. Bradshaw, Tamara Fletcher, Nicholas Herold, Matthew Huber, Amanda Frigola, Matthias Prange, Gregor Knorr, Gerrit Lohmann, Alexander Farnsworth, Yousheng Li, Daniel J. Lunt, Quentin Pillot, Yannick Donnadieu, R. Paul Acosta, Natalie Burls
Software: Catherine D. Bradshaw
Validation: Catherine D. Bradshaw, Tamara Fletcher, Tammo Reichgelt, Pierre Sepulchre
Visualization: Catherine D. Bradshaw
Writing – original draft: Catherine D. Bradshaw, Tamara Fletcher, Tammo Reichgelt, Funda Akgün, David J. Cantrill, Manuel Casas-Gallego, Nela Doláková, Boglárka Erdei, Mine Sezgül Kayseri-Özer, Marianna Kováčová, Diana Ochoa, Matthew Pound, Torsten Utescher, Jiagang Zhao, Pierre Sepulchre, Sarah J. Feakins, Dimiter Ivanov, Shufeng Li, Yunfa Miao, Elżbieta Worobiec, Caroline A. E. Strömberg, Natalie Burls
Writing – review & editing: Catherine D. Bradshaw, Tamara Fletcher, Tammo Reichgelt, Funda Akgün, David J. Cantrill, Manuel Casas-Gallego, Nela Doláková, Boglárka Erdei, Mine Sezgül Kayseri-Özer, Marianna Kováčová, Diana Ochoa, Matthew Pound, Torsten Utescher, Jiagang Zhao, Pierre Sepulchre, Sarah J. Feakins, Dimiter Ivanov, Shufeng Li, Yunfa Miao, Elżbieta Worobiec, Caroline A. E. Strömberg, Joseph Novak, Nicholas Herold, Matthew Huber, Amanda Frigola, Matthias Prange, Gregor Knorr, Alexander Farnsworth, Yousheng Li, Daniel J. Lunt, Quentin Pillot, Yannick Donnadieu, R. Paul Acosta, Natalie Burls

shows global increases in forest cover at all latitudes as compared to today and extensive C_3 grasslands across the high northern latitudes. Data gaps at high latitudes are filled with vegetation models forced by higher CO_2 concentrations than were required at lower latitudes consistent with the inability of current models to simulate Miocene high latitude warmth.

Plain Language Summary The Miocene Climate Optimum was globally the warmest period over the last 25 million years. As a result of this warmth, the vegetation distribution was quite different to today. Climate models need information about that vegetation distribution to simulate the climate of the Miocene but paleobotanical data contains gaps. Vegetation models can be used to fill these gaps but require climate information to run, usually taken from climate models that have difficulty reproducing the warmth of the Miocene seen in the data. To overcome this problem, we use a new more flexible approach to fill the data gaps whereby paleobotanical experts have identified the best models on a regional basis and there is no need for a single model to be used globally. The Miocene vegetation shows more forests than today and more extensive grasslands in the Northern Hemisphere.

1. Introduction

Vegetation distribution assumptions are an important boundary condition for climate model simulations since this can significantly influence regional climate simulation results (e.g., Brovkin, 2002; Crowley & Baum, 1997; Crucifix et al., 2005). The Miocene Climate Optimum (MCO) spanning 16.9–14.7 Ma was the warmest period on Earth over the last ~25 million years (Steinthorsdottir et al., 2021). Atmospheric CO_2 concentrations are thought to be the principal driver for the large-scale warmth and humidity of the period (Burls et al., 2021), with reconstructions equivalent to the end-of-century climate scenario range RCP4.5 to RCP6.0 (Van Vuuren et al., 2011, CenCO2PIP et al., 2023). As a result of the globally warmer conditions, the vegetation distribution of the MCO was very different to today. In addition to global warmth, paleogeography also plays an important role determining in past vegetation distribution. The presence of large water bodies (Hoorn et al., 2022; Kern et al., 2011; Scheiner et al., 2023), the opening and closing of seaways (Vernyhorova et al., 2023; J. Zhang et al., 2023), glaciation (Doláková et al., 2021; Hamon et al., 2012) and tectonic uplift (Henrot et al., 2010; Sobczyk et al., 2024; Tardif et al., 2023) have all been found to matter in determining the regional vegetation of the MCO. Vegetation feedbacks affect climate from the local to the global scale through numerous processes (e.g., Bonan et al., 2024). Vegetation controls the continental albedo and thus the global radiative forcing and associated temperatures. Vegetation also controls most water exchange from the continent to the atmosphere through transpiration associated with photosynthesis (vegetation transpiration is estimated to be 75% of the total evapotranspiration in the modern world, Vicente-Serrano et al., 2022), leading to pivotal feedbacks in the water cycle and increased continental precipitation (Braconnot et al., 1999). With these processes, global vegetation changes can modify climate sensitivity to CO_2 forcing (Bradshaw et al., 2015; Dutton & Barron, 1997; Henrot et al., 2010; Knorr et al., 2011) and ocean circulation (Bradshaw et al., 2021; Lohmann et al., 2015).

Although more and more earth system models (ESMs) embed dynamical global vegetation models (DGVM), including a robust representation of vegetation in paleoclimate model simulations is vital—all ESMs need this information as an initial condition, and those without an integrated DGVM will keep this information fixed throughout the simulations, as a boundary condition. DGVMs can also have a limited application when run for time periods deep into geological history, since vegetation traits determining feedbacks on climate can have evolved (Boyce & Lee, 2017; Bres et al., 2021). Climate model simulations of recent periods of Earth history use the preindustrial vegetation distribution as the boundary condition (e.g., Holocene; Ivanovic et al., 2016 and LGM; Kageyama et al., 2017). Further back in time, vegetation information is primarily derived from the paleobotanical record, which is often supplemented by a single best-fit vegetation model simulation to fill the gaps so that it can be used as a boundary condition for climate models (e.g., Late Miocene: M. J. Pound et al., 2011; Pliocene: Salzmann et al., 2008). However, existing Middle Miocene simulations struggle to reproduce the warmth reconstructed by paleobotanical data, particularly at high latitudes (Burls et al., 2021), as well as the hydrological response to that warmth regardless of the CO_2 concentration imposed (Acosta, Burls, Pound, Bradshaw, De Boer, et al., 2024). This temperature bias in the models, and similar model biases for precipitation, are also seen for other past warm climates such as the Paleocene-Eocene Thermal Maximum

(Korasidis et al., 2022), and the early Eocene (Cramwinckel et al., 2023; Lunt et al., 2021). As a result of these model biases, using a single best-fit model simulations to fill the gaps in the vegetation data for these older time periods will result in inferred vegetation types that are inconsistent with the data.

Here, we bring together the Middle Miocene modeling and data communities using a new regional approach that ensures that the infilled vegetation classes are first, and foremost, consistent with the paleobotanical data. We update previous vegetation reconstructions utilized for climate modeling (Frigola et al., 2018; Herold, Huber, & Müller, 2011; J. Pound et al., 2012; Tong et al., 2009; Wolfe, 1985; You et al., 2009) using new paleobotanical and paleosol data and comparison to the latest climate model simulations for the MCO (MioMIP1: Burls et al., 2021).

2. Methods

The methodology adopted in this study takes a hierarchy of inputs to assign each 2° × 2° grid cell to a single classification using the 28-biome classification system of the BIOME4 model (Kaplan, 2001; Kaplan et al., 2003).

For grid cells with paleobotanical data, the biome classification derived from that data is used to define the biome classification of the grid cell for our vegetation reconstruction. Paleobotanical data used includes any type of fossil plant organ including macroflora, palynoflora and plant silica (phytolith) assemblages from the MCO. Where an appropriate classification has been made in the literature by the original authors, this classification is used. In cases where such a classification is not available, the determination is made through expert judgment. This process involves evaluating the nearest living relatives of the taxa present in the assemblage, considering factors such as morphological similarities, ecological preferences, and paleoenvironmental context to assign the most plausible biome classification. For the remaining grid cells, the grid is first split into regions: Africa, Australasia, East Asia, Europe, the high northern latitudes, the high southern latitudes, North America and South America. The reason for this delineation is that researchers tend to conduct their work according to political boundaries rather than by other geographical features such as river basins or latitudinal banding and therefore using the continental boundaries as the first pass allows us to maximize use of their expertise. For Europe, with a higher density of data and specialists per capita, subregions are defined.

For each region, climate model outputs from the Miocene Model Intercomparison Project 1 (MioMIP1) project (as detailed in the following section) are then used to drive the BIOME4 model itself, and expert judgment is used to determine the most appropriate vegetation model scenario for that region by comparison to the known palaeobotanical record. This process involves consideration of dating uncertainties between different proxies when there were multiple biome options for a given region, whether a particular simulation suggests biomes located adjacent to one another that do not make sense, or if there are transitional biomes missing between them, additional knowledge about the region gained from other proxies or from paleobotanical data in the region before or after the Middle Miocene (under the assumption that the Middle Miocene vegetation is more likely to be similar to the Late Miocene or Early Miocene vegetation than it is to the Pliocene vegetation or modern vegetation). As the MioMIP1 simulations cover a range of CO_2 levels from 200 to 853 ppm, we do not define the CO_2 level for the MCO in this synthesis because we consider it more important that the simulated vegetation is consistent with the paleobotanical data than that the CO_2 level is consistent across the simulations.

2.1. BIOME4 Model

The BIOME4 model is an equilibrium global vegetation model that uses mechanistic processes to simulate 13 plant functional types (PFTs: Tropical Evergreen, Tropical Raingreen, Temperate Broadleaved Evergreen, Temperate Summergreen, Temperate Evergreen Conifer, Boreal Evergreen, Boreal Deciduous, Temperate Grass, Tropical/Warm-Temperate Grass, Desert Woody Plant Type C3 and C4, Tundra Shrub Type, Cold Herbaceous Type and Lichen/Forb Type; Kaplan (2001) and Table S1 in Supporting Information S1) representing the broad distinct plant groups and assigns them into one of 28 biomes (Tropical evergreen forest, Tropical semi-deciduous forest, Tropical deciduous forest/woodland, Temperate deciduous forest, Temperate conifer forest, Warm mixed forest, Cool mixed forest, Cool conifer forest, Cold mixed forest, Evergreen taiga/montane forest, Deciduous taiga/montane forest, Tropical savanna, Tropical xerophytic shrubland, Temperate xerophytic shrubland, Temperate sclerophyll woodland, Temperate broadleaved savanna, Open conifer woodland, Boreal parkland, Tropical grassland, Temperate grassland, Desert, Steppe tundra, Shrub tundra, Dwarf shrub tundra, Prostrate shrub tundra, Cushion-forbs, lichen and moss, Barren and Land ice; Kaplan (2001) and Tables S2 and S3 in

Supporting Information S1). Bioclimatic parameters and the simulation of biogeochemical processes are used to determine the PFTs in each grid cell and for the biome assignment. BIOME4 is driven by the monthly averages of mean temperature, cloudiness and precipitation and the climatological absolute minimum temperature (the lowest temperature during the coldest month of the climatology), as well as user-defined soil characteristics and CO_2 concentrations. We derive new soil parameters for the MCO in this study and we use the CO_2 concentration that was implemented in each simulation in the MioMIP1 ensemble of model outputs in the BIOME4 model simulations. The BIOME4 model is therefore seeing the physiological effect of the CO_2 concentration, not just the climatic effect from the climate model outputs. Each biome is defined by a unique physical structure and PFT composition whereby the BIOME4 model ranks the tree and non-tree PFTs according to the calculated net primary productivity, leaf area index and soil moisture content (for a detailed description, see https://github.com/jedokaplan/BIOME4). BIOME4 has been used in a paleoclimate context in other studies (e.g., Herold, Huber, Greenwood, et al., 2011; Kaplan et al., 2003; M. J. Pound et al., 2011; Prentice and Webb, 1998; Salzmann et al., 2008).

2.2. Soil Data

The BIOME4 model requires information about the soil water holding capacity and saturated hydraulic conductivity for each grid cell. Rather than modern data, we have estimated values appropriate for the MCO. The starting point in this process was to use the Pliocene soil order classifications, which blended climate model simulations and available paleosol data (M. J. Pound et al., 2014). These assignments were rotated back to their estimated positions for 15.5 Ma using GPlates and the Scotese PALEOMAP rotation model (Mather et al., 2023; Müller et al., 2018). For grid cells with Middle Miocene paleosol data (Retallack, 2022), these were similarly rotated back to the estimated positions for 15.5 Ma and used to replace the Pliocene soil orders. The biome assignments of the paleobotanical data sites were also rotated back to their estimated 15.5 Ma positions and translated into an appropriate soil order as defined in Table 1. Note that the soil order assumptions are tied to biomes rather than time periods, so the same translations used for the Pliocene data in M. J. Pound et al. (2014) are applied in our study. Where multiple soil types are associated with a single biome we use the most common global occurrence, for example, both histosol and spodosol soil orders are associated with cool evergreen mixed forest, but alfisol is adopted because it is more widespread (see Table 3.2, Bouwman, 1990). Following the methods of M. J. Pound et al. (2014), all ice-covered Northern Hemisphere grid cells in the Pliocene soil order data were converted to spodosols to account for the absence of ice during the MCO and the expectation of a more northern distribution of boreal and temperate forests. The available Antarctic biome reconstructions suggest gelisols throughout the continent and therefore this is the soil order assumed in this study across Antarctica. The extent of the Antarctic Ice Sheet (AIS) during the MCO is highly uncertain but likely smaller than modern (e.g., Bradshaw et al., 2021; Gasson et al., 2016). To address this uncertainty, we assume an ice-free continent in our study, allowing the climate modelers to replace our vegetation reconstruction with land ice in accordance with their ice sheet configuration. Note that the BIOME4 model does not explicitly predict land ice as an output. Therefore, in cases where the driving climate data contains ice-covered grid cells and the BIOME4 model similarly suggest that these grid cells are too cold or dry to support vegetation, they will be classified as (polar) desert or bare soil. The final step was to perform some manual smoothing of the transitions between the soil orders to avoid abrupt edges and individual grid cell assignments (reassigning up to 9 surrounding grid cells), to fill in any gaps that were left (using the nearest dominant biome assignment), and to extrapolate beyond the modern coastline to accommodate different land-sea masks for the Middle Miocene (extending the same biomes outwards).

Finally, the soil order classifications were converted to estimates for water holding capacity and saturated hydraulic conductivity according to the assumptions in Table 2. The resulting soil order map for the Middle Miocene used as input to the BIOME4 model is shown in Figure 1. Once the final vegetation reconstruction had been generated (Figure 2), the same assumptions from Tables 1 and 2 were applied to fill the gaps in the paleosol data from Data Set S1 in Supporting Information S1, to create a new gridded Middle Miocene soil data set as part of our study (Figure 3).

2.3. Paleobotanical Data

A total of 431 paleobotanical biome classification datapoints were identified from the literature (Figure 4; Table 3; Data Set S2 in Supporting Information S1) and rotated back to their estimated positions for 15.5 Ma using GPlates (Mather et al., 2023; Müller et al., 2018). Data come from all continents but are spatially biased toward

Table 1
Biome to Soil Order Assumptions (cf. M. J. Pound et al., 2014)

Biome number	Biome description	Soil order
1	Tropical evergreen forest	Oxisol
2	Tropical semi-deciduous forest	Oxisol
3	Tropical deciduous forest/woodland	Oxisol
4	Temperate deciduous forest	Alfisol
5	Temperate conifer forest	Alfisol
6	Warm-temperate mixed forest	Ultisol
7	Cool mixed forest	Alfisol
8	Cool conifer forest	Alfisol
9	Cold mixed forest	Alfisol
10	Evergreen taiga/montane forest	Spodosol
11	Deciduous taiga/montane forest	Spodosol
12	Tropical savanna	Vertisol
13	Tropical xerophytic shrubland	Aridisol
14	Temperate xerophytic shrubland	Aridisol
15	Temperate sclerophyll woodland	Mollisol
16	Temperate broadleaved savanna	Mollisol
17	Open conifer woodland	Spodosol
18	Boreal parkland	Spodosol
19	Tropical grassland	Mollisol
20	Temperate grassland	Mollisol
21	Desert	Aridisol
22	Steppe tundra	Gelisol
23	Shrub tundra	Gelisol
24	Dwarf-shrub tundra	Gelisol
25	Prostrate shrub tundra	Gelisol
26	Cushion-forb, lichen, moss tundra	Gelisol
27	Barren	Gelisol
28	Land ice	Gelisol

Europe and East Asia, with Africa and the high latitudes being particularly sparse (<25 data points). Data were assumed to be of MCO age if their age uncertainty crossed the boundaries of the time slice 16.9–14.7 Ma (the MCO definition of Steinthorsdottir et al., 2021). Age assignments were taken from the original publications, and no revisions have been made to reinterpret these assignments based on updated stratigraphy or novel age estimates as this major task is outside the scope of the present study.

In some cases, different data were available across the time slice, such as the data from the Longzhong Basin along the northeastern margins of the Tibetan Plateau (Hui, Zhang, et al., 2018), which show the vegetation shifting from temperate broadleaved savanna to warm-temperate mixed forest across the time slice. In other cases, the data suggest a mix of biomes in close proximity, such as at the AND-2A core site (Warny et al., 2009), which shows that the area consisted of dwarf-shrub tundra and evergreen taiga/montane forest throughout the MCO period. In these cases, one biome had to be chosen over another, and thus the biome thriving under warmer conditions, defined by higher mean annual temperature requirements, was selected for consistency, although the cooler biome could have been equally valid given our uncertainties. Similarly, multiple vegetation interpretations in the same grid cell were a problem in Europe due to the density of available data, potentially capturing micro-scale vegetation variation or short-term vegetation succession. In Europe, we therefore create a higher resolution vegetation reconstruction (1° × 1°) than for other regions (2° × 2°), which may reduce potential data mismatches. Alternatively, the specific taphonomic and production biases associated with macrofossils, palynofloras and phytoliths (see below) may result in vegetation interpretation mismatched within the same grid cell, such as macrofossils and palynofloras indicating forests in Turkey (e.g., Akkiraz et al., 2020; Kayseri & Akgün, 2008; Kayseri-Özer & Emre, 2022; Kayseri-Özer, Akgün, et al., 2014; Kayseri-Özer, Sözbilir, & Akgün, 2014) whereas phytoliths suggest grass-dominated vegetation (Stromberg & Smith, 2007).

In some cases, the paleobotanical data for the MCO has no appropriate biome classification available from the BIOME4 descriptions at all, for example, in Central and Southeastern Europe and in East Asia, thermophilous (often termed as subtropical) broadleaved evergreen and mixed evergreen deciduous vegetation is suggested by the fossil data (Utescher, Erdei, et al., 2007;

Table 2
Soil Order Water Holding Capacity and Saturated Hydraulic Conductivity Assumptions From the Literature (Allen et al., 1998; Arya et al., 1992; Blencowe et al., 1960; Brunel-Saldias et al., 2016; Cox et al., 1999; Das Gupta et al., 2006; Igwe et al., 2013; Nachtergaele et al., 2023)

Soil order number	Soil order	Water holding capacity (mm)	Saturated hydraulic conductivity (mm/hr)
1	Gelisol	75	70
2	Histosol	75	65
3	Spodosol	5	35
4	Oxisol	30	125
5	Vertisol	40	15
6	Aridisol	90	10
7	Ultisol	15	35
8	Mollisol	45	15
9	Alfisol	25	30

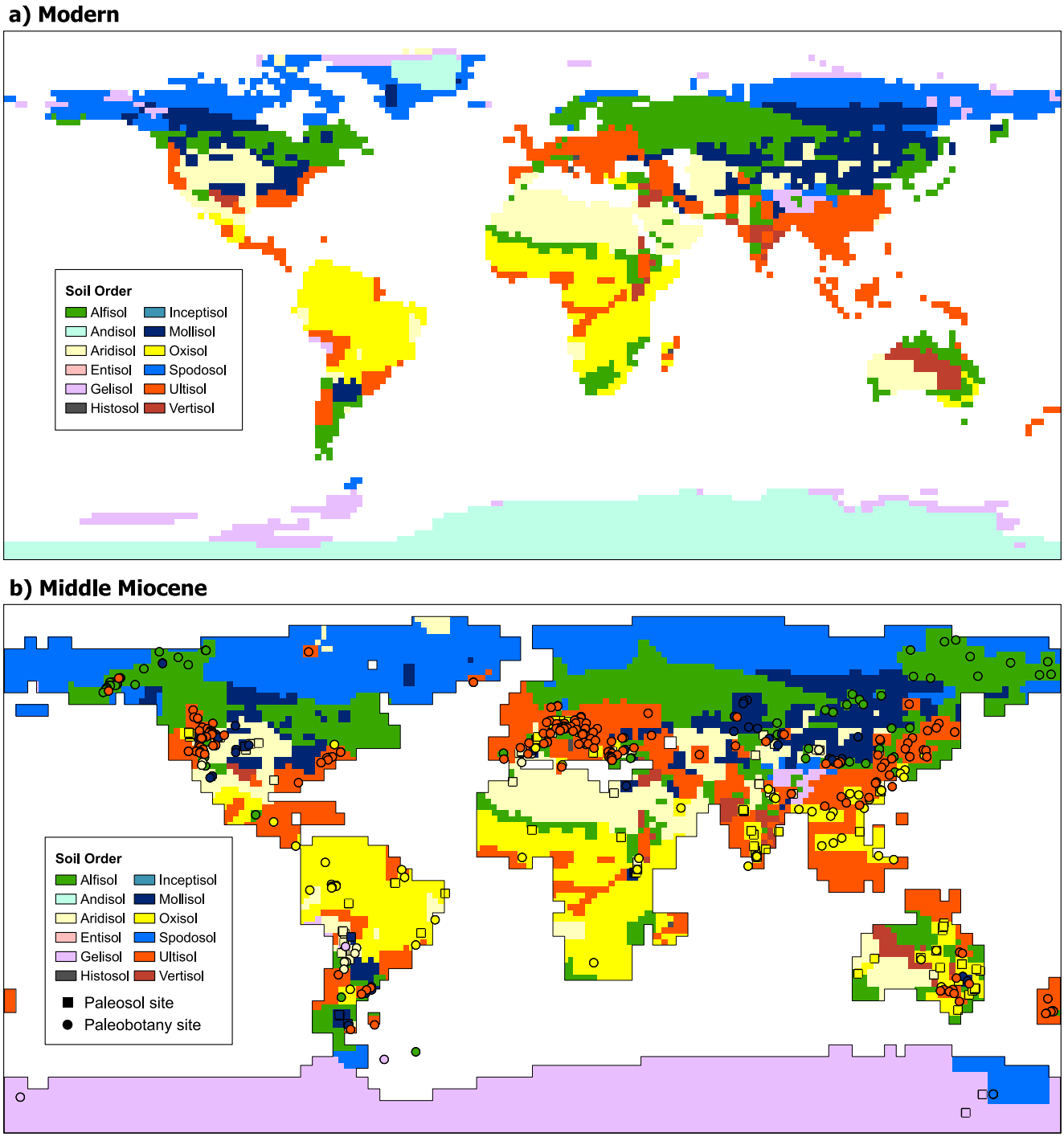

Figure 1. Soil orders. (a) Modern, (b) Middle Miocene soil orders from the paleodata. Squares are data taken from Retallack (2022); refer to Data Set S1 in Supporting Information S1 for full details and references of the paleosol data.

Utescher, Djordjevic-Milutinovic, et al., 2007). However, this category is not represented in BIOME4 (it may be a transition between warm temperate mixed forests, tropical evergreen and tropical semi deciduous forests). These data were assigned to the warm-temperate mixed forest biome. Other data were excluded because of insufficient evidence (i.e., poor data quality, low taxonomic resolution etc.) for selecting a BIOME4 class (e.g., phytolith assemblages from Patagonia, Argentina; Dunn et al., 2015).

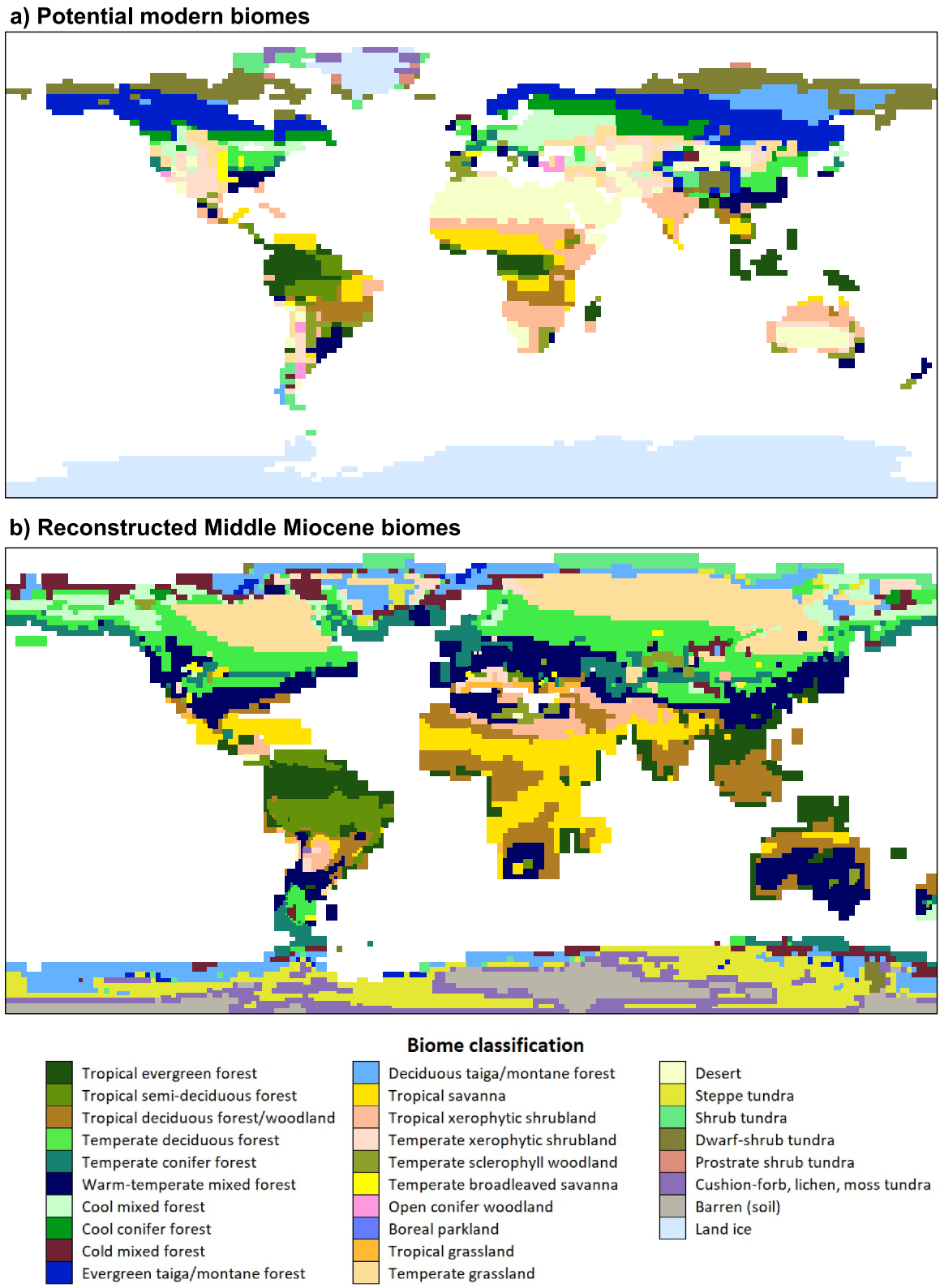

Figure 2. Global Middle Miocene vegetation BIOME4 reconstruction based on our new regional model-data synthesis approach blending simulations from different climate models and boundary conditions compared to potential modern vegetation. (a) Potential Modern biomes (cf. Salzmann et al., 2008); (b) Middle Miocene biomes.

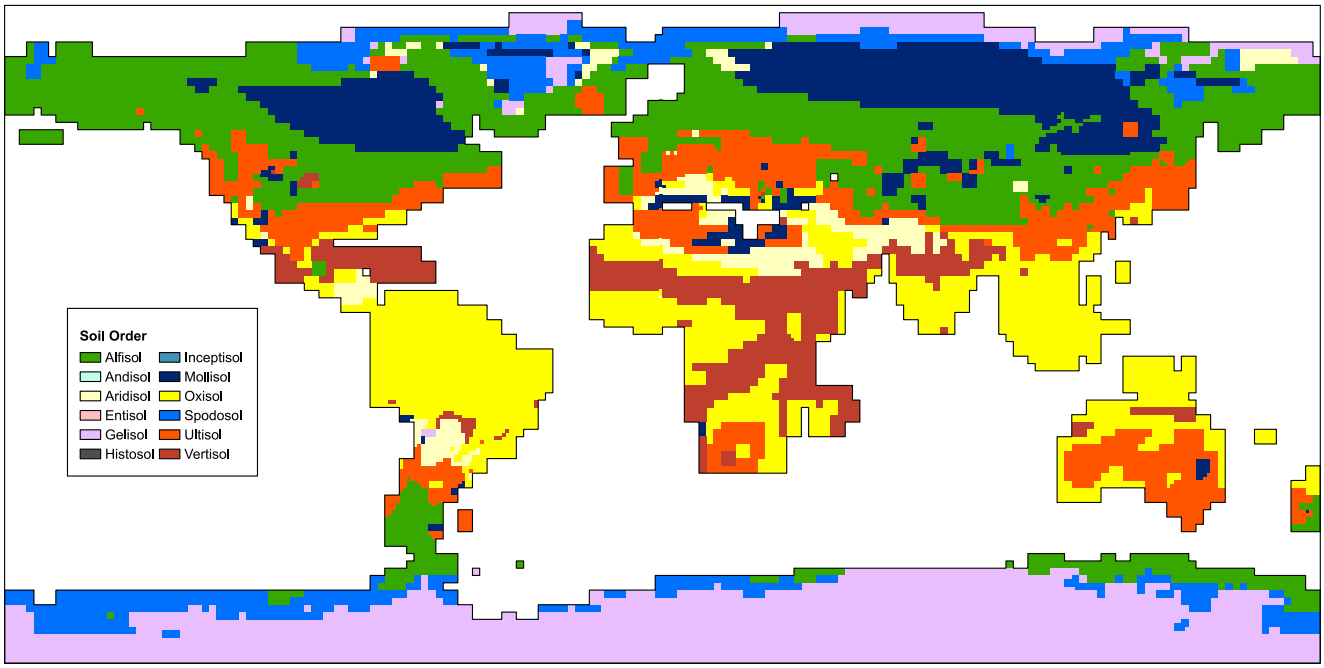

Figure 3. Revised Middle Miocene Soil Orders. These were defined using the paleosol data from Data Set S1 in Supporting Information S1 and supplemented by the vegetation reconstruction shown in Figure 2b with the assumptions from Tables 1 and 2.

Differential taphonomic processes further complicate biome interpretations based on the fossil record. First, because of differential transport and preservation of plant parts, assemblages contain autochthonous and allochthonous taxa to a degree that varies depending on the fossil type. For example, macrofossils, and to some extent, phytolith assemblages, tend to reflect relatively locally growing plants, whereas palynofloras capture pollen and spores from a wider region (e.g., C. A. Strömberg et al., 2018; Traverse, 1988; Wing et al., 1992). Second, different plants parts preserve in different microhabitats and, as a result, reflect different landscape components. Organic fossils, such as leaves and palynofloras, are typically recovered from low energy, unoxidized depositional environments with rapid burial, including wetlands, lakes, and riparian zones. In contrast, plant silica is often preserved in well-oxidized deposits, such as paleosols and sediments deposited further away from water (e.g., C. A. Strömberg et al., 2018). Third, plant fossil types are affected by production bias, resulting in overrepresentation of certain taxa, such as deciduous dicots in leaf assemblages, grasses in phytolith assemblages, and wind-pollinated conifers in palynofloras (e.g., Greenwood & Donovan, 1991; C. A. Strömberg et al., 2018). Expert interpretation is therefore essential to analyze fossil assemblages, both macro- and microfloras, and provide context to determine if specific taxa were true biome constituents or external floral elements preserved within the community. For example, when inferring a biome from palynological assemblages, the "warm temperate mixed forests" biome is usually easily identifiable by the presence of thermophilous conifers and broadleaved taxa such as *Engelhardia* and *Castanopsis*. Palynofloras comprising mainly temperate deciduous components may either represent the deciduous forest biome or riparian vegetation (reflecting the microhabitat in the riparian zone rather than the regional climate), and independent information, such as sedimentary facies, might be needed to distinguish these options. Therefore, aside from often being incomplete, interpretations may be biased toward certain taxa such as species of the anemophilous *Pinus* and *Nothofagus*, which are prolific pollen producers with long-range transport potential (e.g., Gassmann & Pérez, 2006; Harmata & Olech, 1991). As their pollen is potentially transported over long distances, an expert interpretation is needed to assess the pollen assemblage and contextual information to ascertain whether these species were dominant in the region or were transported and perhaps derive from different habitats, e.g., by excluding wind-pollinated taxa from consideration (e.g., Reichgelt et al., 2023). Finally, either model or data-based biome reconstructions assume conservative climatic niche distributions, often derived from the extant nearest relatives of the fossil taxa, which may not be representative of their extinct relatives. Thus, any biome reconstruction contains an inherent uncertainty related to the ecological traits of each fossil taxon.

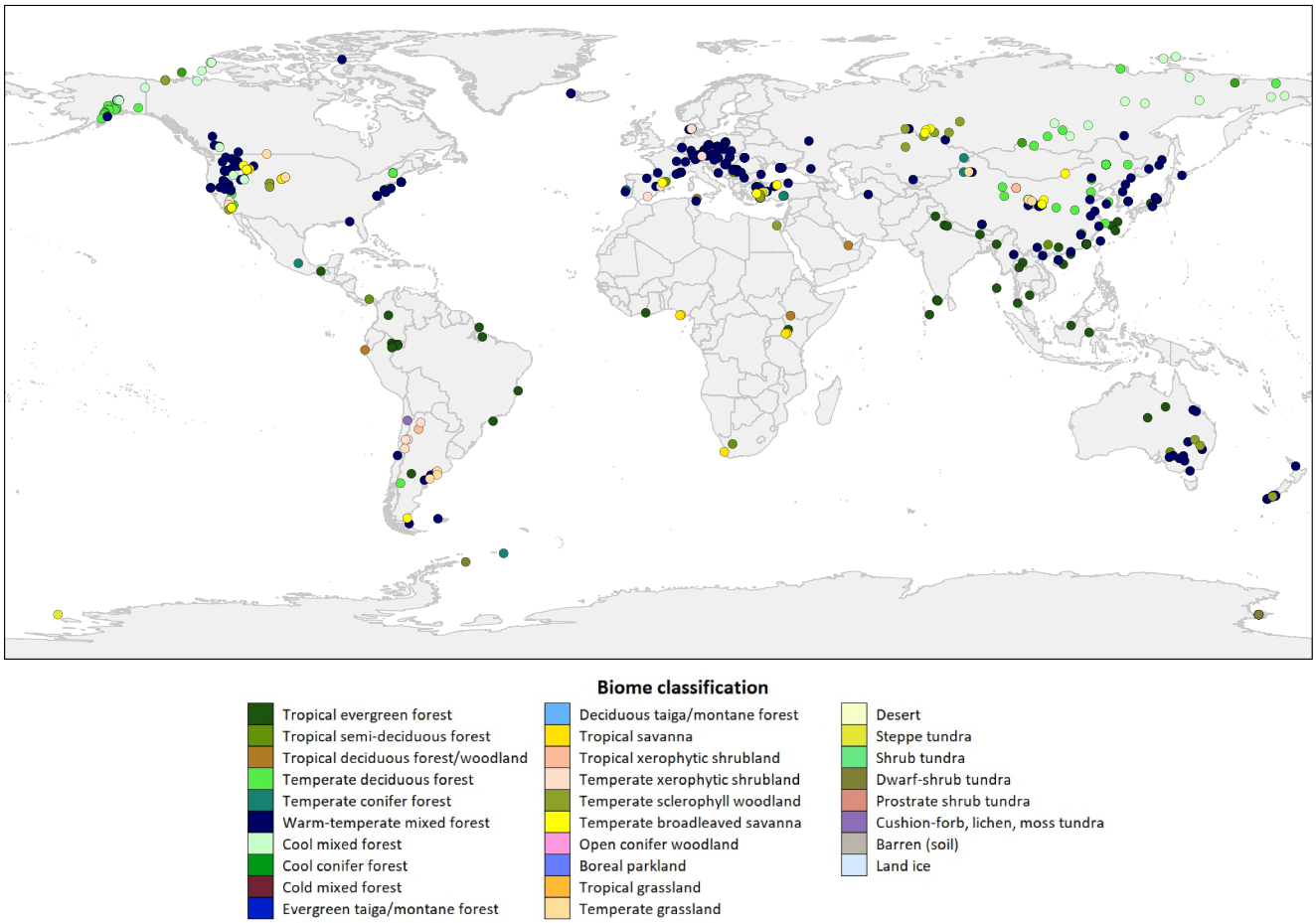

Figure 4. Location of the Miocene Climate Optimum paleobotanical data used for biome classification. Data sites are shown in their modern positions. Refer to Data Set S2 in Supporting Information S1 for full details of the paleobotanical data and references.

2.4. MioMIP1 Simulations

Miocene Model Intercomparison Project 1 was a "MIP of opportunity," whereby each modeling center used their own choice of boundary conditions to investigate different scientific questions such as the role of CO_2 forcing, paleogeography, and ice sheet configurations, but the resulting simulations have been synthesized and interrogated in a systematic way (Burls et al., 2021). Here we have used the 31 Early to Middle Miocene simulations from MioMIP1 with a paleogeography dating between 20 and 11.6 Ma for the BIOME4 modeling, as detailed in Table 4. The land-sea mask is defined as a binary land or sea for some models and as a fraction of landcover for others; we assume all grid cells with a land area greater than 0 are land. As well as producing BIOME4 model results for each of the MioMIP1 ensemble members individually, BIOME4 model results are also produced for the ensemble mean of the MioMIP1 simulations split by CO_2 concentration, whereby the ranges are 200–300 ppm (referred to as the 280 ppm ensemble mean), 350–400 ppm (referred to as the 400 ppm ensemble mean), 500–600 ppm (referred to as the 560 ppm ensemble mean) and 800–853 ppm (referred to as the 850 ppm ensemble mean).

2.5. Data-Model Synthesis

The methodology adopted for the infilling of the data-derived biome gaps with the best-fit model simulated biomes was to first smooth the model data by regridding it to a 2° grid. The MioMIP1 ensemble members are on a variety of spatial resolutions, so this step ensures that all simulations are treated consistently. It also helps to remove any bias toward the model output in the absence of data to back it up, if the climate model used in one region was of higher resolution than the model used in others. The 2° grid was then converted to a 1° grid using a nearest neighbor interpolation, because in some regions there is enough data to warrant a higher resolution for the

Table 3
Contributing Paleobotanical Data

Site	Country	Reference	Latitude	Longitude
1	Russia	Zyryanov (1992)	75.890	142.430
2	Russia	Lavrushin and Alekseev (2005)	75.351	139.036
3	Canada	Lavrushin and Alekseev (2005)	75.110	−87.100
4	Canada	Fletcher et al. (2021)	74.320	−123.250
5	Canada	Williams et al. (2008)	74.300	−123.033
6	Canada	Williams et al. (2008)	74.300	−123.030
7	Russia	Hazin et al. (2019)	72.563	127.185
8	Canada	Fletcher et al. (2021)	71.960	−125.670
9	Canada	Lavrushin and Alekseev (2005)	71.580	−131.220
10	Russia	Laukhin and Rybakova (1981)	70.197	146.181
11	Canada	Norris (1997)	69.500	−135.750
12	Canada	Norris (1997)	69.330	−135.750
13	Canada	Fletcher et al. (2021)	69.200	−127.030
14	Russia	Verkhovskaya and Kundyshev (1991)	68.692	158.700
15	Russia	Aleksandrova (2016)	68.500	170.000
16	USA	J. M. White and Ager (1994)	67.330	−141.330
17	Iceland	Bratseva (1980)	65.773	−24.083
18	Iceland	Grımsson and Denk (2007), Grímsson et al. (2007), Bratseva (1980)	65.773	−24.083
19	Russia	Fletcher et al. (2021)	65.110	172.390
20	Russia	Nikitin (2007)	64.818	168.664
21	USA	Wahrhaftig (1969)	64.000	−148.500
22	USA	Wahrhaftig (1969)	64.000	−148.500
23	USA	Liu and Leopold (1994), J. Pound et al. (2012)	63.900	148.941
24	USA	J. M. White et al. (1997)	63.870	−148.850
25	USA	J. M. White et al. (1997)	63.870	−148.850
26	USA	Wahrhaftig (1969)	63.860	−149.020
27	USA	Leopold and Liu (1994), Grimaldi and Triplehorn (2008), J. M. White et al. (1997)	63.850	−148.376
28	Russia	Baranova et al. (1970), Nikitin (2007)	63.552	128.459
29	Russia	Fletcher et al. (2021)	63.020	133.930
30	USA	Wolfe (1966)	62.420	−150.600
31	USA	Wolfe (1966)	62.330	−151.530
32	USA	Wolfe and Leopold (1967)	61.800	−143.170
33	USA	Wolfe (1966)	61.700	−149.090
34	USA	Wolfe (1966)	61.670	−149.150
35	USA	Wolfe (1966)	61.630	−149.850
36	USA	Wolfe (1966)	61.320	−149.580
37	USA	Wolfe (1966)	61.300	−151.770
38	USA	Wolfe (1966)	61.240	−151.250
39	USA	Wolfe (1966)	60.530	−152.320
40	USA	Wolfe (1966)	60.370	−152.340
41	USA	Wolfe (1966)	60.290	−152.450
42	USA	Wolfe (1966)	60.290	−152.430
43	USA	Wolfe (1966)	59.790	−152.610

Table 3
Continued

Site	Country	Reference	Latitude	Longitude
44	USA	Wolfe (1966)	59.410	−151.740
45	USA	Wolfe and Tanai (1980)	59.400	−151.700
46	USA	Wolfe (1966)	58.840	−153.290
47	Russia	Popova et al. (2012)	58.000	83.000
48	Russia	Belova (1985)	57.500	109.000
49	Russia	Enikeev (2008)	56.970	118.310
50	Denmark	Utescher, Erdei, et al. (2007)	56.175	9.116
51	Russia	Gnibidenko et al. (1999)	56.057	74.790
52	Denmark	Utescher, Erdei, et al. (2007)	56.018	9.116
53	Denmark	Utescher, Erdei, et al. (2007)	56.005	9.112
54	Russia	Popova et al. (2012)	56.000	69.000
55	Russia	Popova et al. (2012)	56.000	68.000
56	Denmark	Larsson et al. (2011)	55.830	8.420
57	Russia	Belova (1985)	55.650	111.270
58	Russia	Gnibidenko et al. (1999)	55.638	73.653
59	Russia	Popova et al. (2012)	55.000	80.000
60	Russia	Popova et al. (2012)	55.000	76.000
61	Russia	Gnibidenko et al. (1999)	54.930	73.362
62	Russia	Kezina and Ol'kin (2000)	54.132	128.239
63	Russia	Belova (1985)	54.000	113.300
64	Kazakhstan	Popova et al. (2012)	54.000	73.000
65	Russia	Belova (1985)	53.935	107.124
66	Canada	Piel (1977)	53.921	−122.778
67	Russia	Popova et al. (2012)	53.000	79.000
68	Russia	Yakubovskaya and Iosifova (1968)	52.664	41.430
69	Poland	Durska (2008)	52.362	18.471
70	Poland	Utescher et al. (2011)	52.344	18.477
71	Russia	Skopintsev and Tregub (2017)	52.194	100.100
72	Poland	Worobiec, Widera, and Worobiec (2022)	52.161	18.314
73	Poland	Worobiec et al. (2021)	52.012	18.374
74	Germany	Mosbrugger et al. (2005)	51.550	13.900
75	Germany	Mosbrugger et al. (2005)	51.550	13.900
76	Germany	Mosbrugger et al. (2005)	51.550	13.900
77	Germany	Mosbrugger et al. (2005)	51.550	13.850
78	Canada	Mathews and Rouse (1984)	51.505	−122.232
79	Germany	Mosbrugger et al. (2005)	51.500	13.780
80	Germany	Eberlein (2015)	51.464	13.615
81	Russia	Belova (1985)	51.400	103.400
82	Canada	Read (2000)	51.193	−120.936
83	Poland	Worobiec, Worobiec, and Kasiński (2022)	51.170	16.380
84	Poland	Worobiec (2009)	51.152	16.154
85	Poland	Worobiec (2009)	51.146	16.136
86	Kazakhstan	Popova et al. (2012)	51.000	68.000

Table 3
Continued

Site	Country	Reference	Latitude	Longitude
87	Canada	Greenwood et al. (2020)	50.940	−120.810
88	Germany	Utescher, Erdei, et al. (2007)	50.900	6.509
89	Germany	Ferguson et al. (1998)	50.758	6.447
90	Poland	Worobiec and Szulc (2010)	50.344	18.046
91	Czechia	Kovar-Eder et al. (1998)	50.197	12.567
92	Poland	Sobczyk et al. (2024)	50.185	16.441
93	Germany	Utescher, Erdei, et al. (2007)	50.040	9,000
94	Poland	Lancucka-Srodoniowa and Zastawniak (1997)	49.980	20.050
95	Canada	Manchester et al. (1991)	49.622	−115.636
96	Germany	Kovar-Eder et al. (1998)	49.311	12.173
97	Germany	Utescher, Erdei, et al. (2007)	49.150	12.100
98	Canada	Stott and Aitken (1993), Holman (1970)	49.086	−107.798
99	Czechia	Kovar-Eder et al. (1998)	49.059	14.715
100	Germany	Utescher, Erdei, et al. (2007)	49.020	11.930
101	Germany	Utescher, Erdei, et al. (2007)	49.000	11.950
102	Germany	Gregor et al. (1989)	48.976	11.954
103	Germany	Gregor et al. (1989)	48.848	10.857
104	Germany	Gregor et al. (1989)	48.577	13.423
105	Germany	Utescher, Erdei, et al. (2007)	48.570	9.530
106	Germany	Rasser et al. (2013)	48.565	9.533
107	Germany	Boehme et al. (2007)	48.550	11.267
108	Germany	Bruch et al. (2004)	48.500	12.000
109	Germany	Mosbrugger et al. (2005)	48.410	11.100
110	Germany	Mosbrugger et al. (2005)	48.400	11.540
111	Hungary	Hably (1985)	48.232	19.657
112	Slovakia	Holcová et al. (1996)	48.225	19.578
113	USA	Manchester et al. (1991)	48.166	−119.087
114	Ukraine	Syabryaj et al. (2007)	48.080	23.730
115	Ukraine	Syabryaj et al. (2007)	48.050	23.700
116	Ukraine	Utescher, Erdei, et al. (2007)	48.050	23.700
117	Kazakhstan	Il'inskaya (1962)	48.036	84.092
118	Czechia and Slovakia	Doláková et al. (2021)	48.000	16.500
119	USA	Manchester et al. (1991)	47.732	−117.348
120	Germany	Utescher, Erdei, et al. (2007)	47.700	10.200
121	Germany	Utescher et al. (2011)	47.700	10.150
122	Germany	Utescher, Erdei, et al. (2007)	47.700	10.200
123	USA	Knowlton (1926)	47.660	−117.420
124	Russia	Lopatina (2001, 2004)	47.491	138.609
125	Austria	Kovar-Eder et al. (2003)	47.480	15.330
126	USA	Manchester et al. (1991)	47.188	−116.222
127	France	Sittler (1958)	47.070	5.000
128	USA	Manchester et al. (1991)	47.023	−115.771
129	USA	C. J. Smiley and Rember (1985)	47.020	−116.260

Table 3
Continued

Site	Country	Reference	Latitude	Longitude
130	Switzerland	Meon-Vilain (1968)	46.947	7.444
131	USA	Wheeler and Dillhoff (2009)	46.940	−120.010
132	USA	C. J. Smiley et al. (1975)	46.940	−116.260
133	USA	Manchester et al. (1991)	46.726	−115.925
134	Hungary	Jiménez-Moreno (2006)	46.533	18.717
135	USA	Manchester et al. (1991)	46.437	−116.563
136	USA	Manchester et al. (1991)	46.309	−115.582
137	Hungary	Hably (2020)	46.249	18.312
138	China	Wan et al. (2014)	46.200	123.200
139	China	Wan et al. (2014)	46.200	123.200
140	China	Wan et al. (2014)	46.200	123.200
141	China	Wan et al. (2014)	46.200	123.200
142	China	Q. H. Huang et al. (2002)	46.167	129.250
143	Hungary	Jiménez-Moreno (2006)	46.166	18.513
144	Russia	Lopatina (2003)	46.020	137.847
145	USA	Strömberg (2005)	45.900	−114.200
146	USA	Manchester et al. (1991)	45.803	−115.663
147	USA	Strömberg (2005)	45.750	−111.430
148	Ukraine	Syabryaj et al. (2007)	45.270	34.030
149	Ukraine	Syabryaj et al. (2007)	45.270	33.430
150	Ukraine	Syabryaj et al. (2007)	45.270	33.430
151	Ukraine	Syabryaj et al. (2007)	45.270	33.430
152	Russia	Bekker-Migdisova (1967)	45.044	41.972
153	Russia	Klimova (1988)	45.000	135.000
154	USA	Martin and Gray (1962)	44.970	−117.520
155	USA	Strömberg (2005)	44.930	−112.550
156	Republic of Serbia	Popova et al. (2012)	44.864	20.658
157	USA	Harris et al. (2017)	44.810	−113.230
158	USA	Harris et al. (2017)	44.810	−113.230
159	USA	Harris et al. (2017)	44.810	−113.230
160	Republic of Serbia	Utescher, Djordjevic-Milutinovic, et al. (2007)	44.809	20.572
161	Republic of Serbia	Utescher, Djordjevic-Milutinovic, et al. (2007)	44.800	21.700
162	USA	Harris et al. (2017)	44.792	−113.314
163	Republic of Serbia	Ercegovac et al. (1997)	44.717	21.233
164	Republic of Serbia	Utescher, Djordjevic-Milutinovic, et al. (2007)	44.700	20.500
165	USA	Chaney (1959)	44.480	−118.760
166	USA	Chaney (1959)	44.460	−119.470
167	USA	Chaney (1925)	44.435	−119.294
168	USA	Oliver (1936)	44.414	−119.086
169	China	Utescher, Djordjevic-Milutinovic, et al. (2007)	44.300	20.600
170	Republic of Serbia	Utescher, Djordjevic-Milutinovic, et al. (2007)	44.200	21.780
171	China	Tang et al. (2011)	44.173	85.457
172	China	J. M. Sun and Zhang (2008)	44.117	84.033

Table 3
Continued

Site	Country	Reference	Latitude	Longitude
173	China	J. M. Sun and Zhang (2008)	44.100	86.333
174	France	Jiménez-Moreno and Suc (2007)	44.030	5.976
175	Bulgaria	Ivanov et al. (2002)	44.029	22.765
176	France	Bialkowski et al. (2006)	44.028	6.234
177	France	Bialkowski et al. (2006)	44.011	6.216
178	Republic of Serbia	Utescher, Djordjevic-Milutinovic, et al. (2007)	44.000	21.000
179	France	Gardère and Pais (2007)	43.928	−0.181
180	Croatia	Jiménez-Moreno et al. (2008)	43.867	16.483
181	USA	Traverse (1994)	43.840	−73.050
182	USA	Tiffney (1994)	43.830	−73.050
183	China	X. Sun and Wang (2005)	43.650	111.967
184	France	Jiménez-Moreno and Suc (2007)	43.536	4.928
185	Bulgaria	Ivanov et al. (2007)	43.493	28.246
186	USA	Lockley and Rice (1990)	43.260	−117.030
187	Japan	Igarashi et al. (2000)	43.211	144.126
188	USA	Strömberg (2005)	42.690	−102.850
189	USA	Elias (1942)	42.680	−102.690
190	USA	Strömberg (2005)	42.640	−102.800
191	Bulgaria	Utescher et al. (2011)	42.533	23.617
192	China	Tao (1997)	42.500	119.250
193	North Korea	Kong (2000)	42.483	130.085
194	Spain	Barrón et al. (2010), Utescher, Erdei, et al. (2007)	42.400	−3.190
195	USA	Axelrod (1964)	42.250	−114.090
196	USA	Strömberg (2005)	42.170	−103.720
197	USA	Strömberg (2005)	42.170	−103.720
198	USA	Axelrod (1964)	42.100	−114.020
199	Kazakhstan	Abusiarova (1966)	42.050	70.125
200	China	Tao et al. (2000), Ping et al. (2001), Z. Zhang (1986)	42.050	119.250
201	USA	Leopold and Denton (1987)	42.000	−115.000
202	USA	Axelrod (1992a)	41.800	−119.800
203	Spain	Utescher et al. (2011)	41.480	2.030
204	USA	Axelrod (1992a)	41.400	−119.290
205	USA	Frederiksen (1984)	41.350	−70.830
206	USA	Frederiksen (1984), Axelrod (2000)	41.323	−70.813
207	USA	Frederiksen (1984)	41.320	−70.820
208	Spain	Jiménez-Moreno and Suc (2007)	41.174	1.102
209	Turkey	Kayseri and Akgün (2008)	41.062	35.732
210	USA	Leopold and Denton (1987)	41.000	−107.000
211	USA	Leopold and Denton (1987)	41.000	−107.000
212	North Korea	Kong (2000)	40.683	128.593
213	USA	Axelrod and Schorn (1994)	40.660	−118.306
214	Turkey	Stromberg and Smith (2007)	40.530	32.640
215	Spain	Barrón et al. (2006)	40.191	−0.652

Table 3
Continued

Site	Country	Reference	Latitude	Longitude
216	Spain	Urban et al. (2010)	40.183	0.650
217	Turkey	Unpublished	40.167	31.915
218	Turkey	Unpublished	40.111	27.643
219	Turkey	Bozcu et al. (2015)	40.022	27.026
220	Turkey	Unpublished	40.016	27.018
221	China	Ma (1991)	40.000	94.717
222	USA	Leopold and Denton (1987)	40.000	−107.000
223	Turkey	Bozcu et al. (2015)	39.966	26.860
224	USA	Axelrod (1995)	39.953	−119.373
225	USA	S. K. Srivastava (1984), L. D. White et al. (1992)	39.900	−120.660
226	USA	Axelrod (1992a, 1992b)	39.883	−119.574
227	USA	Bartley et al. (2010)	39.781	−123.235
228	USA	Tiffney (1994)	39.780	−123.240
229	China	Ma (1993), Fan (1994)	39.717	98.500
230	China	Ma (1993), Fan (1994)	39.717	98.500
231	USA	Kotthoff et al. (2014)	39.630	−73.630
232	USA	Axelrod (1992a, 1992b)	39.600	−119.330
233	Turkey	Unpublished	39.457	28.139
234	USA	Owens (1988)	39.430	−74.760
235	USA	Axelrod (1995)	39.420	−119.300
236	USA	Axelrod (1985)	39.390	−117.630
237	Turkey	Akkiraz et al. (2015, 2020)	39.259	27.738
238	Turkey	Akkiraz et al. (2015, 2020)	39.252	27.736
239	USA	Pazzaglia et al. (1997)	39.200	−75.500
240	Portugal	Utescher, Erdei, et al. (2007)	39.200	−8.900
241	USA	Axelrod (1991)	39.000	−117.680
242	Turkey	Akkiraz et al. (2020)	38.968	27.521
243	Turkey	Akkiraz et al. (2015)	38.831	29.925
244	Turkey	Akkiraz et al. (2015)	38.739	29.752
245	North Korea	Kong (2000)	38.709	127.810
246	Portugal	Antunes and Pais (1984)	38.699	−9.083
247	Turkey	Akkiraz et al. (2015)	38.607	29.202
248	China	Yao et al. (1994)	38.600	119.100
249	Turkey	Unpublished	38.562	27.335
250	Turkey	Unpublished	38.557	27.332
251	USA	McLaughlin et al. (2008)	38.550	−75.060
252	Turkey	Stromberg and Smith (2007)	38.530	28.630
253	Turkey	Kayseri-Özer, Sözbilir, and Akgün (2014)	38.340	27.454
254	Turkey	Kayseri-Özer, Sözbilir, and Akgün (2014)	38.336	27.407
255	Turkey	Kayseri-Özer, Sözbilir, and Akgün (2014)	38.254	27.078
256	Turkey	Kayseri-Özer, Sözbilir, and Akgün (2014)	38.217	27.044
257	Turkey	Emre et al. (2011)	38.090	27.732
258	USA	Axelrod (1992a, 1992b)	38.000	−117.500

Table 3
Continued

Site	Country	Reference	Latitude	Longitude
259	Turkey	Kayseri-Özer and Emre (2022)	37.957	28.072
260	Turkey	Graben (2022)	37.953	57.760
261	Turkey	Kayseri-Özer and Emre (2022)	37.943	28.042
262	Turkey	Graben (2022)	37.892	28.049
263	Turkey	Akgün et al. (2007), Akgün and Akyol (1999)	37.770	27.929
264	Turkey	Kayseri-Özer and Emre (2022)	37.769	28.095
265	Turkey	Akgün et al. (2021)	37.601	34.602
266	USA	Liu and Leopold (1994)	37.540	−77.440
267	USA	Berry (1909), Godfrey and Barnes (2008)	37.533	−77.467
268	Turkey	Akgün et al. (2021)	37.509	34.347
269	China	Jingfang et al. (2020)	37.486	95.212
270	Spain	Jiménez-Moreno and Suc (2007)	37.369	−2.969
271	Turkey	Kayseri-Özer, Akgün, et al. (2014)	37.163	27.894
272	Japan	Fuji (1969)	37.114	136.811
273	Turkey	Kayseri-Özer, Akgün, et al. (2014)	37.046	28.061
274	Turkey	Kayseri-Özer, Akgün, et al. (2014)	37.046	28.061
275	Turkey	Kayseri-Özer and Akgün (2010)	37.043	28.045
276	Tunisia	Moktar and Mannaï-Tayech (2016)	36.826	10.605
277	Japan	Yamanoi (1984)	36.585	137.358
278	China	X. Sun and Wang (2005)	36.567	101.733
279	China	Liu and Leopold (1994), Q. G. Sun et al. (2002)	36.553	118.786
280	China	Chen (2009)	36.517	101.867
281	China	Q. G. Sun (1984)	36.433	102.267
282	China	Jiang and Ding (2008)	36.379	106.099
283	USA	Axelrod (1939)	36.190	−118.110
284	Tunisia	Planderová (1971)	36.134	10.375
285	China	Gu et al. (1992)	36.118	102.801
286	South Korea	Chung and Koh (2005)	36.085	129.310
287	South Korea	Chung and Koh (2005)	36.050	129.361
288	Ocean core	S. Yi et al. (2003)	35.900	123.950
289	China	Ma et al. (1998)	35.508	103.250
290	China	Ma et al. (1998)	35.508	103.250
291	Japan	Yabe and Nakagawa (2018)	35.485	135.546
292	China	Y. Yi (1998)	35.306	123.350
293	China	Hui, Zhang, et al. (2018)	35.266	105.593
294	China	Hui, Zhang, et al. (2018)	35.266	105.593
295	China	Hui, Zhang, et al. (2018)	35.266	105.593
296	USA	Axelrod (1939)	35.214	−118.336
297	USA	Loughney et al. (2020)	35.030	−117.050
298	USA	Loughney et al. (2020)	35.020	−117.020
299	China	Hui et al. (2011)	34.967	105.567
300	China	Hui, Li, et al. (2018)	34.930	101.800
301	China	Hui, Zhang, et al. (2018)	34.778	104.761

Table 3
Continued

Site	Country	Reference	Latitude	Longitude
302	China	Hui, Zhang, et al. (2018)	34.778	104.761
303	China	Hui et al. (2017)	34.700	104.900
304	China	Hui et al. (2017)	34.700	104.900
305	Japan	Matsuoka (1990)	34.658	136.029
306	USA	T. M. Smiley et al. (2018)	34.320	−117.491
307	USA	T. M. Smiley et al. (2018)	34.310	−117.470
308	China	L. Zhao et al. (2018)	34.305	109.499
309	USA	T. M. Smiley et al. (2018)	34.300	−117.470
310	USA	T. M. Smiley et al. (2018)	34.300	−117.470
311	USA	Martin and Gray (1962)	33.780	−118.260
312	China	H. H. Zhao and Guo (1995)	33.633	114.633
313	China	Y. Zheng et al. (1981)	33.345	120.166
314	China	Zhenjiang et al. (2006)	32.033	119.000
315	India	Lakhanpal and Guleria (1986)	31.950	76.267
316	USA	Jarzen et al. (2010), Lott et al. (2019)	30.469	−84.986
317	South Korea	Hu and Sarjeant (1992)	30.421	126.437
318	China	M. R. Sun et al. (1989)	30.000	123.000
319	China	Haomin and Shuangxing (1976), Gengwu and Jianguo (2016), Spicer et al. (2003)	29.717	89.000
320	China	H. Li and Guo (1976)	29.679	89.091
321	India	Prasad (1993)	29.500	78.733
322	Egypt	El Beialy et al. (2005)	29.380	32.600
323	China	Hu and Sarjeant (1992)	29.365	124.818
324	India	Prasad et al. (2004)	29.267	79.517
325	China	Yang et al. (2018)	29.160	121.274
326	Ocean core	Hu and Sarjeant (1992)	27.976	125.819
327	China	Jacques et al. (2011), X. J. Sun and He (1987)	27.220	116.530
328	India	Antal and Prasad (1997)	26.913	88.507
329	China	X. J. Sun and He (1987)	26.833	116.317
330	China	He and Wang (2021)	26.833	116.317
331	Taiwan	Ling (1965), Ho (1966)	25.132	121.706
332	China	Shi et al. (2014), Shi and Li (2010), Jacques et al. (2015), Zixi (2018), B. Wang et al. (2021), Y. Yi (2020)	24.333	117.750
333	China	D. Zheng et al. (2019)	24.250	117.830
334	China	Z. Wang et al. (2019)	24.250	117.890
335	India	Aswal (1993)	24.245	93.107
336	China	Shi et al. (2014), Shi and Li (2010), Jacques et al. (2015), Zixi (2018), B. Wang et al. (2021), Y. Yi (2020)	24.200	117.890
337	China	W. Wang (1988)	24.123	107.259
338	United Arab Emirates	Whybrow and McClure (1980)	23.931	52.268
339	China	L. L. Huang et al. (2021), Y. Li et al. (2021), X. Wu et al. (2021), Song et al. (2023)	23.386	110.165
340	China	J. Huang et al. (2018)	23.350	104.295
341	China	Lei (1985), Zhang et al. (2019)	22.174	113.551
342	China	Lei (1985), Zhang et al. (2019)	21.500	113.500
343	Myanmar	L.-C. Zhao et al. (2004)	21.400	97.817

Table 3
Continued

Site	Country	Reference	Latitude	Longitude
344	Vietnam	Dzanh (1990)	21.098	105.783
345	China	X. Sun et al. (1981)	19.900	110.100
346	China	X. Sun et al. (1981)	19.900	110.100
347	Thailand	Vozenin-Serra et al. (1989)	19.149	100.274
348	Mexico	Lenhardt et al. (2006)	18.996	−99.101
349	China	J.-G. Li and Zhang (1998)	18.716	111.460
350	Thailand	Songtham et al. (2003)	17.836	99.292
351	Mexico	Martínez-Hernández (1992)	16.803	−92.906
352	India	Daneshian et al. (2007)	12.136	93.114
353	Thailand	Highton et al. (1997)	10.190	102.190
354	Panama	Retallack and Kirby (2007)	9.083	−79.625
355	India	R. Srivastava and Awasthi (1994)	8.857	76.616
356	India	Varma et al. (1986)	8.625	76.950
357	Thailand	Watanasak et al. (1995)	8.024	98.882
358	Ivory Coast	Simon et al. (1984)	5.356	−3.495
359	Colombia	Ochoa et al. (2012)	4.860	74.630
360	Nigeria	Oboh (1995)	4.780	6.254
361	Colombia	Wijninga (1996)	4.667	−74.333
362	Nigeria	Oboh (1992)	4.656	5.953
363	Ethiopia	Wheeler et al. (2007)	4.573	36.396
364	Malaysia	Konzalova (2005)	1.850	113.620
365	Brazil	Regali et al. (1974), Jaramillo et al. (2010)	1.361	−49.339
366	Kenya	Behrensmeyer et al. (2002)	0.756	35.772
367	Indonesia	Morley and Morley (2011)	−0.060	118.580
368	Kenya	Dugas and Retallack (1993)	−0.236	35.420
369	Kenya	Wynn and Retallack (2001)	−0.390	35.010
370	Brazil	Behling and Costa (2004)	−1.264	−48.446
371	Peru	Unpublished	−3.012	−73.405
372	Colombia	Hoorn (1994)	−3.387	−71.825
373	Peru	Regali et al. (1974), Jaramillo et al. (2010)	−3.387	−71.825
374	Peru	Regali et al. (1974), Jaramillo et al. (2010)	−3.692	−73.221
375	Colombia	Hoorn (1994)	−3.692	−71.825
376	Peru	Goillot et al. (2007)	−4.023	−73.160
377	Peru	Goillot et al. (2007)	−4.225	−73.364
378	Peru	Berry (1919)	−4.864	−80.788
379	Brazil	Regali et al. (1974), Jaramillo et al. (2010)	−16.129	−38.616
380	Australia	Archer et al. (1991)	−20.550	139.595
381	Australia	Beeston (1994)	−21.382	147.204
382	Australia	Beeston (1994)	−21.819	148.036
383	Australia	Mao and Retallack (2019)	−23.555	134.676
384	Chile	Alpers and Brimhall (1988)	−24.297	−69.068
385	Brazil	Regali et al. (1974), Jaramillo et al. (2010)	−24.492	−45.510
386	Argentina	Quattrocchio et al. (2003)	−24.862	−65.409

Table 3
Continued

Site	Country	Reference	Latitude	Longitude
387	Argentina	Anzótegui and Herbst (2004)	−26.710	−66.020
388	Argentina	Barreda et al. (2003)	−29.539	−68.929
389	Australia	Carpenter et al. (2011)	−29.600	147.700
390	Argentina	Caccavari and Barreda (2000)	−29.620	−69.600
391	Australia	Martin (1997)	−30.184	145.793
392	South Africa	De Wit and Bamford (1993)	−30.772	20.415
393	Australia	Holmes and Andereson (2019)	−31.213	149.150
394	Argentina	Ottone et al. (1998)	−32.044	−69.793
395	Australia	McCurry et al. (2022)	−32.270	149.700
396	South Africa	Coetzee and Rogers (1982)	−32.923	18.134
397	Australia	Truswell et al. (1984)	−32.990	140.910
398	Chile	Hinojosa (2010)	−33.950	−71.800
399	Australia	Martin (1993)	−34.000	141.744
400	Australia	Martin (1993)	−34.044	144.520
401	Australia	Martin (1993)	−34.428	140.662
402	Australia	Martin (1993)	−34.751	143.416
403	Australia	Martin (1993)	−35.421	144.859
404	New Zealand	Moore and Wallace (2000)	−36.860	175.434
405	Australia	Kershaw (1997)	−38.185	146.354
406	Argentina	Quattrocchio and Guerstein (1989)	−38.286	−60.895
407	Argentina	Barreda et al. (2008)	−38.670	−61.266
408	Argentina	Dunn et al. (2015)	−38.963	−68.007
409	Argentina	Quattrocchio and Guerstein (1989)	−39.286	−60.895
410	Argentina	Barreda et al. (2008)	−39.360	−62.672
411	Argentina	Quattrocchio and Guerstein (1989)	−40.346	−62.910
412	Argentina	Barreda et al. (2008)	−40.723	−64.400
413	Argentina	Caviglia and Zamaloa (2014)	−41.580	−71.000
414	New Zealand	Reichgelt et al. (2015)	−44.900	169.800
415	New Zealand	Reichgelt et al. (2015)	−45.000	169.300
416	New Zealand	Reichgelt et al. (2015)	−45.000	169.300
417	New Zealand	Reichgelt et al. (2015)	−45.100	169.900
418	New Zealand	Pole and Douglas (1998), Reichgelt et al. (2015)	−45.200	169.100
419	New Zealand	Reichgelt et al. (2015)	−45.200	169.100
420	New Zealand	Mildenhall and Pocknall (1984)	−45.873	167.696
421	New Zealand	Field et al. (2009)	−45.960	167.554
422	Argentina	Raigemborn et al. (2018)	−51.200	−69.150
423	Falkland Islands	Macphail and Cantrill (2006)	−51.353	−60.692
424	Argentina	Zamaloa (2000), Zamaloa and Romero (2005)	−52.724	−68.606
425	Ocean core	Mohr (2001)	−60.896	−42.615
426	Ocean core	Anderson et al. (2011)	−63.260	−53.040
427	Ocean core	Warny et al. (2009)	−77.750	−165.283
428	Ocean core	Warny et al. (2009)	−77.760	165.280
429	Ocean core	Warny et al. (2009)	−77.760	165.280

Table 3
Continued

Site	Country	Reference	Latitude	Longitude
430	Ocean core	Warny et al. (2009)	−77.760	165.280
431	Ocean core	Warny et al. (2009)	−77.760	165.280

Note. Refer to Data Set S2 in Supporting Information S1 for full details.

vegetation reconstruction (i.e., Europe). Grid cells containing data points (and grid cells around those data points to account for the uncertainty in the paleolocation of the data and to avoid abrupt transitions) were then converted to the data-derived biome classification. Where a grid cell contained more than one datapoint of contradictory biomes, the biome assignment made was to the biome with the highest number of agreeing datapoints. The resulting vegetation reconstruction is made available at 1° resolution.

3. Results

3.1. BIOME4 Model Simulated Biome Distributions

We begin by describing the broad patterns resulting from the globally consistent model simulations. The BIOME4 model simulated a wide range of biome distributions for each of the simulations in the MioMIP1 ensemble (Figure 5). For the middle to high northern latitudes (~40–90°N), these distributions are largely driven by the atmospheric CO_2 concentration whereby similar biome distributions are generated across the MioMIP1 simulations within a given CO_2 range. The lowest CO_2 group, 280 ppm, results in large regions of the deciduous taiga/montane forest and steppe tundra biomes, which is replaced by the temperate grassland biome as the CO_2 concentration increases. Some Saharan Desert biome is simulated for most of the vegetation models driven by the MioMIP1 simulations, but the Sahara is largely replaced by tropical xerophytic shrubland. No MioMIP1 simulations result in a modern-like Amazon Forest in the MCO when driving BIOME4, and whether trees are simulated in that region or not is highly variable across the climate models, ice sheet configurations and CO_2 concentration. The biome predictions for Antarctica are very sensitive to CO_2 concentration, with tundra biomes, grassland biomes and forest biomes all featuring in the simulations depending on CO_2 levels (the high CO_2 concentration simulations resulting in more grasslands and forests than the lower CO_2 concentration simulations, perhaps due more to the direct physiological effect of the CO_2 than the climatic effect).

3.2. Model-Data Comparison

All the BIOME4 simulations driven by the MioMIP1 multimodel climate ensemble were considered by paleobotanists and vegetation modeling experts on a regional basis, and where possible, a best-fit model was identified for each region. Figure 6 shows the regional boundaries used.

3.2.1. Northern High Latitudes

Vegetation proxy data for the Northern High Latitudes is clustered in the western part of the North American Arctic and central to eastern Siberia (Figure 7). Dominating these reconstructions is the cool mixed forest biome (Fletcher et al., 2021; J. M. White & Ager, 1994). Marine and terrestrial records from the North Sea Basin show the occurrence of mixed deciduous/evergreen forests and *Taxodium* coastal swamp forests (e.g., Friis, 1979; Larsson et al., 2006, 2011) and therefore the BIOME4 simulations with large areas of taiga and tundra biomes in high northern Europe are inconsistent with the proxy data. In Eurasia, paleobotanical data showed most agreement with biomes generated by the BIOME4 model run on the model osutputs of "CESM1 (CAM5) 20–14 Ma 840 ppm" (Figure 7). Despite best fit, the central Siberian region model output has temperate grassland or deciduous taiga/montane forest simulated where cool mixed forest was reconstructed from paleobotanical data, cold mixed forest simulated where temperate conifer forest was reconstructed, and temperate conifer forest simulated where warm-temperate mixed forest was reconstructed, suggesting an overall cooler and drier bias of the model. This data-model mismatch resulting from the inability to simulate Arctic amplification of temperature by the paleoclimate models has been a frequent feature of data-model comparisons of other past warm periods (e.g., the mid-Piacenzian Warm Period: de Nooijer et al., 2020; Tindall et al., 2022; and the Paleocene-Eocene Thermal Maximum: Korasidis et al., 2022), and of the MioMIP1 models (Burls et al., 2021). It is also possible that

Table 4
Details of the Middle to Early Miocene Simulations From the Miocene Model Intercomparison Project 1 Multimodel Ensemble; Full Details Can Be Found in Burls et al. (2021)

ID used in this study	Model name	Paleography period	CO_2 level (ppm)	Ice sheets	Reference
CCSM-NH3 20–14 Ma 355 ppm	CCSM-NH3	20–14 Ma	355	AIS from Herold et al. (2008) GIS from Herold et al. (2008)	Herold, Huber, Greenwood, et al. (2011), Herold, Huber, and Müller (2011), Herold et al. (2012)
CCSM-NH3 20–14 Ma 560 ppm	CCSM-NH3	20–14 Ma	560	AIS from Herold et al. (2008) GIS from Herold et al. (2008)	Herold, Huber, Greenwood, et al. (2011), Herold, Huber, and Müller (2011), Herold et al. (2012)
CCSM3 T42 MCO 200ppm	CCSM3 T42	MCO	200	AIS 6 million km^3 No GIS	Frigola et al. (2018)
CCSM3 T42 MCO 400 ppm	CCSM3 T42	MCO	400	AIS 6 million km^3 No GIS	Frigola et al. (2018)
CCSM3 T42 MMG 200 ppm	CCSM3 T42	MMG	200	AIS 23 million km^3 No GIS	Frigola et al. (2018)
CCSM3 T42 MMG 400 ppm	CCSM3 T42	MMG	400	AIS 23 million km^3 No GIS	Frigola et al. (2018)
CCSM4 20–14 Ma 400 ppm	CCSM4	20–14 Ma	400	AIS 6.5 million km^3 GIS 0.3 million km^3	Burls et al. (2021)
CESM1 (CAM5) 20–14 Ma 400 ppm	CESM1 (CAM5)	20–14 Ma	400	AIS 6.5 million km^3 GIS 0.3 million km^3	Burls et al. (2021)
CESM1 (CAM5) 20–14 Ma 280 ppm	CESM1 (CAM5)	20–14 Ma	280	AIS 6.5 million km^3 GIS 0.3 million km^3	Acosta et al. (2022)
CESM1 (CAM5) 20–14 Ma 560 ppm	CESM1 (CAM5)	20–14 Ma	560	AIS 6.5 million km^3 GIS 0.3 million km^3	Acosta et al. (2022)
CESM1 (CAM5) 20–14 Ma 840 ppm	CESM1 (CAM5)	20–14 Ma	840	AIS 6.5 million km^3 GIS 0.3 million km^3	Acosta et al. (2022)
COSMOS T31 20–14 Ma 278 ppm	COSMOS T31	20–14 Ma	278	AIS from Herold et al. (2008) No GIS	Stärz et al. (2017)
COSMOS T31 20–14 Ma 450 ppm	COSMOS T31	20–14 Ma	450	AIS from Herold et al. (2008) No GIS	Stärz et al. (2017)
HadCM3L Mid Miocene 90SLE 853 ppm	HadCM3L	Mid Miocene	853	AIS 90 m SLE No GIS	Bradshaw et al. (2021)
HadCM3L Mid Miocene 90SLE 560 ppm	HadCM3L	Mid Miocene	560	AIS 90 m SLE No GIS	Bradshaw et al. (2021)
HadCM3L Mid Miocene 90SLE 400 ppm	HadCM3L	Mid Miocene	400	AIS 90 m SLE No GIS	Bradshaw et al. (2021)
HadCM3L Mid Miocene 90SLE 280 ppm	HadCM3L	Mid Miocene	280	AIS 90 m SLE No GIS	Bradshaw et al. (2021)
HadCM3L Mid Miocene 55SLE 853 ppm	HadCM3L	Mid Miocene	853	AIS 55 m SLE No GIS	Bradshaw et al. (2021)
HadCM3L Mid Miocene 55SLE 560 ppm	HadCM3L	Mid Miocene	560	AIS 55 m SLE No GIS	Bradshaw et al. (2021)

Table 4
Continued

ID used in this study	Model name	Paleography period	CO_2 level (ppm)	Ice sheets	Reference
HadCM3L Mid Miocene 55SLE 400 ppm	HadCM3L	Mid Miocene	400	AIS 55 m SLE No GIS	Bradshaw et al. (2021)
HadCM3L Mid Miocene 55SLE 280 ppm	HadCM3L	Mid Miocene	280	AIS 55 m SLE No GIS	Bradshaw et al. (2021)
HadCM3L Mid Miocene NoICE 853 ppm	HadCM3L	Mid Miocene	853	No AIS No GIS	Bradshaw et al. (2021)
HadCM3L Mid Miocene NoICE 560 ppm	HadCM3L	Mid Miocene	560	No AIS No GIS	Bradshaw et al. (2021)
HadCM3L Mid Miocene NoICE 400 ppm	HadCM3L	Mid Miocene	400	No AIS No GIS	Bradshaw et al. (2021)
HadCM3L Mid Miocene NoICE 280 ppm	HadCM3L	Mid Miocene	280	No AIS No GIS	Bradshaw et al. (2021)
HadCM3L Langhian 280 ppm	HadCM3L	Langhian	280	AIS from Getech Plc. No GIS	Farnsworth et al. (2019)
HadCM3L Langhian 400 ppm	HadCM3L	Langhian	400	AIS from Getech Plc. No GIS	Farnsworth et al. (2019)
HadCM3L Langhian 560 ppm	HadCM3L	Langhian	560	AIS from Getech Plc. No GIS	Farnsworth et al. (2019)
IPSLCM5A2 20 Ma 840 ppm	IPSLCM5A2	20 Ma	840	AIS as modern GIS as modern	Burls et al. (2021)
IPSLCM5A2 20 Ma 560 ppm	IPSLCM5A2	20 Ma	560	AIS as modern GIS as modern	Burls et al. (2021)
IPSLCM5A2 20 Ma 420 ppm	IPSLCM5A2	20 Ma	420	AIS as modern GIS as modern	Burls et al. (2021)
IPSLCM5A2 20 Ma No GIS 560 ppm	IPSLCM5A2	20 Ma (No GIS)	560	AIS as modern No GIS	Pillot et al. (2022)

Note. SLE = sea level equivalent; AIS = Antarctic Ice Sheet; GIS = Greenland Ice Sheet. Note that the required variables from the MioMIP NorESM simulations were not available at the time of the study.

preservation bias is playing a role: riparian and near-(lake)shore environments are more likely to be preserved and are also more likely to have arborescent taxa (Kowalski & Dilcher, 2003) that are not necessarily representative of regional vegetation.

The onset of habitats dominated by C_3 grasslands occurred in the Early-Middle Miocene in central Europe, but these ecosystems did not cover large areas during the Middle Miocene, let alone in such northern latitudes. Grass-dominated vegetation spread first in central North America roughly during the Oligocene-Miocene transition and subsequently expanded to parts of Eurasia and Africa in the Early-Middle Miocene (Barbolini et al., 2020; Harris et al., 2017; Peppe et al., 2023; C. A. E. Strömberg, 2011). At present, there is no proxy data supporting the extensive temperate grassland simulated at high northern latitudes.

Nonetheless, we produce a blend of the available paleobotanical data and the model simulations for the northern high latitudes (Figure 7), which represents a best compromise accounting for these inconsistencies.

3.2.2. North America

Most biome reconstructions across North America were warm-temperate mixed forest (Figure 8). In eastern North America, this is consistent with a recent analysis suggesting widespread and continuous, though

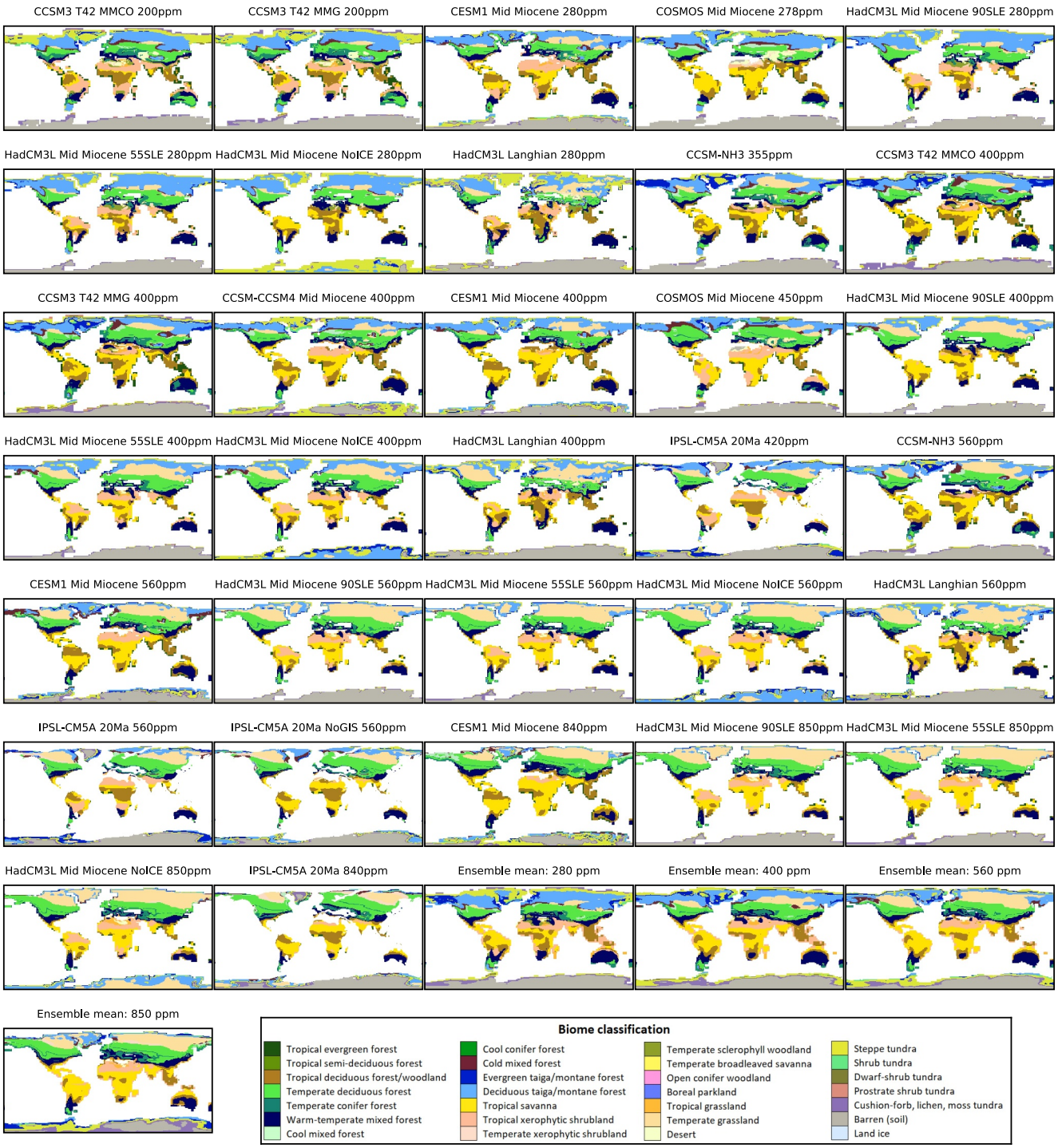

Figure 5. BIOME4 model simulated biome distributions for the Miocene Model Intercomparison Project 1 multimodel ensemble.

taxonomically heterogeneous, Miocene temperate seasonal forests (O'Keefe et al., 2024; Reichgelt et al., 2023). Tropical taxa are generally absent, except for Louisiana, which may have had tropical floral elements and generally lacks temperate floral elements. Conversely, a Middle Miocene flora from northern Florida, where more tropical floral elements would be expected, is distinctly temperate in its vegetation composition (Lott et al., 2019), although fossil fungi indicate tropical conditions (O'Keefe et al., 2024). The model that best fits Middle Miocene vegetation from paleobotanical data in North America is "HadCM3L Mid Miocene 55SLE 560 ppm." In this

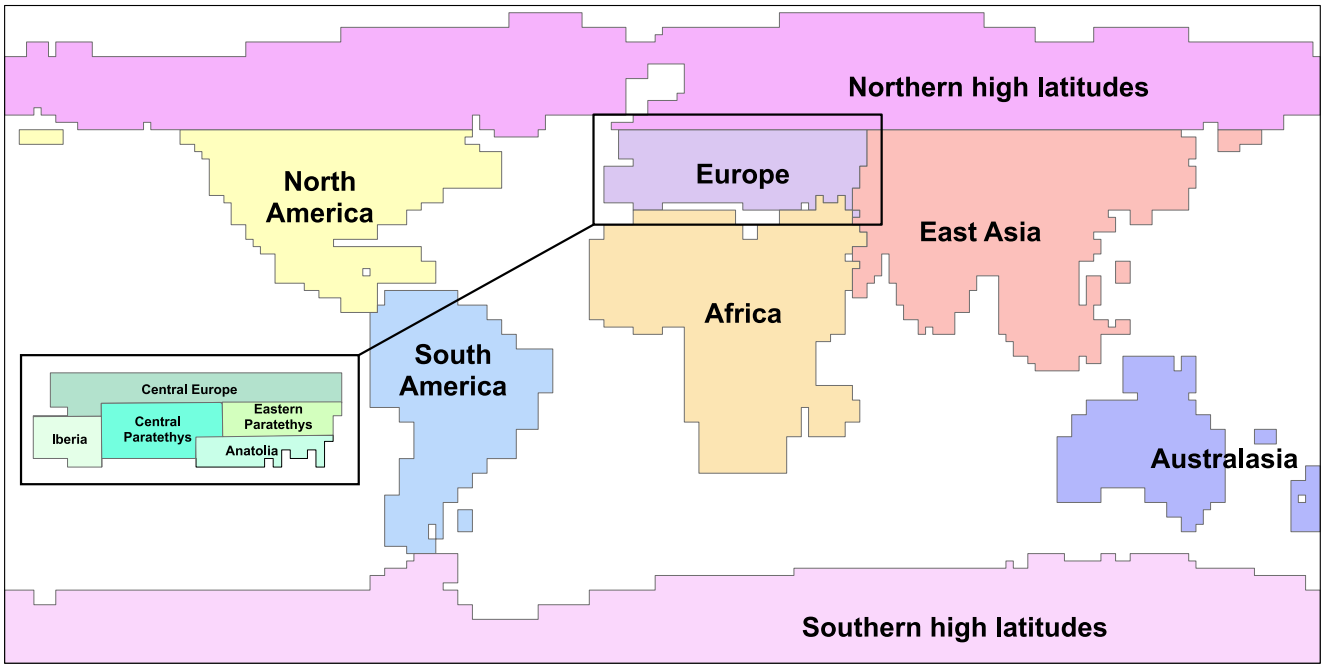

Figure 6. Model-data comparison regions.

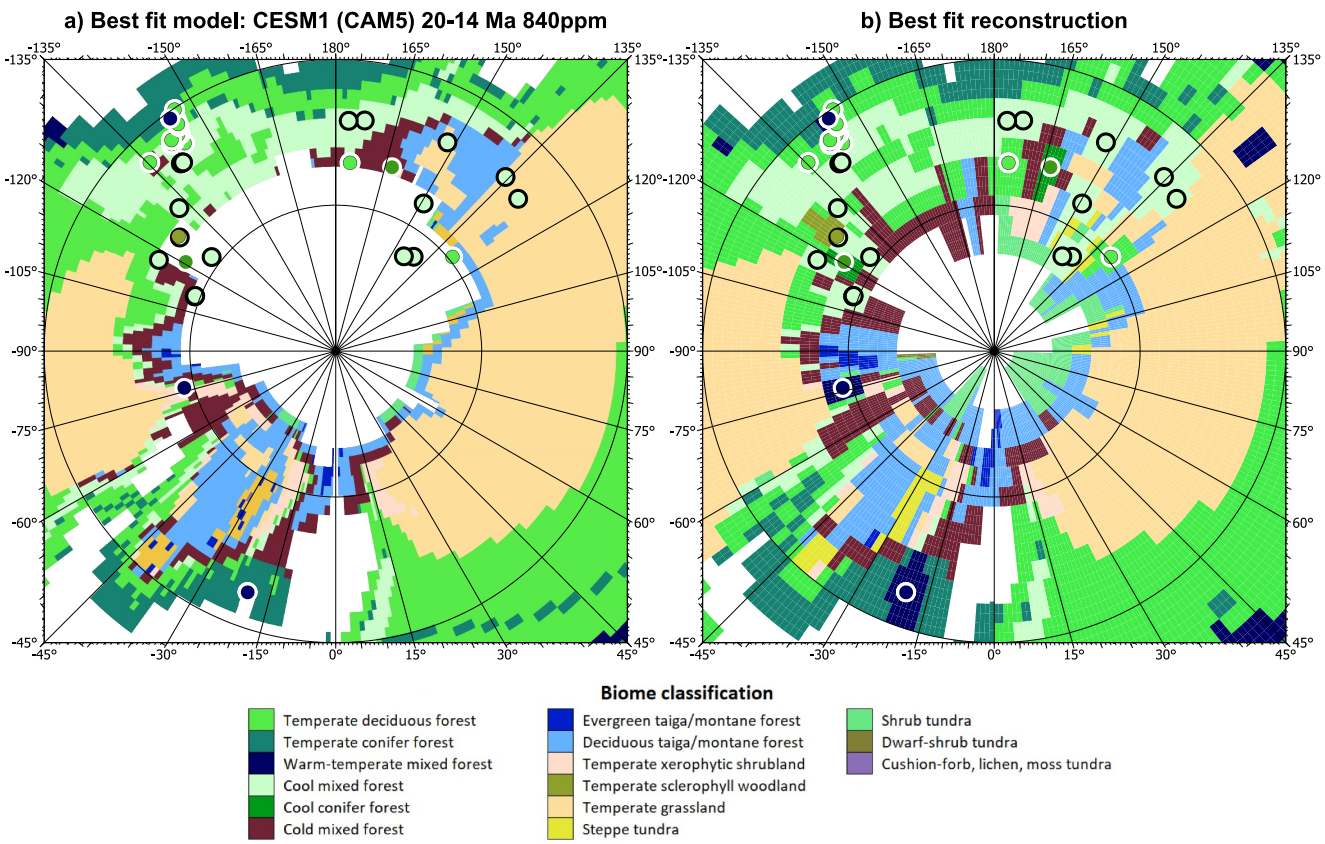

Figure 7. Vegetation reconstruction for the northern high latitudes. (a) Best fit model from model-data comparison; (b) Best fit reconstruction based on paleobotanical data and model blending.

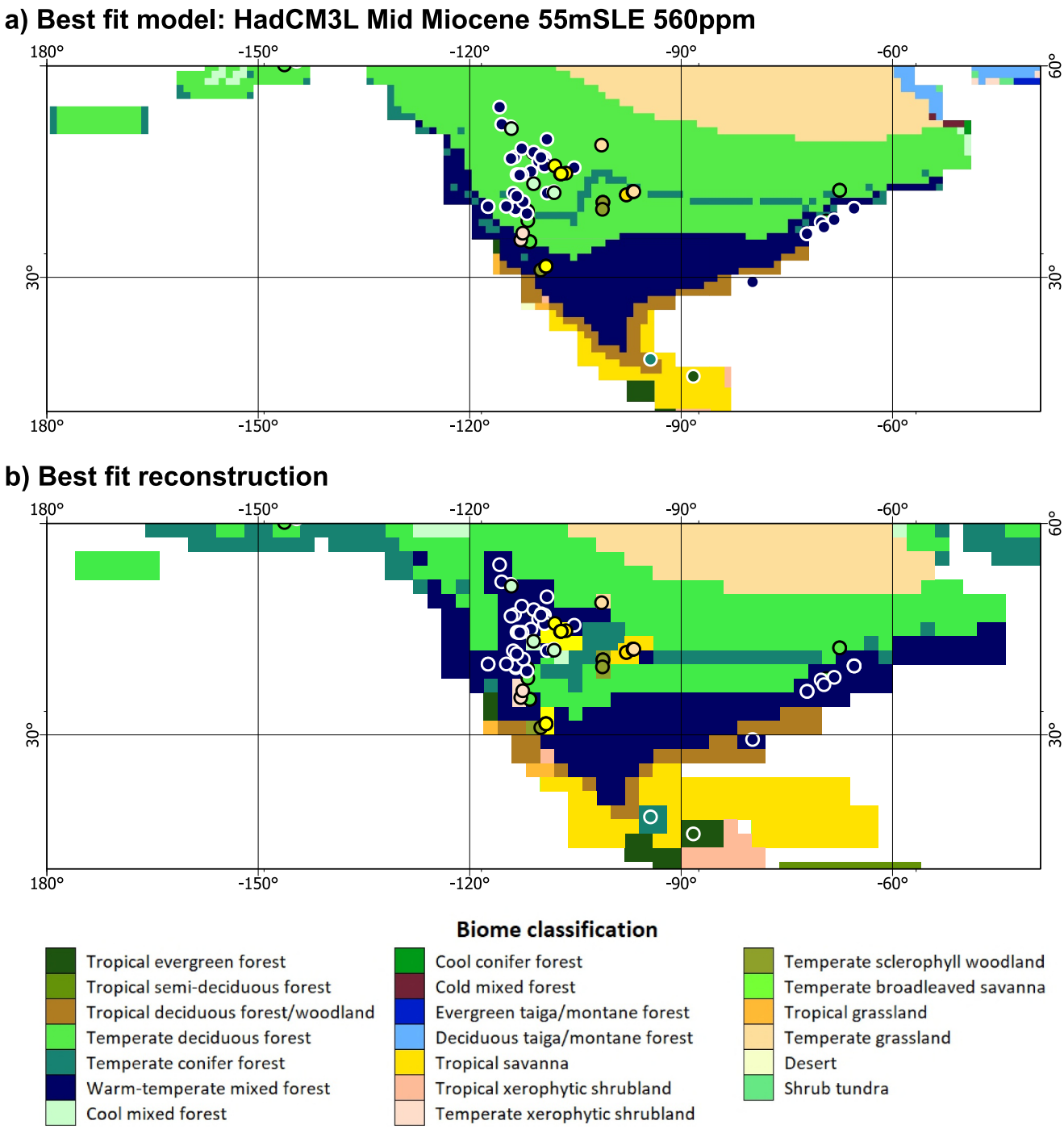

Figure 8. Vegetation reconstruction for North America. (a) Best fit model from model-data comparison; (b) Best fit reconstruction based on paleobotanical data and model blending.

simulation, the east coast climatic homogeneity is well captured, with tropical vegetation represented on the southeastern coast.

In the mountain west, proxies have been interpreted as warm-temperate mixed forests, while most simulations, including the "HadCM3L Mid Miocene 55SLE 560 ppm" simulation, predict deciduous forests. The contrast between the models and the proxies could indicate that the prescribed paleoaltitude was too high, or climate too cool, to support warm temperate forest in the models. Alternatively, the reconstruction of warm-temperate mixed

forests in this area from the proxy record may be too simplistic as the floral components of the Middle Miocene of western North America are frequently described as similar to eastern deciduous taxa (Axelrod, 1992a; Greenwood et al., 2020; Wheeler & Dillhoff, 2009). In northwestern North America, the biomes of the "HadCM3L Mid Miocene 55SLE 560 ppm" simulation fit better with the northern high latitude reconstruction chosen above (Figure 7), than those with cold mixed forest or deciduous taiga/montane forests, although the northeast coast is colder than its northern high latitude adjacent cells.

Phytolith assemblages and soil carbonate and plant wax carbon isotope geochemistry show the presence of grassland biomes, such as savannas, in the Early-Middle Miocene of the continental interior of North America (Harris et al., 2017; Kukla et al., 2022; Loughney et al., 2020; C. A. E. Strömberg, 2005; Tipple & Pagani, 2010). Savanna or grasslands and forest are bistable (alternate stable state) ecologies in some climates (Staver et al., 2011) whereby different strongly contrasting vegetation types may develop under identical initial climatic conditions due to internal feedback cycles, relating to factors such as nutrient cycling, fire recurrence, shading, under-canopy humidity, and/or herbivore browsing. For instance, there are many modern-day areas in the central USA that have natural prairie ecosystems but are within the climate range of temperate deciduous trees (R. C. Anderson, 2006). Fire recurrence in grass-dominated ecosystems does not allow for maturation of forest tree seedlings, whereas savannah vegetation may be fire-adapted (Hoffmann, 2000). If fire recurrence, or any other persistent vegetation perturbation, for example, herbivory by large mammals such as gomphotheres or equids (Janis et al., 2004; Y. Wu et al., 2018), is not incorporated into a vegetation model, then grasslands may be underrepresented. This appears to have been the case in central North America, where the absence of savannah and grasslands in the model is at odds with the proxy record. The MioVeg1 MCO blended data-model vegetation reconstruction for North America is shown in Figure 8.

3.2.3. Europe

In Europe, identifying a single best-fit model to the paleobotanical data was complicated because models that fit well in some parts of the region did not fit well in others. Therefore, a blend of the BIOME4 simulations driven by the MioMIP1 models was used, as described below according to the sub-regions defined in Figure 6.

Most simulations indicate the presence of three main latitudinal vegetation belts comprising temperate deciduous forest in the north-east, warm-temperate mixed forest and temperate conifer forest in the center and west, and warmer and drier biomes in the south.

For northwestern Central Europe, the paleobotanical data indicates the presence of warm temperate mixed forests composed of broadleaved evergreen, deciduous trees, thermophilous conifers at varying proportions, and a diverse shrub layer (e.g., M. J. Pound & McCoy, 2021; Utescher et al., 2021), yet the BIOME4 model primarily simulates temperate deciduous forests. This may indicate that the model is being driven by temperatures that are too cool, but these mismatches may not be so significant, especially where warm temperate mixed forest biomes are simulated nearby. For northeastern Central Europe, most of the best-fitting models (MioMIP1 ensemble mean scenario under the 850 ppm CO_2 scenario, "CCSM3 T42 MCO 400 ppm," "CESM1 (CAM5) 20–14 Ma 840 ppm," the HadCM3L model under all 560 ppm CO_2 scenarios, and the IPSL-CM5A model under the 400, 560 and 850 ppm CO_2 scenarios; refer to Figure 9) simulate temperate deciduous forest and therefore this biome is the selected for this region.

In the Central Paratethys region, the paleobotanical data suggest the dominance of warm temperate evergreen and warm temperate evergreen-deciduous broadleaved forests (note that these are often referred to as "mixed" in the literature but this is not the same as broadleaved-coniferous mixed forests) with a varying conifer component partly as extra- or azonal elements (e.g., Doláková et al., 2021; Kvaček et al., 2006). The BIOME4 model simulations for the Central Paratethys region suffer from overestimation of temperate deciduous and temperate conifer forests when driven by the MioMIP1 models. Paleobotanical data also suggest somewhat drier conditions in the southern Central Paratethys region because of the occurrence of sclerophyllous taxa (e.g., Erdei et al., 2007; Hably, 2020; Kvaček et al., 2006).

The "CESM1 (CAM5) 20–14 Ma 840 ppm" simulation provides the best fit for the Central and Eastern Paratethys paleovegetation. It shows a belt of warm temperate mixed forests and drier vegetation (Vernyhorova et al., 2023) such as the tropical deciduous woodland to the south, though that may not meet the strict definition of "tropical" (i.e., cold month mean temperature above 18°C).

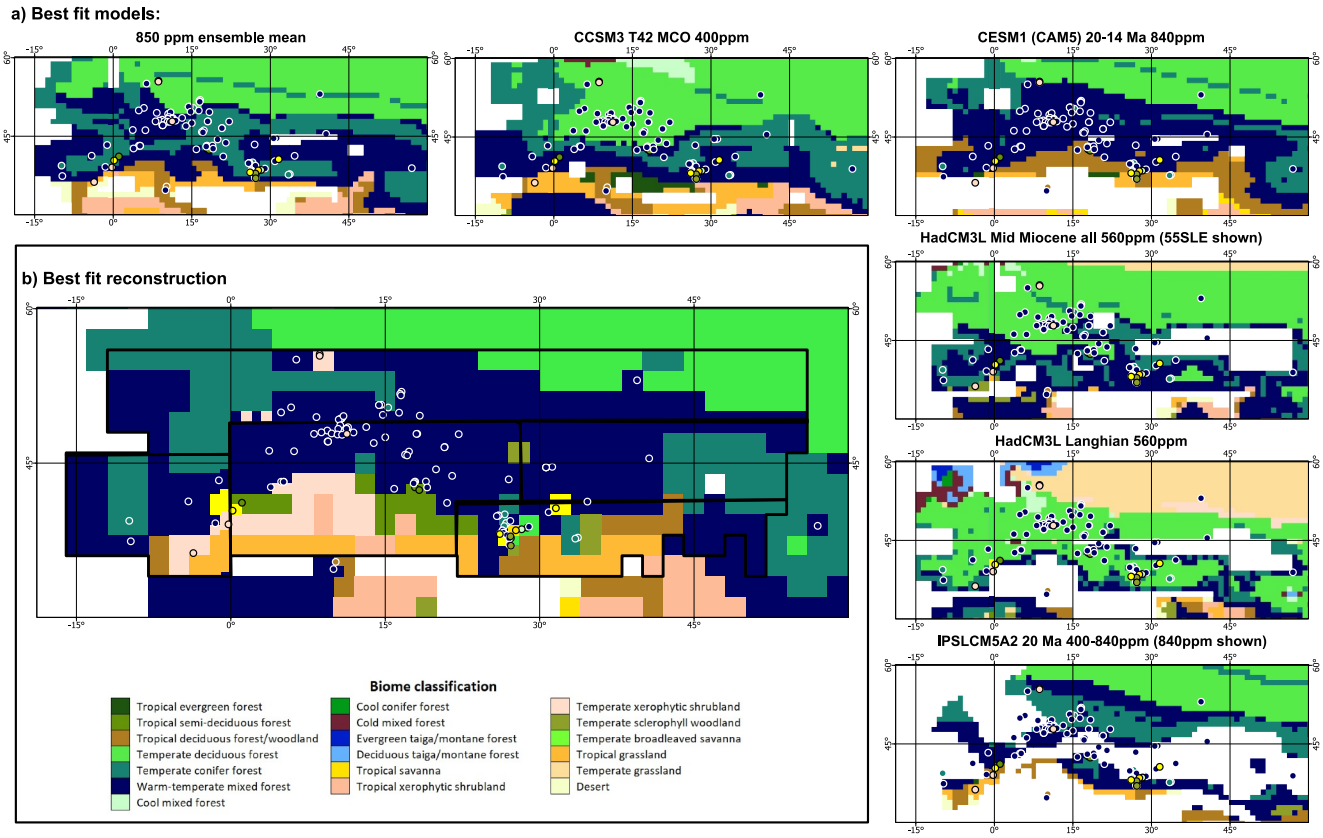

Figure 9. Vegetation reconstruction for Europe. (a) Best fit models from model-data comparison (refer to the text in Section 3.2.3 for details of the models used for each region); (b) Best fit reconstruction based on paleobotanical data and model blending (Europe subregions shown by thick black lines).

The macrofloral and palynofloral records suggest that the Anatolia region was predominantly characterized by warm temperate mixed forest during the MCO, transitioning to temperate coniferous forest in the northwest, as a result of the tectonic activity during the Miocene such as Graben Tectonism (Bozkurt & Sözbilir, 2004) and movement along the North Anatolian Fault (Şengör & Canitez, 1982). The macrofloral and palynofloral data from Anatolia and the Paratethys regions have similar reconstructed forest biomes despite the differences in the paleogeography and the influence of marine conditions (Doláková et al., 2021; Harzhauser et al., 2024), but the percentage abundance of specific taxa varies. This means that some cooler biomes (temperate deciduous, cool mixed and cold mixed forest) are assigned to the Anatolian region compared to the Paratethys regions and these cooler conditions are also simulated by the BIOME4 model driven by many of the MioMIP1 models. The simulations indicate the possibility of an expansion of arid conditions in the eastern Mediterranean region and southern Anatolia, which is supported by phytolith assemblages indicating woodland-savanna vegetation in central and western Anatolia (Stromberg & Smith, 2007). However, the reconstructed biomes based on other types of proxies in southernmost Anatolia do not support these conditions at scale and so the data-model blend represents a mosaic landscape in this region (Figure 9). The best-fitting models for Anatolia were "CCSM3 T42 MCO 400ppm," "CCSM3 T42 MMG 400 ppm," and the HadCM3L model under the 400–560 ppm CO_2 scenarios.

For Iberia, most of the BIOME4 simulations predict warm-temperate mixed forest and temperate conifer forest, often suggesting a southwest-northeast divide between them. In this region, the proxy data are generally consistent with the simulated biomes, comprising paleobotanical assemblages characterized by a mixture of evergreen thermophilous taxa and temperate deciduous taxa with consistent presence of conifers in part of the region (Barrón et al., 2010; Jiménez-Moreno et al., 2010). In southern Iberia and in the proto-Mediterranean region of the Central Paratethys, BIOME4 simulations also predict warmer and drier biomes such as temperate and tropical xerophytic shrubland, tropical deciduous forest and tropical semi-deciduous forest. The occurrence of such biomes is supported by fossil records from central and southern Iberia spanning the MCO or

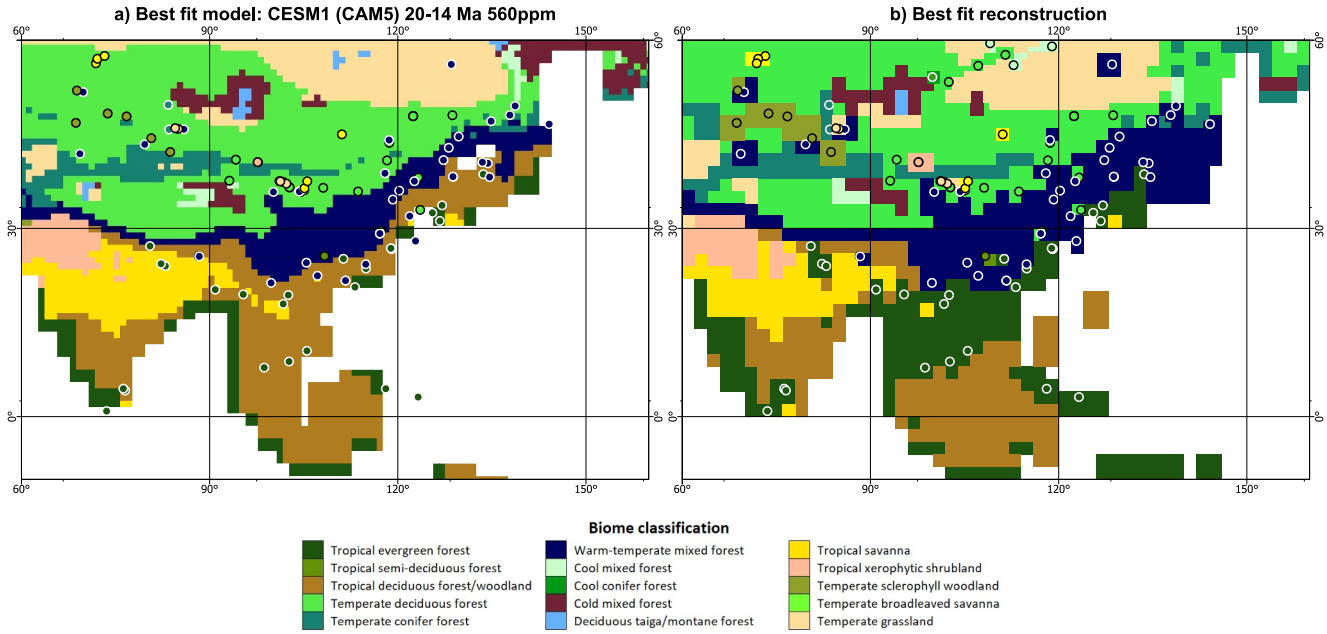

Figure 10. Vegetation reconstruction for East Asia. (a) Best fit model from model-data comparison; (b) Best fit reconstruction based on paleobotanical data and model blending.

chronologically close to this climatic event. These records indicate the presence of high abundances of herbaceous taxa and shrubs, reflecting a temperate xerophytic shrubland biome (Casas-Gallego et al., 2021; Jiménez-Moreno et al., 2010).

The combined European reconstruction assumed for the MCO in MioVeg1 can be found in Figure 9.

3.2.4. East Asia

With a relative wealth of biome proxy data, it was possible to compare large scale patterns in the biome reconstructions of East Asia (Figure 4). The first is a band of tropical evergreen forest along the south from India, across the Indochinese peninsula, and up the eastern coast of China. To the north and west of the band of tropical evergreen forest is a band of sites mostly reconstructed as warm temperate mixed forest. Temperate deciduous forest is common further inland, with a band of temperate sclerophyll woodland reconstructed to the north-west.

None of the models simulate the tropical evergreen forest band, but some reconstruct coastal areas with evergreen tropical forest, with most reconstructing tropical savanna and tropical deciduous forest/woodland, with varying amounts of xerophytic shrubland. This inability to simulate tropical evergreen forest could indicate the models are under-simulating moisture availability or a taphonomic bias to vegetation from wetter sites. Simulations that suggest tropical forest types are taken as a better match to the data than those simulating savanna or shrubland. The overall width and northerly extent of the warm temperate mixed forest band varied greatly with both model and CO_2 concentration. Many models reconstructed a broad continental interior of temperate deciduous forest, some with temperate xerophytic shrubland patches, although not exactly aligning with the data. None of the models resulted in the temperate sclerophyll woodland band in the northwest of the East Asia region. To best represent these trends, we selected "CESM1 (CAM5) 20–14 Ma 560 ppm" as the simulation to infill the paleobotanical data gaps in East Asia (Figure 10).

3.2.5. Africa

Biome data for the Miocene of Africa is scarce. One site in the north (~30°N) is reconstructed from the proxy data as temperate sclerophyll woodland. The remainder are reconstructed as tropical biomes. Tropical evergreen forest is simulated only in limited coastal regions in any of the models. Warm temperate mixed forest was most commonly simulated in southern Africa, where tropical semi-deciduous forest and tropical savanna are reconstructed, with "CESM1 (CAM5) 20–14 Ma 840 ppm" a notable exception. However, "CESM1 (CAM5) 20–

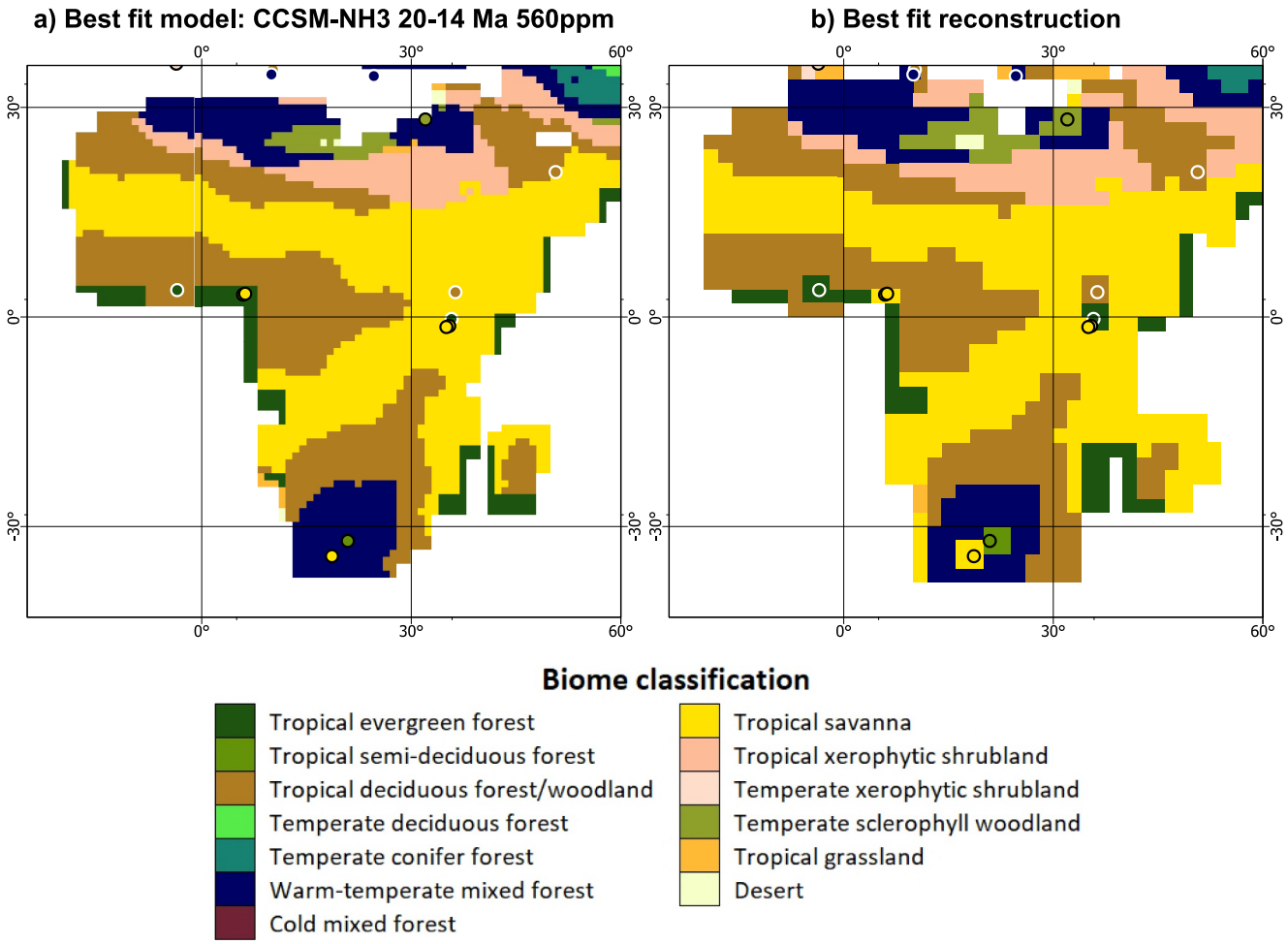

Figure 11. Vegetation reconstruction for Africa. (a) Best fit model from model-data comparison; (b) Best fit reconstruction based on paleobotanical data and model blending.

14 Ma 840 ppm" appears too dry in the north, producing tropical xerophytic shrubland where temperate sclerophyll woodland and tropical deciduous forest/woodland were reconstructed from paleobotanical data, and generally simulating little forest cover. The best match for the largely still warm and wet adapted African vegetation of the Middle Miocene (Jacobs et al., 2010) combined with relatively open C_3–C_4 savanna (Peppe et al., 2023), is "CCSM-NH3 20-14 Ma 560 ppm" (Figure 11).

3.2.6. South America

South America is the only region where all of the models were in strong disagreement with the paleobotanical data. All the BIOME4 simulations driven by the MioMIP1 models had a dry bias as compared to the data which led them to underestimate the presence of tropical rainforest, indicating a widespread tendency toward extensive areas of tropical xerophytic shrublands or tropical savannas. This data-model mismatch is perhaps linked in some models to the lack of Pebas Mega-Wetland System in most of the prior paleogeographic reconstructions. The Pebas Mega-Wetland System, which characterized Amazonia in the Miocene, reached its maximum extent during the MCO (Hoorn et al., 2022; Jaramillo et al., 2017) and could have provided the moisture source to support the tropical forested biomes documented in the paleobotanical data. The HadCM3L simulations of Farnsworth et al. (2019) are the only simulations to include a Pebas Mega-Wetland System, but in this model the addition of the large water body is insufficient to counteract the dry bias when compared to the paleobotanical data. The data-model mismatch could also be linked to incorrect paleotopography for the Andes: lower elevations leading to weaker reconstruction of the South American monsoon (Acosta et al., 2022). However, drying of tropical and subtropical regions of the Southern Hemisphere, including South America, was also a feature of the Pliocene Model

Intercomparison Project simulations, which ascribed the drying to dynamical effects from an interhemispheric temperature gradient (Pontes et al., 2020). It seems, therefore, that this dry bias in the MioMIP1 model ensemble may have multiple sources and it is thus beyond the scope of this study to remedy. Many of the climate inputs from the MioMIP1 models also result in floras associated with cooler-than-expected environments simulated in BIOME4 for the southernmost tip of South America being simulated in the BIOME4 model. This result is consistent with the insufficient polar amplification of temperature in climate models, discussed for the high northern latitudes, above.

The approach taken within MioVeg1 for South America is therefore as follows. We aimed to identify the model that had (a) the highest number of overlaps with the data reconstructions, (b) best represented the transition and position of tropical forests and savannas in northern South America, (c) best represented the transitions of biomes associated with the Andean highs and eastern slopes, (d) best represented the overall transition between biomes and representation of more local biomes, such as those expected for the Parana River area and the mangrove to dry forest transition in Ecuador-Peru, and (e) had the ability to depict biome transitions along southeast Brazil, Paraguay, Uruguay, and northern Argentina, alongside minimal overestimation of cooler high latitude biomes. Two models were deemed to best fit these criteria: "CESM1 (CAM5) 20–14 Ma 280 ppm" and "HadCM3L Langhian 560 ppm." That a climate model driven by such a low CO_2 concentration provided one of the best matches to the data is surprising, considering that available CO_2 reconstructions for the MCO suggest a mean of 500 ppm (CenCO2PIP et al., 2023). Given the high climate sensitivity of the CESM1 (CAM5) model (Meehl et al., 2013), we conducted sensitivity tests of the BIOME4 model using the "CESM1 (CAM5) 20–14 Ma 280 ppm" simulation climate data but increasing the CO_2 constraint within the BIOME4 model (Figure 12). We found that increasing the water use efficiency by forcing the biomes to be determined at higher CO_2 resulted in wetter biomes in the arid subtropics and a distribution here that looks more like the "HadCM3L Langhian 560 ppm" simulation. Due to the slightly closer match to the forest data in the north and south in the biome maps from "CESM1 (CAM5) 20–14 Ma 280 ppm" the climate simulation outputs from this model were chosen to fill in the data gaps for the region north of 20°S and south of 40°S. However, due to the reduction in the xerophytic shrubland resulting in the Amazonian basin, we used our sensitivity test version "CESM1 (CAM5) 20–14 Ma 280 ppm" combined with the BIOME4 model forced with a 400 ppm CO_2 concentration (Figure 12). For the region 20–40°S, where the proxy data suggest more sparse vegetation, we used the biome reconstruction of the "HadCM3L Langhian 560 ppm" simulation. We adjusted the simulated biomes with the greatest dry bias as compared to the paleobotanical data to the next wettest biome in the BIOME4 scheme—mostly impacting the region north of 20°S. For example, we convert the tropical deciduous biome to the tropical evergreen biome and the tropical savanna biome to the tropical semi-deciduous biome. In the absence of the updated paleogeography for MioMIP2, we cover the Pebas Mega-Wetland System region with vegetation in our reconstruction. Model-based reconstructions of Miocene vegetation in the Atacama Desert present conflicting evidence, showing both arid (e.g., Micheels et al., 2007) and mesic conditions (M. J. Pound et al., 2011). In contrast, paleo archives suggest periodic reductions of arid conditions in the Atacama Desert and lower western Andean slopes during the Middle Miocene (e.g., Oerter et al., 2016; Rech et al., 2019). This discrepancy may result from models integrating flora from both the narrow lowlands (0–1,500 m), broader western Andean slopes (1,500–3,500 m), and even the Altiplano (>3,500 m). We thus highlight that the desert biome represented in the best-fit models for the Central Andes (14°S to 29°S) reflects the arid to semi-arid conditions of both the Atacama Desert lowlands and the western slopes of the Central Andes, which were 1.0–1.5 km lower during the MCO (e.g., Kar et al., 2016; Martinez et al., 2020). The resultant MioVeg1 MCO blended data-model vegetation reconstruction for South America is given in Figure 13.

3.2.7. Australasia

Biomes with definitions based on Northern Hemisphere ecosystems are often difficult to apply to the Southern Hemisphere. This is apparent in Australasia, where conifer forests were frequently produced by the climate of the models, such as temperate needle-leaf forests and taiga. However, the most important biome-defining conifers in the Northern Hemisphere, the Pinaceae, are absent from the Southern Hemisphere. Instead, Southern Hemisphere conifers are in the Araucariaceae, Cupressaceae (specifically the Athrotaxidoideae and Callitroideae) and Podocarpaceae. These Southern Hemisphere conifers form different climate-vegetation associations than Northern Hemisphere conifers (e.g., Brodribb, 2011) and while they may constitute the dominant woody vegetation component (e.g., Gibson et al., 1991; Leathwick, 2001), Southern Hemisphere conifer-dominated

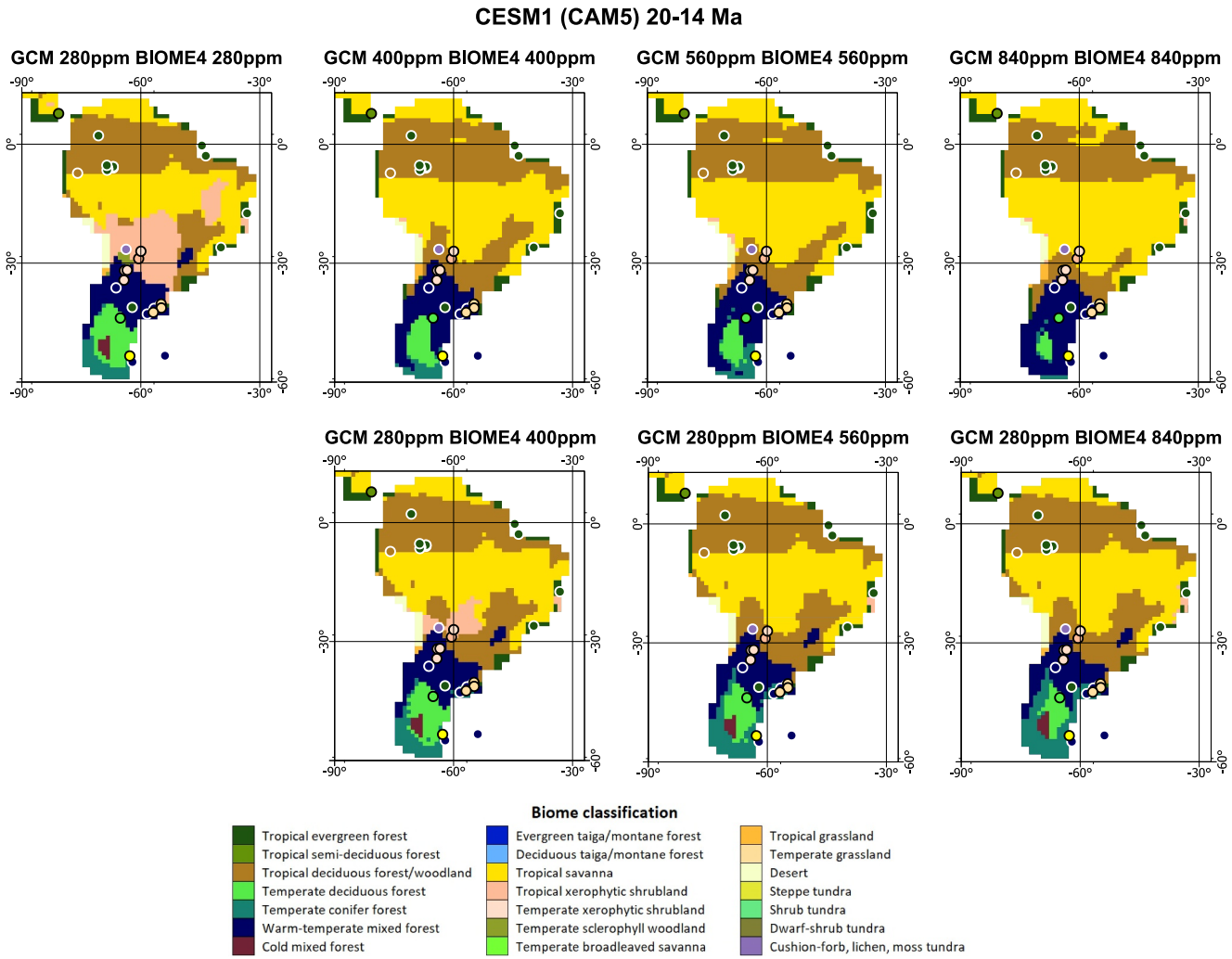

Figure 12. Vegetation reconstruction for South America CO_2 sensitivity to BIOME4 model CO_2 test.

ecosystems are functionally different from conifer-dominated ecosystems in the Northern Hemisphere. Additionally, in widespread temperate ecosystems in the Southern Hemisphere, in southern South America, New Zealand, southeastern Australia including Tasmania and the highlands of New Guinea and New Caledonia, the dominant woody vegetation components are in the angiosperm family Nothofagaceae (Veblen et al., 1996), which in many places also make up the treeline. Nothofagaceae likely also dominated temperate Miocene ecosystems in the Southern Hemisphere (Pujana et al., 2021; Reichgelt et al., 2022), including the last woody vegetation of Antarctica (Askin & Raine, 2000; Cantrill & Poole, 2012; Truswell & Macphail, 2009).

Model reconstructions that produced colder climate biomes than are known from the Middle Miocene of Australia were excluded. In the model chosen to best represent the known biomes from Australia and New Zealand, "HadCM3L Langhian 560 ppm," Australia has large, homogeneous areas of warm temperate mixed forest. In Australia, this is likely to have included sclerophyllous vegetation (Byrne & Murphy, 2020; Carpenter et al., 2011) for which the functional similarity to Northern Hemisphere warm temperate mixed forest is not clear.

In the northern regions of Australia, Papua New Guinea and Indonesia, more tropical rainforest, or even tropical semi-deciduous forest was expected than the tropical deciduous forest/woodland that dominated according to the models. This may indicate the models are under-simulating moisture availability, perhaps seasonally, or over-estimating tropical evapotranspiration. If this were the case, the overestimation of tropical evapotranspiration is either local (northern Australia) or the overestimated value is below the minimum level required for sustaining a tropical forest in South America (which models fail to reproduce). Alternatively, there may be taphonomic bias to

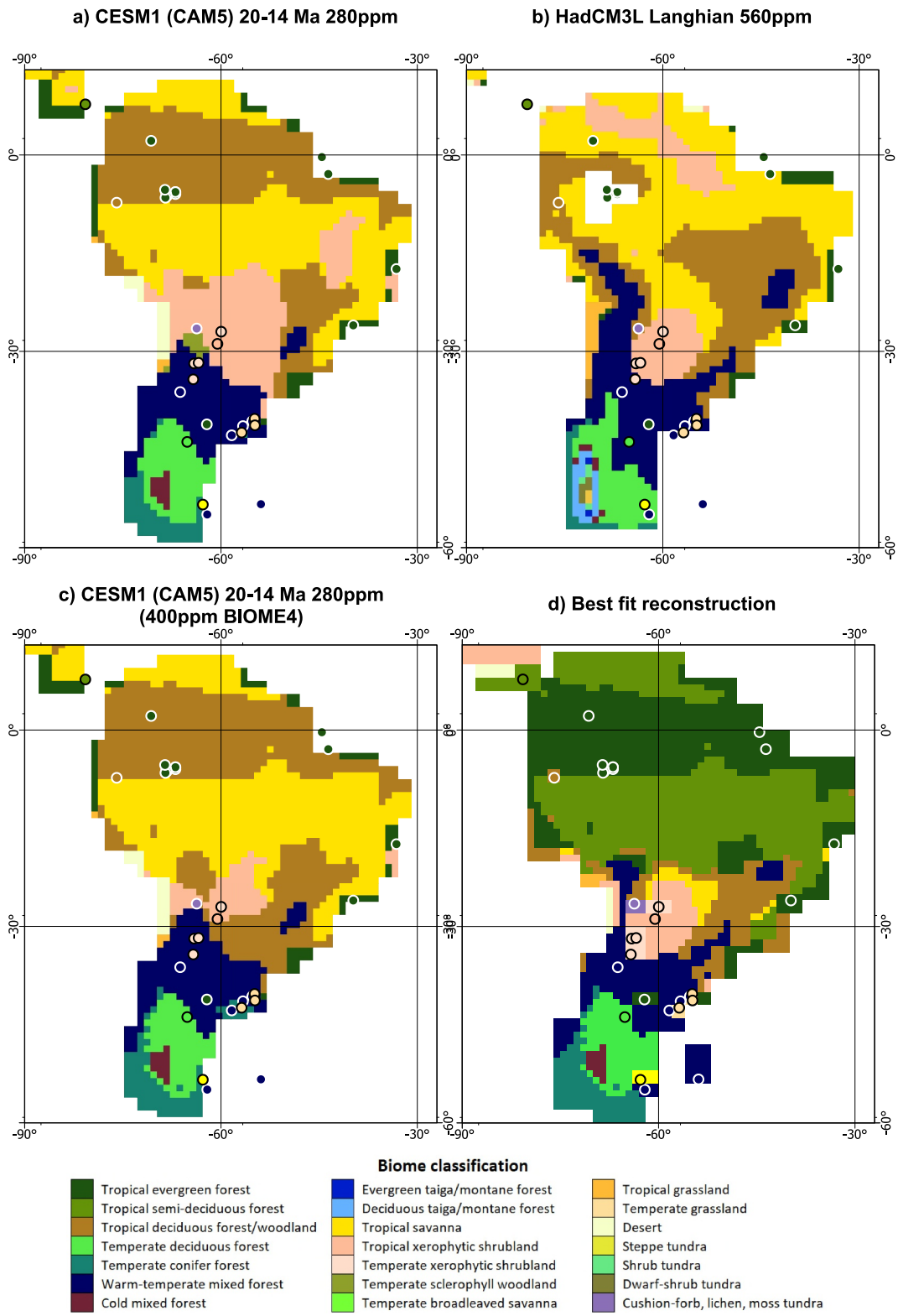

Figure 13. Vegetation reconstruction for South America. (a) Best fit model from model-data comparison for the region north of 20°S and south of 40°S; (b) Best fit model from model-data comparison for the region 20–40°S; (a) Best fit model from model-data comparison for the Amazonian basin; (d) Best fit reconstruction based on paleobotanical data and model blending.

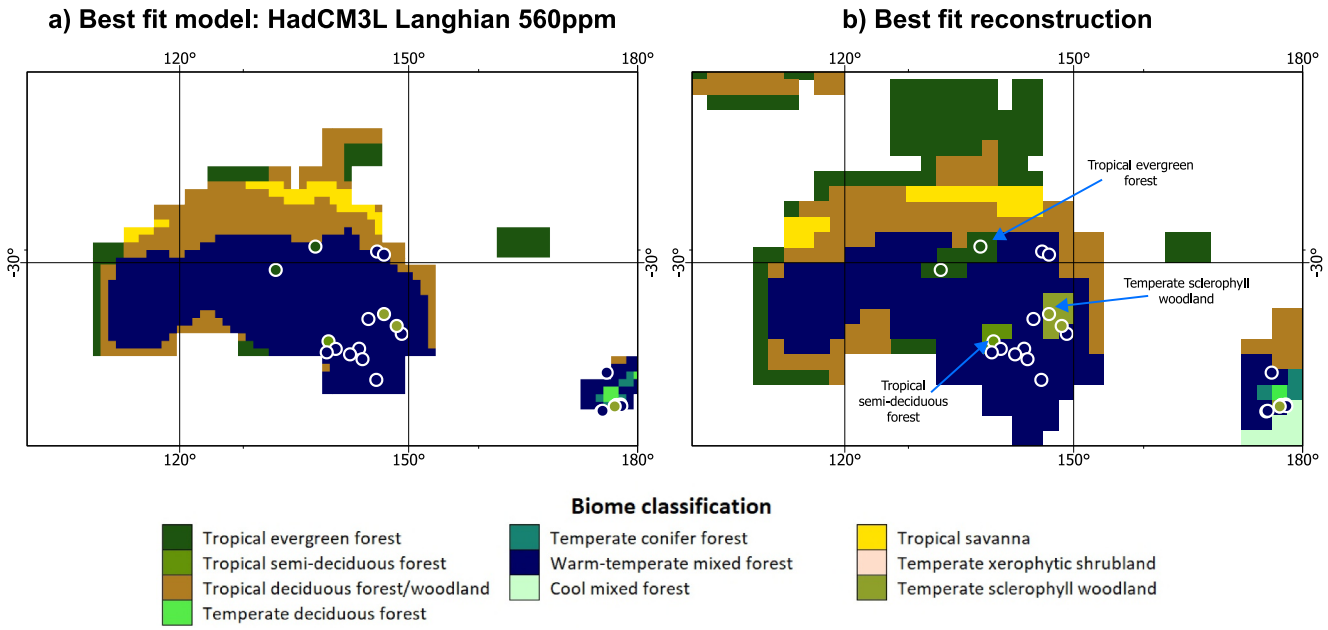

Figure 14. Vegetation reconstruction for Australasia. (a) Best fit model from model-data comparison; (b) Best fit reconstruction based on paleobotanical data and model blending.

vegetation around permanent bodies of water because sedimentary records from IODP Sites U1459 and U1464 suggest that northern Australia was arid during the Middle Miocene (Groeneveld et al., 2017).

"HadCM3L Langhian 560 ppm" simulates an appropriate variety of biomes in New Zealand, from tropical deciduous in the north to warm temperate mixed, temperate deciduous, and temperate conifer forest in the south. There is evidence for increased seasonality in the Middle Miocene of New Zealand that may have led to vegetation mosaics that included angiosperm- and conifer-dominated evergreen and deciduous forests (Pole, 2003; Reichgelt et al., 2015, 2019, 2022). The MioVeg1 MCO reconstruction that blends the "HadCM3L Langhian 560 ppm" with the paleobotanical data Australasia can be seen in Figure 14.

3.2.8. High Southern Latitudes

The MCO is likely the last time arboreal vegetation grew on Antarctica, and even during this period of peak warmth, it was likely limited to the coastal margins, the Antarctic Peninsula, and the South Orkney Islands (Mohr, 2001; Sangiorgi et al., 2018; Warny et al., 2009). In the Dry Valleys, evidence of tundra persists until just prior to 14 Ma (Lewis et al., 2008), coinciding with the Middle Miocene Climate Transition (Raitzsch et al., 2021) after which the last area to support tundra with woody plants was the Antarctic Peninsula (J. B. Anderson et al., 2011). Today, the Antarctic bioregions are restricted to the ice-free areas. These ice-free areas are divided into maritime and continental biomes. The maritime Antarctic Bioregion has a lush and diverse flora consisting largely of mosses and liverworts, as well as two species of herbaceous angiosperms (Poaceae and Carophyllaceae) native to the continent. This bioregion exists only in the northern half of the Antarctic Peninsula (Colesie et al., 2023; Terauds & Lee, 2016) and can be categorized as cushion-forb, lichen, moss tundra under the scheme used here. Conversely, the continental biome constitutes dry, ice-free areas, sometimes reaching deep into the continent. Lichen dominated here during the MCO (Terauds & Lee, 2016) and they are therefore considered "barren."

None of the BIOME4 models driven by the MioMIP1 climate models capture the patterns of vegetation of both the coastal regions and vegetation of the Dry Valleys; "CESM1 (CAM5) 20–14 Ma 840 ppm" was ultimately chosen as the best trade-off between the two. Notably, all the ice-free simulations from MioMIP1 result in too extensive forest, or even grassland biomes.

Again, fitting this Southern Hemisphere vegetation to a Northern Hemisphere based scheme may be problematic, as the main Antarctic woody vegetation constituents were in the Nothofagaceae (Askin & Raine, 2000; Griener

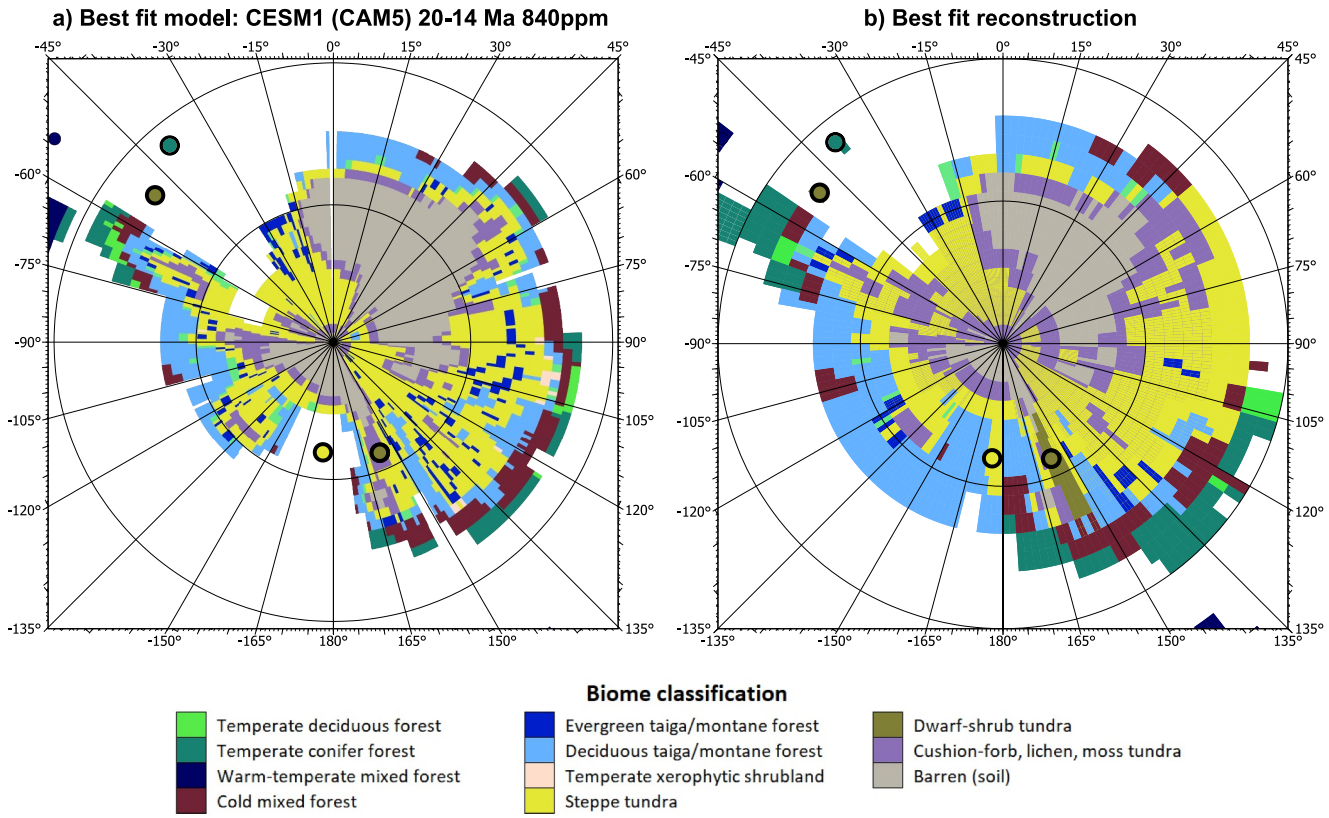

Figure 15. Vegetation reconstruction for the southern high latitudes. (a) Best fit model from model-data comparison; (b) Best fit reconstruction based on paleobotanical data and model blending.

et al., 2015). Furthermore, the extent and degree of transience of Middle Miocene Antarctic ice sheets to be prescribed in MioMIP2 is highly uncertain because of differences in the proxy signals and apparent high variability in atmospheric CO_2 concentrations and ice sheet extents (Bradshaw et al., 2021; Feakins et al., 2012; Gasson et al., 2016; Halberstadt et al., 2021; Levy et al., 2016; Passchier et al., 2011; Sangiorgi et al., 2018). Ice sheet and CO_2 variation may impact this region significantly, and the uncertainties are compounded by limited vegetation data from this region, and that Antarctica was isolated from source regions for plants to reinvade under more suitable climatic conditions. Notwithstanding these uncertainties, we have combined the sparse paleobotanical data for this region with the simulation (Figure 15).

4. Discussion

The final vegetation reconstruction for the Middle Miocene (Figure 2b) can be compared to the potential modern situation (Figure 2a), and the simplified megabiome comparisons (broader categories that group the biome classifications together) can be made based on Figure 16. Compared to today, notable differences include the absence of large desert regions in the Middle Miocene, indicative of wetter conditions followed by a drying trend that led to widespread aridification in the modern desert regions. The absence of large deserts in our reconstruction is consistent with the previous Middle Miocene vegetation reconstruction (Frigola et al., 2018). However, we note that the paleobotanical record is particularly scarce in regions covered by desert today, resulting in high uncertainty in our vegetation reconstruction in these areas and we cannot rule out the past presence of fragmented desert or other equally xerophytic biomes such as savannas or scrublands. Modeling studies suggest that aridification of the Sahara Desert post-dates the MCO and is linked to global cooling during the Middle Miocene Climate Transition or during the Late Miocene, and to the closure of Tethyan seaway (Z. Zhang et al., 2014; J. Zhang et al., 2023).

The Middle Miocene is also characterized by a marked increase in the amount of forest globally, with 69% of the Middle Miocene land area being classified as a forest biome (~155 million km^2) compared to 43% for the

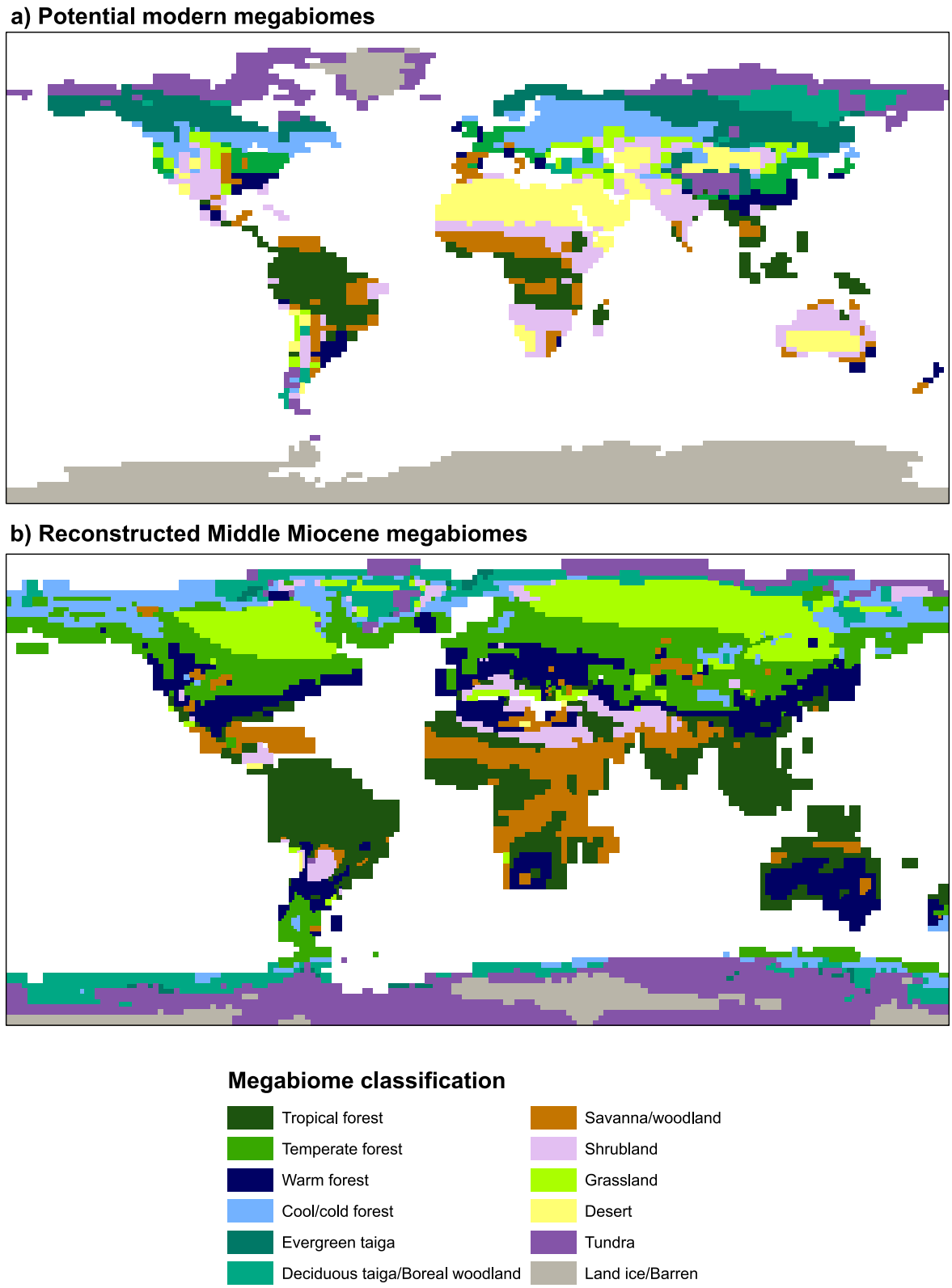

Figure 16. Global Middle Miocene vegetation megabiome reconstruction based on our new regional model-data synthesis approach blending simulations from different climate models and boundary conditions compared to potential modern vegetation. (a) Potential modern Megabiomes (cf. Salzmann et al., 2008); (b) Middle Miocene Megabiomes. Megabiomes classified according to Dallmeyer et al. (2017).

potential modern situation (~63 million km^2); ~75% of the Greenland Ice Sheet grid cells and ~25% of the AIS grid cells are covered in forest in our MCO vegetation reconstruction, representing ~12% of the new forested areas. The BIOME4 simulations driven by the individual MioMIP1 ensemble members have a total forested area that ranges from 46% to 71% of land area (note that ensemble members differ in their land-sea mask and that most contain more land than today; refer to Table S4 in Supporting Information S1). The results from the individual ensemble members show that the area of forest decreases as CO_2 concentration increases, consistent with projections for future climate change (IPCC, 2019). Most of the non-ice sheet area increase of forest in our reconstruction comes from tropical forest biomes in the Middle Miocene across the low latitudes and the occurrence of temperate forest biomes increases across the mid-latitudes. There is good evidence in the paleobotanical record for the occurrence of these vegetation types (Utescher, Erdei, et al., 2007; Utescher, Djordjevic-Milutinovic, et al., 2007; Figure 4), and temperate forest expansion, specifically, is consistent with recent regional reanalysis of the leaf macrofossil data (Reichgelt & West, 2025). Occurrences of taiga/montane forest biomes are reduced at the high northern latitudes as compared to the modern distribution, replaced by cool mixed forests, temperate deciduous forests, and extensive temperate grasslands. Whilst vegetation models other than BIOME4 suggest the presence of temperate grasslands in the high northern latitudes during the Middle Miocene (Henrot et al., 2017), there is no evidence for extensive temperate grasslands across the high northern latitudes during the Middle Miocene in our paleobotanical record and none was included in the most recent previous Middle Miocene vegetation reconstruction (Frigola et al., 2018). Fossil evidence for grassland biomes in the Northern Hemisphere during the MCO—as well as before and after—is currently limited to the mid-latitudes and is documented primarily through phytolith assemblages (e.g., Harris et al., 2017; Hyland et al., 2018; Kukla et al., 2022; Loughney et al., 2020; T. M. Smiley et al., 2018; C. A. E. Strömberg, 2005; Stromberg & Smith, 2007). In these regions, phytolith data lend support to the model-derived results. In contrast, phytolith assemblages have not been studied from high northern latitudes (Figure 4), which may explain the lack of evidence for grassland biomes given the potential underrepresentation of grasslands in the macroflora and palynoflora record, particularly in arid environments. Evidence from faunal hypsodonty and tooth wear, paleosol morphology, and stable carbon isotopes can complement paleobotanical information, allowing for recognition of grass-dominated vegetation in the past (C. A. E. Strömberg, 2011). Future iterations of the MioVeg1 data set should therefore incorporate more reconstructions from these complementary records. Further data collecting should target the high northern latitudes, alongside northern Europe, central North America, Africa, and Western Australia; these areas are particularly data-sparse in our data set due to erosive processes dominating these regions rather than Miocene tectonic activity that would favor sediment deposition (e.g., Isphording, 1970). In general, the tropics are under-sampled, in part due to extensive extant vegetation cover in these regions (but see C. A. Strömberg et al., 2024). More data availability for these regions would allow a similar approach to improving the reconstruction as was conducted for the South America region.

Major differences between our new vegetation reconstruction and the previous version from Frigola et al. (2018) include the presence of savanna and woodlands in Africa whereas Frigola et al. (2018) have tropical broadleaf evergreen forests. Our new reconstruction also contains more shrublands in central South America than Frigola et al. (2018) and we reconstruct an absence of shrublands in Australia whereas Frigola et al. (2018) have a western band of shrublands on the continent. The broad categories in Europe and East Asia are similar between our reconstructions but MioVeg1 contains much more detail than Frigola et al. (2018). Additionally, broadly in agreement between the two Middle Miocene reconstructions are the suggested locations of tundra in Antarctica. The biomes from the new vegetation reconstruction have been used to define an updated soils data set for the Middle Miocene using the assumptions in Tables 1 and 2 as shown in Figure 16.

Figure 17 highlights that the Middle Miocene warmth in the polar regions is best captured by the MioMIP1 models run with the highest CO_2 concentrations (840 ppm), whereas the vegetation reconstructions in the mid and low latitudes favor MioMIP1 models run with lower CO_2 concentrations (typically 560 ppm). These results confirm the general finding that climate models have difficulty reproducing the latitudinal temperature gradient of the Middle Miocene (Burls et al., 2021; Henrot et al., 2017), but outstanding data-model mismatches could also be due to data captured during time periods with paleogeographic configurations or CO_2 concentrations not simulated in the MioMIP1 ensemble. An approach that could be considered in future studies is to modify the sea-surface temperatures in the ESMs such that they are in line with proxy temperature reconstructions. By forcing the surface ocean to represent the warmer equator-to-pole temperature gradient of the Miocene, a recent study

Figure 17. Middle Miocene regional vegetation reconstruction by atmospheric CO_2 concentration.

has shown that the resulting vegetation simulated by the BIOME4 model is more consistent with the fossil evidence (Acosta, Burls, Pound, Bradshaw, McCoy, et al., 2024).

An especially anomalous region in the global reconstruction is South America. It was particularly difficult to select the best model simulation in this region, and the model simulation ultimately used to fill some of the data gaps was driven by the climatic conditions under the lowest CO_2 concentration: 280 ppm. The reasons for this anomaly are not clear, but perhaps related to paleogeographic uncertainties as most of the MioMIP1 models did not include the Pebas Mega-Wetland System in their boundary conditions and therefore an important water source could be missing from the simulations. However, accurate modeling of this large continental scale mega-wetland is complicated by poor constraints on the vegetation in its interior, which would affect the water balance, evapotranspiration, and soil formation, and, hence, how the system functions as a hydroclimatic control. This region should therefore be a priority target for future paleobotanical and paleogeographic data exploration. Some of the difficulty in classifying South American vegetation types might also relate to untested assumptions about the autecology of extinct plants. The non-analog nature of South American vegetation, containing a mix of taxa that currently inhabit primarily the Neotropics (e.g., palms) and high southern latitudes (e.g., *Nothofagus*) from the Eocene onward, has long been recognized by paleobotanists (e.g., Barreda & Palazzesi, 2007; Dunn et al., 2015; Hinojosa, 2005; Hinojosa et al., 2006). Future work should include broadening the vegetation classes in BIOME4 to incorporate the novel biome classifications identified from paleobotanical data for the Middle Miocene.

Our study is the first to bring together at scale the international paleobotanical community to work with the modeling community in the generation of vegetation boundary conditions for climate modeling purposes. In creating this new collaboration, we have been able to draw on the individual expertise of those researchers who have studied Miocene vegetation in each region at depth in a way that would be extremely difficult to do at the global scale by an individual researcher. Our new regional approach to biome classifications has allowed us to reconstruct the most consistent depiction of Middle Miocene vegetation to date. The fact that our approach has led to the blending of model simulations from different models forced by different paleogeographies and different CO_2 concentrations to fill in the gaps in the data highlights the problems of reconstructing past high latitude warmth in the models (e.g., Burls et al., 2021). Outstanding data-model mismatches could also be due to data captured during time periods with paleogeographic configurations or CO_2 concentrations not simulated in the MioMIP1 ensemble. Our approach, however, provides the opportunity to identify which models work best in different regions and contributes a baseline against which to test the impact of modifications made in MioMIP2. By constraining the biome reconstructions independently of CO_2, we also gain greater insights into the dominant controls shaping the ecosystems, such as the hydrological cycle. Determining the reasons why certain models seem to work better in certain regions is beyond the scope of our study, but MioMIP1 has shown that there is model dependence in hydrological cycle sensitivity to prescribed CO_2 (Acosta, Burls, Pound, Bradshaw, De Boer, et al., 2024) suggesting that key processes driving the hydrological cycle response to Miocene boundary

conditions needs to be resolved and/or that there are other boundary conditions or processes not yet considered that are critical to reproducing Miocene hydroclimate. The MioMIP2 effort using our new vegetation boundary conditions will therefore be a vital component leading to improvements in simulations of Miocene climate.

5. Conclusions

We have derived a new global vegetation reconstruction for the Middle Miocene that can be used in future modeling studies such as the forthcoming MioMIP2 project. Due to well documented mismatches between model simulations and the paleorecord, we have adopted a new methodology for the reconstruction where we have relaxed the requirement for a vegetation simulation, as driven by a single climate model output to be used to fill the gaps in the paleobotanical record. Expert judgment was used to determine which of the BIOME4 vegetation model simulations driven by the climate outputs of the MioMIP1 project at a variety of CO_2 concentrations, best fit the 431 paleobotanical datapoints on a regional basis. The results of the exercise confirm that the lower latitudinal temperature gradient of the Middle Miocene can only be met by using models run with higher CO_2 concentrations toward the poles.

Conflict of Interest

The authors declare no conflicts of interest relevant to this study.

Data Availability Statement

The new synthesis of biome and soil data generated from the paleobotanical record for the Middle Miocene can be found in the Zenodo repository Bradshaw et al. (2025), together with NetCDF files containing the updated Middle Miocene vegetation and soil boundary conditions (MCO_biome.nc, MCO_soil.nc, MCO_whc.nc, MCO_k-sat.nc).

Code Availability Statement: Code for the BIOME4 model is provided in the Github repository https://github.com/jedokaplan/BIOME4. We have archived our NetCDF files containing the BIOME4 model inputs and outputs generated from the MioMIP1 climate data (as listed in Table 4) and the BIOME4 namelist files in the Zenodo repository Bradshaw et al. (2025). All figures were made using ArcMap Pro 3.2.1.

Acknowledgments
C. D. Bradshaw acknowledges NERC Grant NE/I006281/1 and a NERC PhD studentship. D. Ochoa acknowledges funding from the European Union's Horizon 2020 research and innovation program under the Marie Skłodowska-Curie grant agreement No. 101034371. M. Pound acknowledges funding from the Royal Society (IECR2202086) and NERC (NE/V01501X/1). N. J. Burls acknowledge support from NSF AGS-1844380, and NSF EAR-2303417. Some of the palynological studies of Anatolia were supported by TUBITAK projects numbered 116Y140, 110Y065, 104Y297. T. Fletcher acknowledges funding from the European Union's Horizon 2020 research and innovation program under the Marie Skłodowska-Curie grant agreement No 101017833, and the support of the Ramsay Fellowship. M. Kováčová acknowledges funding from the Slovak Research and Development Agency under project number APVV-23-0227 and from the Scientific Agency of the Ministry of Education, Research, Development and Youth of the Slovak Republic under project number VEGA 1/0336/25. C.A.E. Strömberg acknowledges funding from the U.S. National Science Foundation (EAR-1924390). J.B. Novak acknowledges funding from the U.S. National Science Foundation (NNA 22–02918). For the purpose of open access, the author has applied a Creative Commons Attribution (CC BY) license to any Author Accepted Manuscript version arising from this submission.

References

Abusiarova, R. Y. (1966). Neogene flora of the mountain regions of middle Asia and southern Kazakhstan. In *The importance of palynologycal analysis for the stratigraphic and paleofloristic investigations* (p. 168). Nauca.

Acosta, R. P., Burls, N., Pound, M., Bradshaw, C., McCoy, J., Gibson, M., et al. (2024). Climate conundrum: A wet or dry European and Northern African climate during the middle Miocene. *Geophysical Research Letters*, *51*(21), e2024GL109499. https://doi.org/10.1029/2024gl109499

Acosta, R. P., Burls, N. J., Pound, M. J., Bradshaw, C. D., De Boer, A. M., Herold, N., et al. (2024). A model-data comparison of the hydrological response to Miocene warmth: Leveraging the MioMIP1 opportunistic multi-model ensemble. *Paleoceanography and Paleoclimatology*, *39*(1), e2023PA004726. https://doi.org/10.1029/2023pa004726

Acosta, R. P., Ladant, J. B., Zhu, J., & Poulsen, C. J. (2022). Evolution of the Atlantic Intertropical Convergence Zone, and the South American and African monsoons over the past 95-Myr and their impact on the tropical rainforests. *Paleoceanography and Paleoclimatology*, *37*(7), e2021PA004383. https://doi.org/10.1029/2021pa004383

Akgün, F., & Akyol, E. (1999). Palynostratigraphy of the coal-bearing Neogene deposits Graben in Büyük Menderes Western Anatolia. *Geobios*, *32*(3), 367–383. https://doi.org/10.1016/s0016-6995(99)80013-8

Akgün, F., Kayseri, M. S., & Akkiraz, M. S. (2007). Palaeoclimatic evolution and vegetational changes during the Late Oligocene–Miocene period in Western and Central Anatolia (Turkey). *Palaeogeography, Palaeoclimatology, Palaeoecology*, *253*(1–2), 56–90. https://doi.org/10.1016/j.palaeo.2007.03.034

Akgün, F., Kayseri-Özer, M. S., Tekin, E., Varol, B., Şen, Ş., Herece, E., et al. (2021). Late Eocene to Late Miocene palaeoecological and palaeoenvironmental dynamics of the Ereğli-Ulukışla Basin (Southern Central Anatolia). *Geological Journal*, *56*(2), 673–703. https://doi.org/10.1002/gj.4021

Akkiraz, M. S., Akgün, F., Utescher, T., Vılde, V., Bruch, A., Mosbrugger, V., & Durak, S. D. Ü. (2015). Erken-Orta Miyosen Yaşlı Kömürlü Tortulların Paleoekolojisi: Erken-orta Miyosen Yaşlı Kömürlü Tortulların Paleoekolojisi. *Turkiye Jeoloji Bulteni*, *58*(3), 39–60. Retrieved from https://dergipark.org.tr/tr/pub/tjb/issue/28092/298483

Akkiraz, M. S., Utescher, T., Bruch, A. A., Wilde, V., Durak, S. D., & Mosbrugger, V. (2020). Early Miocene palaeoflora and palaeoecology of the Soma Basin, Western Turkey. *Palaeobiodiversity and Palaeoenvironments*, *100*(4), 921–938. https://doi.org/10.1007/s12549-020-00434-3

Aleksandrova, G. N. (2016). Geological development of the Chauna Depression (Northeastern Russia) in the Paleogene and Neogene 2. Neogene. *Bulletin of Moscow Society of Naturalists. Geological Series*, *91*(6), 11–35.

Allen, R. G., Pereira, L. S., Raes, D., & Smith, M. (1998). *Crop evapotranspiration—Guidelines for computing crop water requirements-FAO irrigation and drainage paper 56* (Vol. 300, p. D05109). Fao.

Alpers, C. N., & Brimhall, G. H. (1988). Middle Miocene climatic change in the Atacama Desert, northern Chile: Evidence from supergene mineralization at La Escondida. *Bulletin of the Geological Society of America*, *100*(10), 1640–1656. https://doi.org/10.1130/0016-7606(1988)100<1640:mmccit>2.3.co;2

Anderson, J. B., Warny, S., Askin, R. A., Wellner, J. S., Bohaty, S. M., Kirshner, A. E., et al. (2011). Progressive Cenozoic cooling and the demise of Antarctica's last refugium. *Proceedings of the National Academy of Sciences*, *108*(28), 11356–11360. https://doi.org/10.1073/pnas.1014885108

Anderson, R. C. (2006). Evolution and origin of the Central Grassland of North America: Climate, fire, and mammalian grazers. *Journal of the Torrey Botanical Society*, *133*(4), 626–647. https://doi.org/10.3159/1095-5674(2006)133[626:eaootc]2.0.co;2

Antal, J. S., & Prasad, M. (1997). Angiospermous fossil leaves from Siwalik sediments (Middle Miocene) of Darjeeling District, West Bengal. *Palaeobotanist*, *46*(3), 95–104. https://doi.org/10.54991/jop.1997.1353

Antunes, M. T., & Pais, J. (1984). Climate during Miocene in Portugal and its evolution. *Paleobiologie Continentale*, *14*(2), 75–89.

Anzótegui, L. M., & Herbst, R. (2004). Megaflora (hojas y frutos) de la Formación San José (Mioceno medio) en río Seco, departamento Santa María, provincia de Catamarca, Argentina. *Ameghiniana*, *41*(3), 423–436.

Archer, M., Hand, S. J., & Godthelp, H. (1991). *Riversleigh.* Reed Books.

Arya, L. M., Dierolf, T. S., Rusman, B., Sofyan, A., & Widjaja-Adhi, I. P. G. (1992). Soil structure effects on hydrologic processes and crop water availability in Ultisols and Oxisols of Sitiung, Indonesia. In *Soil Management CRSP Bulletin 92-03*.

Askin, R. A., & Raine, J. I. (2000). Oligocene and early Miocene terrestrial palynology of the Cape Roberts drillhole CRP-2/2A, Victoria Land Basin, Antarctica. *Terra Antarctica*, *7*, 493–501.

Aswal, H. S. (1993). Palynostratigraphy of Kharkhublen Anticline (central part) Central and Southern District, Manipur, India. In *Proceedings of the 2nd seminar on petroliferous basins of India* (Vol. 1, pp. 477–491).

Axelrod, D. I. (1939). *A Miocene flora from the western border of the Mohave Desert* (Vol. 516, pp. 1–129). Carnergie Institution. Retrieved from https://books.google.com.pa/books/about/A_Miocene_Flora_from_the_Western_Border.html?id=sc1OAQAAIAAJ

Axelrod, D. I. (1964). The Miocene Trapper Creek flora of southern Idaho. Retrieved from https://books.google.com.pa/books/about/The_Miocene_Trapper_Creek_Flora_of_South.html?id=leVQAQAAIAAJ

Axelrod, D. I. (1985). *Miocene floras from the Middlegate Basin, west-central Nevada* (Vol. 129). University of California Press. Retrieved from https://books.google.com.pa/books/about/Miocene_Floras_from_the_Middlegate_Basin.html?id=Nbjx9yd8UY8C

Axelrod, D. I. (1991). The Early Miocene buffalo canyon flora of western Nevada. Retrieved from https://ifpni.org/publication.htm?id=2D20A3AD-9866-E149-586B-6E220CEE8483

Axelrod, D. I. (1992a). Miocene floristic change at 15 Ma, Nevada to Washington, U.S.A. *Palaeobotanist*, *41*, 234–239. https://doi.org/10.54991/jop.1992.1127

Axelrod, D. I. (1992b). *The Middle Miocene Pyramid flora of Western Nevada: Berkeley* (Vol. 137, pp. 1–50). University of California Press, Bulletin of the Department of Geological Sciences.

Axelrod, D. I. (1995). *The Miocene purple Mountain flora of Western Nevada* (Vol. 139, pp. 1–63). University of California Publications: Geological Sciences.

Axelrod, D. I. (2000). *A Miocene (10–12 Ma) evergreen Laurel-Oak forest from Carmel Valley, California* (Vol. 145, pp. 1–34). University of California Publications: Geological Sciences.

Axelrod, D. I., & Schorn, H. E. (1994). The 15 Ma floristic crisis at Gilliam Spring, Washoe County, Northwestern Nevada. *PaleoBios*, *16*(2), 1–10.

Baranova, Y. P., Kul'kova, I. A., Nikitin, V. P., & Shvareva, N. Y. (1970). New data on the Miocene of Mount Mamontovaya (Aldan). *Doklady Akademii Nauk SSSR*, *193*, 77–79.

Barbolini, N., Woutersen, A., Dupont-Nivet, G., Silvestro, D., Tardif, D., Coster, P. M. C., et al. (2020). Cenozoic evolution of the steppe-desert biome in Central Asia. *Science Advances*, *6*(41), eabb8227. https://doi.org/10.1126/sciadv.abb8227

Barreda, V., Guler, V., & Palazzesi, L. (2008). Late Miocene continental and marine palynological assemblages from Patagonia. *Developments in Quaternary Science*, *11*, 343–350. https://doi.org/10.1016/s1571-0866(07)10016-6

Barreda, V., Limarino, C., Fauqué, L., Tripaldi, A., & Net, L. (2003). Primer registro palinológico del miembro inferior de la Formación Cerro Morado (Mioceno), Precordillera de La Rioja. *Ameghiniana*, *40*(1), 81–87.

Barreda, V., & Palazzesi, L. (2007). Patagonian vegetation turnovers during the Paleogene-early Neogene: Origin of arid-adapted floras. *The Botanical Review*, *73*(1), 31–50. https://doi.org/10.1663/0006-8101(2007)73[31:pvtdtp]2.0.co;2

Barrón, E., Lassaletta, L., & Alcalde-Olivares, C. (2006). Changes in the Early Miocene palynoflora and vegetation in the east of the Rubielos de Mora basin (SE Iberian Ranges, Spain). *Neues Jahrbuch Fur Geologie Und Palaontologie-Abhandlungen*, *242*(2–3), 171–204. https://doi.org/10.1127/njgpa/242/2006/171

Barrón, E., Rivas-Carballo, R., Postigo-Mijarra, J. M., Alcalde-Olivares, C., Vieira, M., Castro, L., et al. (2010). The Cenozoic vegetation of the Iberian Peninsula: A synthesis. *Review of Palaeobotany and Palynology*, *162*(3), 382–402. https://doi.org/10.1016/j.revpalbo.2009.11.007

Bartley, R. H., Bartley, S. E., Springer, D. J., & Erwin, D. M. (2010). New observations on the Middle Fork Eel River coal-bearing beds, Mendocino County, California, USA. *International Journal of Coal Geology*, *83*(2–3), 204–228. https://doi.org/10.1016/j.coal.2010.01.001

Beeston, J. W. (1994). Tertiary palynology in the Mount Coolon and Riverside areas. *Queensland Geology*, *6*, 127–179.

Behling, H., & Costa, M. L. D. (2004). Mineralogy, geochemistry, and palynology of modern and late Tertiary mangrove deposits in the Barreiras Formation of Mosqueiro Island, northeastern para' state, eastern Amazonia. *Journal of South American Earth Sciences*, *17*(4), 285–295. https://doi.org/10.1016/j.jsames.2004.08.002

Behrensmeyer, A. K., Deino, A. L., Hill, A., Kingston, J. D., & Saunders, J. J. (2002). Geology and geochronology of the middle Miocene Kipsaramon site complex, Muruyur beds, Tugen Hills, Kenya. *Journal of Human Evolution*, *42*(1–2), 11–38. https://doi.org/10.1006/jhev.2001.0519

Bekker-Migdisova, E. E. (1967). Tertiary Homoptera of Stavropol and a method of reconstruction of continental palaeobiocoenoses. *Palaeontology*, *10*, 542–553.

Belova, V. A. (1985). *Vegetation and Climate of the Late Cenozoic of the south of Eastern Siberia* (p. 160). Nauka. (in Russian) [Belova V.A. Rastitel'nost' i klimat pozdnego kainozoya yuga Vostochnoi Sibiri. Novosibirsk: Nauka, 1985. 160 s.]

Berry, E. W. (1909). A Miocene flora from the Virginia coastal plain. *The Journal of Geology*, *17*(1), 19–30. https://doi.org/10.1086/621583

Berry, E. W. (1919). *Miocene fossil plants from northern Peru*. Proceedings of the United States National Museum. Retrieved from https://repository.si.edu/bitstream/handle/10088/14744/USNMP-55_2270_1919.pdf

Bialkowski, A., Châteauneuf, J. J., Cojan, I., & Bauer, H. (2006). Integrated stratigraphy and paleoenvironmental reconstruction of the Miocene series of the Châteauredon Dome, SE France. *Eclogae Geologicae Helvetiae*, *99*, 1–15.

Blencowe, J. P. B., Moore, S. D., Young, G. J., Shearer, R. C., Hagerstrom, R., Conley, W. M., & Potter, J. S. (1960). Soil Department of Agriculture Bulletin (Vol. *462*).

Boehme, M., Bruch, A. A., & Selmeier, A. (2007). The reconstruction of early and Middle Miocene climate and vegetation in Southern Germany as determined from the fossil wood flora. *Palaeogeography, Palaeoclimatology, Palaeoecology*, *253*(1–2), 91–114. https://doi.org/10.1016/j.palaeo.2007.03.035

Bonan, G. B., Lucier, O., Coen, D. R., Foster, A. C., Shuman, J. K., Laguë, M. M., et al. (2024). Reimagining Earth in the Earth system. *Journal of Advances in Modeling Earth Systems*, *16*(8), e2023MS004017. https://doi.org/10.1029/2023ms004017

Bouwman, A. F. (1990). Global distribution of the major soils and land cover types. In A. F. Bouwman (Ed.) *Soils and the greenhouse effect* (pp. 33–59). John Wiley & Sons Ltd.

Boyce, C. K., & Lee, J. E. (2017). Plant evolution and climate over geological timescales. *Annual Review of Earth and Planetary Sciences*, *45*(1), 61–87. https://doi.org/10.1146/annurev-earth-063016-015629

Bozcu, M., Akgün, F., Gürdal, G., Bozcu, A., Yeşilyurt, S. K., Karaca, Ö., & Akkiraz, M. S. (2015). Evolution of Çan-Etili (Çanakkale-NW Turkey) lignite basin: Sedimentology, petrology, palynology and lignite characterization. *International Journal of Sediment Research*, *30*(3), 190–207.

Bozkurt, E., & Sözbilir, H. (2004). Tectonic evolution of the Gediz Graben: Field evidence for an episodic, two-stage extension in western Turkey. *Geological Magazine*, *141*(1), 63–79. https://doi.org/10.1017/s0016756803008379

Braconnot, P., Joussaume, S., Marti, O., & De Noblet, N. (1999). Synergistic feedbacks from ocean and vegetation on the African monsoon response to mid-Holocene insolation. *Geophysical Research Letters*, *26*(16), 2481–2484. https://doi.org/10.1029/1999gl006047

Bradshaw, C. D., Fletcher, T., Reichgelt, T., Akgün, F., Cantrill, D. J., Casas-Gallego, M., et al. (2025). Supplementary Data for MioVeg1: A global Middle Miocene vegetation reconstruction for climate modelling [Dataset]. *Zenodo*. https://doi.org/10.5281/zenodo.17166072

Bradshaw, C. D., Langebroek, P. M., Lear, C. H., Lunt, D. J., Coxall, H. K., Sosdian, S. M., & de Boer, A. M. (2021). Hydrological impact of Middle Miocene Antarctic ice-free areas coupled to deep ocean temperatures. *Nature Geoscience*, *14*(6), 429–436. https://doi.org/10.1038/s41561-021-00745-w

Bradshaw, C. D., Lunt, D. J., Flecker, R., & Davies-Barnard, T. (2015). Disentangling the roles of late Miocene palaeogeography and vegetation—Implications for climate sensitivity. *Palaeogeography, Palaeoclimatology, Palaeoecology*, *417*, 17–34. https://doi.org/10.1016/j.palaeo.2014.10.003

Bratseva, G. M. (1980). Neogene palynoflora of Iceland. In *Proceedings of the fourth international palynological conference, 1976* (pp. 744–746). Birbal Sahni Institute of Palaeobotany.

Bres, J., Sepulchre, P., Viovy, N., & Vuichard, N. (2021). The Cretaceous physiological adaptation of angiosperms to a declining pCO_2: A modeling approach emulating paleo-traits. *Biogeosciences*, *18*(20), 5729–5750. https://doi.org/10.5194/bg-18-5729-2021

Brodribb, T. J. (2011). A functional analysis of Podocarp ecology. In B. L. Turner & L. A. CernUSAk (Eds.), *Smithsonian contributions to botany* (pp. 165–173). Smithsonian Institution Scholarly Press.

Brovkin, V. (2002). Climate-vegetation interaction. *Journal de Physique IV*, *12*(10), 57–72. https://doi.org/10.1051/jp4:20020452

Bruch, A. A., Utescher, T., Olivares, C. A., Doláková, N., Ivanov, D., & Mosbrugger, V. (2004). Middle and Late Miocene spatial temperature patterns and gradients in Europe-preliminary results based on palaeobotanical climate reconstructions. *Courier Forschungsinstitut Senckenberg*, 15–28.

Brunel-Saldias, N., MartinezI, S. O., Ovalle, C., & Acevedo, E. (2016). Structural characterization of a compacted alfisol under different tillage systems. *Journal of Soil Science and Plant Nutrition*, *16*, 689–701.

Burls, N. J., Bradshaw, C. D., De Boer, A. M., Herold, N., Huber, M., Pound, M., et al. (2021). Simulating miocene warmth: Insights from an opportunistic multi-model ensemble (MioMIP1). *Paleoceanography and Paleoclimatology*, *36*(5), e2020PA004054. https://doi.org/10.1029/2020pa004054

Byrne, M., & Murphy, D. J. (2020). The origins and evolutionary history of xerophytic vegetation in Australia. *Australian Journal of Botany*, *68*(3), 195–207. https://doi.org/10.1071/bt20022

Caccavari, M., & Barreda, V. (2000). A new calymmate mimosoid polyad from the Miocene of Argentina. *Review of Palaeobotany and Palynology*, *109*(3–4), 197–203. https://doi.org/10.1016/s0034-6667(99)00051-2

Cantrill, D. J., & Poole, I. (2012). *The vegetation of Antarctica through geological time* (pp. 1–480). Cambridge University Press.

Carpenter, R. J., Goodwin, M. P., Hill, R. S., & Kanold, K. (2011). Silcrete plant fossils from Lightning Ridge, New South Wales: New evidence for climate change and monsoon elements in the Australian Cenozoic. *Australian Journal of Botany*, *59*(5), 399–425. https://doi.org/10.1071/bt11037

Casas-Gallego, M., Postigo-Mijarra, J. M., Rivas-Carballo, M. R., Valle-Hernández, M. F., Morín-de Pablos, J., & Barrón, E. (2021). Early evidence of continental aridity and open-habitat grasslands in Europe as revealed by the Middle Miocene microflora of the Madrid Basin. *Palaeogeography, Palaeoclimatology, Palaeoecology*, *581*(1), 110603. https://doi.org/10.1016/j.palaeo.2021.110603

Caviglia, N., & Zamaloa, M. D. C. (2014). Flora angiospérmica de Pico Quemado, Formación Ñirihuau (Oligoceno Tardío), Provincia de Río Negro, Argentina. *Ameghiniana*, *51*(3), 209–225. https://doi.org/10.5710/AMGH.24.02.2014.800

Cenozoic CO_2 Proxy Integration Project (CenCO2PIP) Consortium, Hönisch, B., Royer, D. L., Breecker, D. O., Polissar, P. J., Bowen, G. J., et al. (2023). Toward a Cenozoic history of atmospheric CO_2. *Science*, *382*(6675), eadi5177. https://doi.org/10.1126/science.adi5177

Chaney, R. W. (1925). The Mascall flora: Its distribution and climatic relation. In *Contributions to paleontology from the Carnegie Institution of Washington* (Vol. 349, pp. 23–48).

Chaney, R. W. (1959). *Miocene floras of the Columbia Plateau* (Vol. 617, pp. 1–229). Carnegie Institution Washington, Publication. Retrieved from https://books.google.com.pa/books/about/Miocene_Floras_of_the_Columbia_Plateau.html?id=-fkA96PHbqkC

Chen, C. F. (2009). *Cenozoic pollen records and palaoenvironmental evolution in Xining Basin, Northeastern Tibetan Plateau. MSc dissertation* (pp. 1–1344). China Lanzhou University. (in Chinese with English abstract).

Chung, C.-H., & Koh, Y.-K. (2005). Palynostratigraphic and palaeoclimatic investigations on the Miocene deposits in the Pohang area, South Korea. *Review of Palaeobotany and Palynology*, *135*(1–2), 1–11. https://doi.org/10.1016/j.revpalbo.2005.02.002

Coetzee, J. A., & Rogers, J. (1982). Palynological and lithological evidence for the Miocene palaeoenvironment in the Saldanha region (South Africa). *Palaeogeography, Palaeoclimatology, Palaeoecology*, *39*(1–2), 71–85. https://doi.org/10.1016/0031-0182(82)90073-6

Colesie, C., Walshaw, C. V., Sancho, L. G., Davey, M. P., & Gray, A. (2023). Antarctica's vegetation in a changing climate. *Wiley Interdisciplinary Reviews: Climate Change*, *14*(1), e810. https://doi.org/10.1002/wcc.810

Cox, P. M., Betts, R. A., Bunton, C. B., Essery, R. L. H., Rowntree, P. R., & Smith, J. (1999). The impact of new land surface physics on the GCM simulation of climate and climate sensitivity. *Climate Dynamics*, *15*(3), 183–203. https://doi.org/10.1007/s003820050276

Cramwinckel, M. J., Burls, N. J., Fahad, A. A., Knapp, S., West, C. K., Reichgelt, T., et al. (2023). Global and zonal-mean hydrological response to early Eocene warmth. *Paleoceanography and Paleoclimatology*, *38*(6), e2022PA004542. https://doi.org/10.1029/2022pa004542

Crowley, T. J., & Baum, S. K. (1997). Effect of vegetation on an ice-age climate model simulation. *Journal of Geophysical Research*, *102*(D14), 16463–16480. https://doi.org/10.1029/97jd00536

Crucifix, M., Betts, R. A., & Cox, P. M. (2005). Vegetation and climate variability: A GCM modelling study. *Climate Dynamics*, *24*(5), 457–467. https://doi.org/10.1007/s00382-004-0504-z

Dallmeyer, A., Claussen, M., Ni, J., Cao, X., Wang, Y., Fischer, N., et al. (2017). Biome changes in Asia since the mid-Holocene—An analysis of different transient Earth system model simulations. *Climate of the Past*, *13*(2), 107–134. https://doi.org/10.5194/cp-13-107-2017

Daneshian, J., Sarkar, S., & Sharma, V. (2007). Miocene palynoflora from Inglis Island, Andaman Sea and its palaeoecological implication. *Geological Society of India*, *70*(1), 147–157.

Das Gupta, S., Mohanty, B. P., & Köhne, J. M. (2006). Soil hydraulic conductivities and their spatial and temporal variations in a vertisol. *Science Society of America Journal*, *70*, 1872–1881.

de Nooijer, W., Zhang, Q., Li, Q., Zhang, Q., Li, X., Zhang, Z., et al. (2020). Evaluation of Arctic warming in mid-Pliocene climate simulations. *Climate of the Past*, *16*(6), 2325–2341. https://doi.org/10.5194/cp-16-2325-2020

De Wit, M. C. J., & Bamford, M. K. (1993). Fossil wood from the Brandvlei Area, Bushmanland as an indication of palaeoenvironmental changes during the Cainozoic. *Palaeontologia Africana*, *30*, 81–89.

Doláková, N., Kováčová, M., & Utescher, T. (2021). Vegetation and climate changes during the Miocene climatic optimum and Miocene climatic transition in the northwestern part of Central Paratethys. *Geological Journal*, *56*(2), 729–743. https://doi.org/10.1002/gj.4056

Dugas, D. P., & Retallack, G. J. (1993). Middle Miocene fossil grasses from fort Ternan, Kenya. *Journal of Paleontology*, *67*(1), 113–128. https://doi.org/10.1017/s0022336000021223

Dunn, R. E., Strömberg, C. A. E., Madden, R. H., Kohn, M. J., & Carlini, A. A. (2015). Linked canopy, climate and faunal evolution in the Cenozoic of Patagonia. *Science*, *347*(6219), 258–261. https://doi.org/10.1126/science.1260947

Durska, E. (2008). A 90 m-thick coal seam in the Lubstów lignite deposit (Central Poland): Palynological analysis and sedimentary environment. *Geological Quarterly*, *52*(3), 281.

Dutton, J. F., & Barron, E. J. (1997). Miocene to present vegetation changes: A possible piece of the Cenozoic cooling puzzle. *Geology*, *25*(1), 39–41. https://doi.org/10.1130/0091-7613(1997)025<0039:mtpvca>2.3.co;2

Dzanh, T. (1990). Neogene events in Vietnam from the point of view of flora and Mollusca. In R. Tsuchi (Ed.), *Pacific Neogene events* (pp. 129–135). University of Tokyo Press.

Eberlein, M. (2015). *Bestimmungs-und Verbreitungsatlas der Tertiärflora Sachsens—Angiospermenblätter und Ginkgo [dissertation]* (p. 144). Technische Universität Dresden, Fakultät Umweltwissenschaften. urn:nbn:de:bsz:14-qucosa-171947.

El Beialy, S. Y., Mahmoud, M. S., & Ali, A. S. (2005). Insights on the age, climate and depositional environments of the Rudeis and Kareem Formations, GS-78-1 well, Gulf of Suez, Egypt: A palynological approach. *Revista Espanola de Micropaleontologia*, *37*(2), 273–289.

Elias, M. K. (1942). *Tertiary prairie grasses and other herbs from the High Plains* (Vol. 41, pp. 7–171). Geological Society of America. https://doi.org/10.1130/spe41-p7

Emre, T., Tavlan, M., Akkiraz, M. S., & Işintek, I. (2011). Stratigraphy, sedimentology and palynology of the Neogene-Pleistocene (?) rocks around Akçaşehir-Tire-İzmir (Küçük Menderes graben, Western Anatolia). *Turkish Journal of Earth Sciences*, *20*(1), 27–56.

Enikeev, F. I. (2008). The late Cenozoic of northern transbaikalia and paleoclimates of southern East Siberia. *Russian Geology and Geophysics*, *49*(8), 602–610. https://doi.org/10.1016/j.rgg.2007.11.013

Ercegovac, M. D., Jeremić, M. M., & Djajić, S. B. (1997). Miocene sedimentary organic facies and palynofacies in Drmno depression (Serbia). *Annales Geologiques de la Peninsule Balkanique*, *61*, 143–165.

Erdei, B., Hably, L., Kázmér, M., Utescher, T., & Bruch, A. A. (2007). Neogene flora and vegetation development of the Pannonian domain in relation to palaeoclimate and palaeogeography. *Palaeogeography, Palaeoclimatology, Palaeoecology*, *253*(1–2), 115–140. https://doi.org/10.1016/j.palaeo.2007.03.036

Fan, Y. (1994). *Tertiary oil and gas region of China II northwest oil and gas region partition*. Petroleum Industry Press.

Farnsworth, A., Lunt, D. J., O'Brien, C. L., Foster, G. L., Inglis, G. N., Markwick, P., et al. (2019). Climate sensitivity on geological timescales controlled by nonlinear feedbacks and ocean circulation. *Geophysical Research Letters*, *46*(16), 9880–9889. https://doi.org/10.1029/2019gl083574

Feakins, S. J., Warny, S., & Lee, J. E. (2012). Hydrologic cycling over Antarctica during the middle Miocene warming. *Nature Geoscience*, *5*(8), 557–560. https://doi.org/10.1038/ngeo1498

Ferguson, D. K., Pingen, M., Zetter, R., & Hofmann, C.-C. (1998). Advances in our knowledge of the Miocene plant assemblage from Kreuzau, Germany. *Review of Palaeobotany and Palynology*, *101*(1–4), 147–177. https://doi.org/10.1016/s0034-6667(97)00074-2

Field, B. D., Crundwell, M. P., Lyon, G. L., Mildenhall, D. C., Morgans, H. E. G., Ohneiser, C., et al. (2009). Middle Miocene paleoclimate change at Bryce Burn, southern New Zealand. *New Zealand Journal of Geology and Geophysics*, *52*(4), 321–333. https://doi.org/10.1080/00288306.2009.9518461

Fletcher, T. L., Telka, A., Rybczynski, N., & Matthews, J. V., Jr. (2021). Neogene and early Pleistocene flora from Alaska and Arctic/Subarctic Canada: New data, intercontinental comparisons and correlations. *Palaeontologia Electronica*, *24*, a07. https://doi.org/10.26879/1121

Frederiksen, N. O. (1984). Stratigraphic, paleoclimatic and paleobiogeographic significance of Tertiary sporomorphs from Massachusetts. In *U.S. Geological Survey Professional Paper 1308* (pp. 1–25). Retrieved from https://pubs.usgs.gov/pp/1308/report.pdf

Frigola, A., Prange, M., & Schulz, M. (2018). Boundary conditions for the Middle Miocene Climate Transition (MMCT v1. 0). *Geoscientific Model Development*, *11*(4), 1607–1626. https://doi.org/10.5194/gmd-11-1607-2018

Friis, E. M. (1979). The Damgaard flora: A new Middle Miocene flora from Denmark. *Bulletin of the Geological Society of Denmark*, *27*, 117–142. https://doi.org/10.37570/bgsd-1978-27-12

Fuji, N. (1969). Fossil spores and pollen grains from the Neogene deposits in Noto Peninsula, Central Japan-II a palynological study of the Middle Miocene Yamatoda member. *Transactions of the Proceedings of the Palaeontological Society of Japan, N.S.*, *74*, 51–80.

Gardère, P., & Pais, J. (2007). Palynologic data from aquitaine (SW France) Middle Miocene sables fauves Formation. Climatic evolution. *Ciencias da Terra*, *15*, 151–161.

Gassmann, M. I., & Pérez, C. F. (2006). Trajectories associated to regional and extra-regional pollen transport in the southeast of Buenos Aires province, Mar del Plata (Argentina). *International Journal of Biometeorology*, *50*(5), 280–291. https://doi.org/10.1007/s00484-005-0021-8

Gasson, E., DeConto, R., Pollard, D., & Levy, R. H. (2016). Dynamic Antarctic ice sheet during the early to mid-Miocene. *Proceedings of the National Academy of Sciences*, *113*(13), 3459–3464. https://doi.org/10.1073/pnas.1516130113

Gengwu, L., & Jianguo, L. (2016). Miocene plant fossil horizons and related stratigraphic issues in Wuyu Basin, Nanmulin, Tibet. *Journal of Stratigraphy*, *40*(1), 92–99.

Gibson, N., Davies, J., & Brown, M. J. (1991). The ecology of Lagarostrobos franklinii (Hook.f.) Quinn (Podocarpaceae) in Tasmania. 1. Distribution, floristics and environmental correlates. *Australian Journal of Ecology*, *16*(2), 215–222. https://doi.org/10.1111/j.1442-9993.1991.tb01048.x

Gnibidenko, Z. N., Martynov, V. A., Nikitin, V. P., & Semakov, N. N. (1999). Magnetostratigraphic and paleobotanical description of the Miocene deposits in the Beshcheul Horizon of West Siberia. *Russian Geology and Geophysics*, *40*, 1776–1788.
Godfrey, S. J., & Barnes, L. G. (2008). A new genus and species of late Miocene pontoporiid dolphin (Cetacea: Odontoceti) from the St. Marys Formation in Maryland. *Journal of Vertebrate Paleontology*, *28*(2), 520–528. https://doi.org/10.1671/0272-4634(2008)28[520:angaso]2.0.co;2
Goillot, C., Franceschi, D. D., Pons, D., & Antoine, P.-O. (2007). Exceptionally preserved microfossils in the Middle Miocene of Amazonian Peru: Preliminary palaeoenvironmental implications. In E. Diaz-Martinez & I. Rabano (Eds.), *4th European meeting on the palaeontology and stratigraphy of Latin America* (pp. 161–165). Instituto Geologico y Minero de Espana.
Graben, M., & Emre, T. (2022). Palaeovegetation and paleoclimate in the SW Turkey—A study based on the early-middle Miocene coal-bearing sediments from the Büyük. *Review of Palaeobotany and Palynology*, *297*, 104560. https://doi.org/10.1016/j.revpalbo.2021.104560
Greenwood, D. R., & Donovan, S. K. (1991). The taphonomy of plant macrofossils. In *The processes of fossilization* (pp. 141–169).
Greenwood, D. R., West, C. K., & Basinger, J. F. (2020). The Miocene Red Lake Macroflora of the Deadman River Formation (Chilcotin Group), Interior Plateau, British Columbia, Canada. *Acta Palaeobotanica*, *60*(2), 213–250. https://doi.org/10.35535/acpa-2020-0011
Gregor, H. J., Hottenrott, M., Knobloch, E., & Planderova, E. (1989). Neue mega- und mikrofloristische Untersuchungen in der jungtertiaren Molasse Bayerns. *Geologica Bavarica*, *94*, 281–369.
Griener, K. W., Warny, S., Askin, R. A., & Acton, G. (2015). Early to middle Miocene vegetation history of Antarctica supports eccentricity-paced warming intervals during the Antarctic icehouse phase. *Global and Planetary Change*, *127*, 67–78. https://doi.org/10.1016/j.gloplacha.2015.01.006
Grimaldi, D. A., & Triplehorn, D. M. (2008). Insects from the upper Miocene grubstake Formation of Alaska. *American Museum Novitates*, *3612*, 1–19. https://doi.org/10.1206/602.1
Grımsson, F., & Denk, T. (2007). Floristic turnover in Iceland from 15 to 6 Ma—Extracting biogeographical signals from fossil floral assemblages. *Journal of Biogeography*, *34*(9), 1490–1504. https://doi.org/10.1111/j.1365-2699.2007.01712.x
Grímsson, F., Denk, T., & Símonarson, L. A. (2007). Middle Miocene floras of Iceland—The early colonization of an island? *Review of Palaeobotany and Palynology*, *144*(3–4), 181–219. https://doi.org/10.1016/j.revpalbo.2006.07.003
Groeneveld, J., Henderiks, J., Renema, W., McHugh, C. M., De Vleeschouwer, D., Christensen, B. A., et al. (2017). Australian shelf sediments reveal shifts in Miocene Southern Hemisphere westerlies. *Science Advances*, *3*(5), e1602567. https://doi.org/10.1126/sciadv.1602567
Gu, Z. G., Bai, S., Zhang, X. T., Ma, Y. Z., Wang, S. H., & Li, B. Y. (1992). Neogene subdivision and correlation of sediments within the Guide and Hualong basins of Qinghai province. *Journal of Stratigraphy*, *16*(2), 96–104.
Hably, L. (1985). Ipolytarnóc alsó-miocén korú flórája. Geologica hungarica. *Series geologica*, *44–46*, 77–255.
Hably, L. (2020). The Karpatian (late early Miocene) flora of the Mecsek area. *Acta Palaeobotanica*, *60*(1), 51–122. https://doi.org/10.35535/acpa-2020-0003
Halberstadt, A. R. W., Chorley, H., Levy, R. H., Naish, T., DeConto, R. M., Gasson, E., & Kowalewski, D. E. (2021). CO_2 and tectonic controls on Antarctic climate and ice-sheet evolution in the mid-Miocene. *Earth and Planetary Science Letters*, *564*, 116908. https://doi.org/10.1016/j.epsl.2021.116908
Hamon, N., Sepulchre, P., Donnadieu, Y., Henrot, A.-J., François, L., Jaeger, J.-J., & Ramstein, G. (2012). Growth of subtropical forests in Miocene Europe: The roles of carbon dioxide and Antarctic ice volume. *Geology*, *40*(6), 567–570. https://doi.org/10.1130/g32990.1
Haomin, L., & Shuangxing, G. (1976). Miocene flora of Nanmulin, Tibet. *Acta Palaeontologica Sinica*, *15*, 7–17.
Harmata, K., & Olech, M. (1991). Transect for aerobiological studies from Antarctica to Poland. *Grana*, *30*(2), 458–463. https://doi.org/10.1080/00173139109432009
Harris, E. B., Strömberg, C. A. E., Sheldon, N. D., Smith, S. Y., & Vilhena, D. A. (2017). Vegetation response during the lead-up to the middle Miocene warming event in the Northern Rocky Mountains, USA. *Palaeogeography, Palaeoclimatology, Palaeoecology*, *485*, 401–415. https://doi.org/10.1016/j.palaeo.2017.06.029
Harzhauser, M., Landau, B., Mandic, O., & Neubauer, T. A. (2024). The Central Paratethys Sea—Rise and demise of a Miocene European marine biodiversity hotspot. *Scientific Reports*, *14*(1), 16288. https://doi.org/10.1038/s41598-024-67370-6
Hazin, L. B., Kuzmina, O. B., Hazina, I. V., Lashchinskii, N. N., Kartozia, A. A., & Kashirtsev, V. A. (2019). First discovery of fossil leaf prints in Cenozoic sediments of the Island Sardakh-Sise (Lena River Delta). In *Reports of the Russian Academy of Sciences* (Vol. 487, pp. 185–188).
He, W.-L., & Wang, X.-J. (2021). A Miocene flora from the Toupi Formation in Jiangxi Province, southeastern China. *Palaeoworld*, *30*(4), 757–769. https://doi.org/10.1016/j.palwor.2020.12.006
Henrot, A.-J., François, L., Favre, E., Butzin, M., Ouberdous, M., & Munhoven, G. (2010). Effects of CO_2, continental distribution, topography and vegetation changes on the climate at the Middle Miocene: A model study. *Climate of the Past*, *6*, 675–694.
Henrot, A. J., Utescher, T., Erdei, B., Dury, M., Hamon, N., Ramstein, G., et al. (2017). Middle Miocene climate and vegetation models and their validation with proxy data. *Palaeogeography, Palaeoclimatology, Palaeoecology*, *467*, 95–119. https://doi.org/10.1016/j.palaeo.2016.05.026
Herold, N., Huber, M., Greenwood, D. R., Müller, R. D., & Seton, M. (2011). Early to middle Miocene monsoon climate in Australia. *Geology*, *39*(1), 3–6. https://doi.org/10.1130/g31208.1
Herold, N., Huber, M., & Müller, R. D. (2011). Modeling the Miocene climatic optimum. Part I: Land and atmosphere. *Journal of Climate*, *24*, 6353–6372. https://doi.org/10.1175/2011jcli4035.1
Herold, N., Huber, M., Müller, R. D., & Seton, M. (2012). Modeling the Miocene climatic optimum: Ocean circulation. *Paleoceanography*, *27*(1), PA1209. https://doi.org/10.1029/2010pa002041
Herold, N., Seton, M., Müller, R. D., You, Y., & Huber, M. (2008). Middle Miocene tectonic boundary conditions for use in climate models. *Geochemistry, Geophysics, Geosystems*, *9*(10), Q10009. https://doi.org/10.1029/2008gc002046
Highton, P. J. C., Racey, A., Wakefield, M. I., Carmichael, A. J., & Glendinning, N. R. W. (1997). Quantitative biostratigraphy: An example from the Neogene of the Gulf of Thailand. In *The international conference on stratigraphy and tectonic evolution of Southeast Asia and the South Pacific, Bangkok, Thailand* (pp. 563–585).
Hinojosa, L. F. (2005). Climatic and vegetational changes inferred from Cenozoic Southern South America paleoflora. *Revista Geologica de Chile*, *32*, 95–115.
Hinojosa, L. F. (2010). Climatic and vegetational changes inferred from Cenozoic Southern Southamerica paleoflora. *Andean Geology*, *32*(1), 95–116.
Hinojosa, L. F., Armesto, J. J., & Villagran, C. (2006). Are Chilean coastal forests pre-pleistocene relicts? Evidence from foliar physiognomy, palaeoclimate, and phytogeography. *Journal of Biogeography*, *33*(2), 331–341. https://doi.org/10.1111/j.1365-2699.2005.01350.x
Ho, C. S. (1966). The shihti Formation in northern Taiwan. *Bulletin of the Geological Survey of Taiwan*, *17*, 1–25.
Hoffmann, W. A. (2000). Post-Establishment seedling success in the Brazilian Cerrado: A comparison of Savanna and forest species 1. *Biotropica*, *32*, 62–69. https://doi.org/10.1646/0006-3606(2000)032[0062:pessit]2.0.co;2

Holcová, K., Doláková, N., Vass, D., Zagorsek, K., & Zelenka, J. (1996). Foraminifera, Bryozoa, Ostracoda and palynomorphs like indicators of marine environment in the Lower Badenian of Strhare-Trenc graben. *Mineralia Slovaca*, *28*, 99–119.

Holman, J. A. (1970). Herpetofauna of the Wood Mountain Formation (Upper Miocene) of Saskatchewan. *Canadian Journal of Earth Sciences*, *7*(5), 1317–1325. https://doi.org/10.1139/e70-124

Holmes, W., & Andereson, H. (2019). The Middle Miocene flora of the chalk Mountain Formation, Warrumbungle Volcano complex, NSW, Australia. *Proceedings of the Linnean Society of New South Wales*, *141*, S19–S32.

Hoorn, C. (1994). An environmental reconstruction of the palaeo-Amazon river system (Middle–Late Miocene, NW Amazonia). *Palaeogeography, Palaeoclimatology, Palaeoecology*, *112*(3–4), 187–238. https://doi.org/10.1016/0031-0182(94)90074-4

Hoorn, C., Boschman, L. M., Kukla, T., Sciumbata, M., & Val, P. (2022). The Miocene wetland of western Amazonia and its role in neotropical biogeography. *Botanical Journal of the Linnean Society*, *199*(1), 25–35. https://doi.org/10.1093/botlinnean/boab098

Hu, Z., & Sarjeant, W. A. S. (1992). Cenozoic spore-pollen assemblage zones from the shelf of the East China Sea. *Review of Palaeobotany and Palynology*, *72*(1–2), 103–118. https://doi.org/10.1016/0034-6667(92)90178-j

Huang, J., Su, T., Jia, L. B., Spicer, T., & Zhou, Z. K. (2018). A fossil fig from the Miocene of southwestern China: Indication of persistent deep time karst vegetation. *Review of Palaeobotany and Palynology*, *258*, 133–145. https://doi.org/10.1016/j.revpalbo.2018.07.005

Huang, L. L., Jin, J. H., Quan, C., & Oskolski, A. A. (2021). New occurrences of Altingiaceae fossil woods from the Miocene and upper Pleistocene of South China with phytogeographic implications. *Journal of Palaeogeography*, *10*(4), 482–493. https://doi.org/10.1016/j.jop.2021.11.001

Huang, Q. H., Kong, H., & Dong, J. Y. (2002). The palynomorph assemblage and its stratigraphic sequence in the Fangzheng fault depression of the Yilan-Yitong Graben. *Acta Micropalaeontologica Sinica*, *19*(2), 193–198.

Hui, Z., Li, J., Song, C., Chang, J., Zhang, J., Liu, J., et al. (2017). Vegetation and climatic changes during the Middle Miocene in the Wushan Basin, northeastern Tibetan Plateau: Evidence from a high-resolution palynological record. *Journal of Asian Earth Sciences*, *147*, 116–127. https://doi.org/10.1016/j.jseaes.2017.07.008

Hui, Z., Li, J., Xu, Q., Song, C., Zhang, J., Wu, F., & Zhao, Z. (2011). Miocene vegetation and climatic changes reconstructed from a sporopollen record of the Tianshui Basin, NE Tibetan Plateau. *Palaeogeography, Palaeoclimatology, Palaeoecology*, *308*(3–4), 373–382. https://doi.org/10.1016/j.palaeo.2011.05.043

Hui, Z., Li, X., Ma, Z., Xiao, L., Zhang, J., & Chang, J. (2018). Miocene pollen assemblages from the Zeku Basin, northeastern Tibetan Plateau, and their palaeoecological and palaeoaltimetric implications. *Palaeogeography, Palaeoclimatology, Palaeoecology*, *511*, 419–432. https://doi.org/10.1016/j.palaeo.2018.09.009

Hui, Z., Zhang, J., Ma, Z., Li, X., Peng, T., Li, J., & Wang, B. (2018). Global warming and rainfall: Lessons from an analysis of Mid-Miocene climate data. *Palaeogeography, Palaeoclimatology, Palaeoecology*, *512*, 106–117. https://doi.org/10.1016/j.palaeo.2018.10.025

Hyland, E. G., Huntington, K. W., Sheldon, N. D., & Reichgelt, T. (2018). Temperature seasonality in the North American continental interior during the Early Eocene Climatic Optimum. *Climate of the Past*, *14*(10), 1391–1404. https://doi.org/10.5194/cp-14-1391-2018

Igarashi, Y., Yahata, M., & Kimura, M. (2000). Fossil pollen stratigraphy of Miocene Tonokita Formation, Akan-cho, east Hokkaido. *Bulletin of Ashoro Museum of Paleontology*, *1*, 85–90.

Igwe, C. A., Zarei, M., & Stahr, K. (2013). Soil hydraulic and physico-chemical properties of ultisols and inceptisols in south-eastern Nigeria. *Archives of Agronomy and Soil Science*, *59*(4), 491–504. https://doi.org/10.1080/03650340.2011.649475

Il'inskaya, I. A. (1962). On the changes in the flora of the Zaysan Basin from the end of the Late Cretaceous to the end of the Miocene. *Doklady Akademii Nauk SSSR*, *146*, 181–185.

IPCC. (2019). Summary for policymakers. In P. R. Shukla, J. Skea, E. Calvo Buendia, V. Masson-Delmotte, H.-O. Pörtner, D. C. Roberts, et al. (Eds.), *Climate change and land: An IPCC special report on climate change, desertification, land degradation, sustainable land management, food security, and greenhouse gas fluxes in terrestrial ecosystems*.

Isphording, W. C. (1970). Late tertiary paleoclimate of eastern United States. *The American Association of Petroleum Geologists Bulletin*, *54*(2), 334–343. https://doi.org/10.1306/5d25c999-16c1-11d7-8645000102c1865d

Ivanov, D. A., Ashraf, A. R., & Mosbrugger, V. (2007). Late Oligocene and Miocene climate and vegetation in the Eastern Paratethys area (northeast Bulgaria), based on pollen data. *Palaeogeography, Palaeoclimatology, Palaeoecology*, *255*(3–4), 342–360. https://doi.org/10.1016/j.palaeo.2007.08.003

Ivanov, D. A., Ashraf, A. R., Mosbrugger, V., & Palamarev, E. (2002). Palynological evidence for Miocene climate change in the Forecarpathian Basin (Central Paratethys, NW Bulgaria). *Palaeogeography, Palaeoclimatology, Palaeoecology*, *178*(1–2), 19–37. https://doi.org/10.1016/s0031-0182(01)00365-0

Ivanovic, R. F., Gregoire, L. J., Kageyama, M., Roche, D. M., Valdes, P. J., Burke, A., et al. (2016). Transient climate simulations of the deglaciation 21–9 thousand years before present (version 1)—PMIP4 Core experiment design and boundary conditions. *Geoscientific Model Development*, *9*(7), 2563–2587. https://doi.org/10.5194/gmd-9-2563-2016

Jacobs, B. F., Pan, A. D., Scotese, C. R., Werdelin, L., & Sanders, W. J. (2010). A review of the Cenozoic vegetation history of Africa. *Cenozoic mammals of Africa*, *5*, 57–74.

Jacques, F. M. B., Shi, G., Su, T., & Zhou, Z. (2015). A tropical forest of the middle Miocene of Fujian (SE China) reveals Sino-Indian biogeographic affinities. *Review of Palaeobotany and Palynology*, *216*, 76–91. https://doi.org/10.1016/j.revpalbo.2015.02.001

Jacques, F. M. B., Shi, G., & Wang, W. (2011). Reconstruction of Neogene zonal vegetation in South China using the Integrated Plant Record (IPR) analysis. *Palaeogeography, Palaeoclimatology, Palaeoecology*, *307*(1–4), 272–284. https://doi.org/10.1016/j.palaeo.2011.05.025

Janis, C. M., Damuth, J., & Theodor, J. M. (2004). The species richness of Miocene browsers, and implications for habitat type and primary productivity in the North American grassland biome. *Palaeogeography, Palaeoclimatology, Palaeoecology*, *207*(3–4), 371–398. https://doi.org/10.1016/s0031-0182(04)00048-3

Jaramillo, C., Hoorn, C., Silva, S. A. F., Leite, F. F. H., Quiroz, L., Dino, R., & Antonioli, L. (2010). The origin of the modern Amazon rainforest: Implications of the palynological and palaeobotanical record. In C. Hoorn & F. P. Wesselingh (Eds.), *Amazonia, Landscape and Species Evolution: A look into the past* (pp. 317–334). Blackwell Publishing.

Jaramillo, C., Romero, I., D'Apolito, C., Bayona, G., Duarte, E., Louwye, S., et al. (2017). Miocene flooding events of western Amazonia. *Science Advances*, *3*(5), e1601693. https://doi.org/10.1126/sciadv.1601693

Jarzen, D. M., Corbett, S. L., & Manchester, S. R. (2010). Palynology and paleoecology of the Middle Miocene Alum Bluff flora, Liberty County, Florida, USA. *Palynology*, *34*(2), 261–286. https://doi.org/10.1080/01916122.2010.510824

Jiang, H., & Ding, Z. (2008). A 20Ma pollen record of East-Asian summer monsoon evolution from Guyuan, Ningxia, China. *Palaeogeography, Palaeoclimatology, Palaeoecology*, *265*(1–2), 30–38. https://doi.org/10.1016/j.palaeo.2008.04.016

Jiménez-Moreno, G. (2006). Progressive substitution of a subtropical forest for a temperate one during the middle Miocene climate cooling in Central Europe according to palynological data from cores Tengelic-2 and Hidas-53 (Pannonian Basin, Hungary). *Review of Palaeobotany and Palynology*, *142*(1–2), 1–14. https://doi.org/10.1016/j.revpalbo.2006.05.004

Jiménez-Moreno, G., Fauquette, S., & Suc, J. P. (2010). Miocene to Pliocene vegetation reconstruction and climate estimates in the Iberian Peninsula from pollen data. *Review of Palaeobotany and Palynology*, *162*(3), 403–415. https://doi.org/10.1016/j.revpalbo.2009.08.001

Jiménez-Moreno, G., Mandic, O., Harzhauser, M., Pavelić, D., & Vranjković, A. (2008). Vegetation and climate dynamics during the early middle Miocene from Lake Sinj (Dinaride Lake system, SE Croatia). *Review of Palaeobotany and Palynology*, *152*(3-4), 237–245.

Jiménez-Moreno, G., & Suc, J.-P. (2007). Middle Miocene latitudinal climatic gradient in Western Europe: Evidence from pollen records. *Palaeogeography, Palaeoclimatology, Palaeoecology*, *253*(1–2), 208–225. https://doi.org/10.1016/j.palaeo.2007.03.040

Jingfang, L., Kexin, Z., Bowen, S., Yadong, X., Zhiyu, Z., Wei, H., & Daolai, Z. (2020). Eocene-Pliocene sporopollen records and climate change in Dahonggou area, Qaidam Basin. *Modern Geology*, *34*(4), 732–744.

Kageyama, M., Albani, S., Braconnot, P., Harrison, S. P., Hopcroft, P. O., Ivanovic, R. F., et al. (2017). The PMIP4 contribution to CMIP6–Part 4: Scientific objectives and experimental design of the PMIP4-CMIP6 last Glacial Maximum experiments and PMIP4 sensitivity experiments. *Geoscientific Model Development*, *10*(11), 4035–4055. https://doi.org/10.5194/gmd-10-4035-2017

Kaplan, J. O. (2001). Geophysical applications of vegetation modeling. PhD thesis (Lund, Sweden). Retrieved from https://infoscience.epfl.ch/record/136645

Kaplan, J. O., Bigelow, N. H., Prentice, I. C., Harrison, S. P., Bartlein, P. J., Christensen, T. R., et al. (2003). Climate change and Arctic ecosystems: 2. Modeling, paleodata-model comparisons, and future projections. *Journal of Geophysical Research*, *108*(D19), 8171. https://doi.org/10.1029/2002jd002559

Kar, N., Garzione, C. N., Jaramillo, C., Shanahan, T., Carlotto, V., Pullen, A., et al. (2016). Rapid regional surface uplift of the northern Altiplano plateau revealed by multiproxy paleoclimate reconstruction. *Earth and Planetary Science Letters*, *447*, 33–47. https://doi.org/10.1016/j.epsl.2016.04.025

Kayseri, M. S., & Akgün, F. (2008). Palynostratigraphic, palaeovegetational and palaeoclimatic investigations on the Miocene deposits in Central Anatolia (Çorum Region and Sivas Basin). *Turkish Journal of Earth Sciences*, *17*(2), 361–403. https://journals.tubitak.gov.tr/earth/vol17/iss2/7/

Kayseri-Özer, M. S., & Akgün, F. (2010). The late Burdigalian-Langhian interval in Turkey and the palaeoenvironmental and palaeoclimatic implications and correlation of Europe and Turkey: Late Burdigalian-Langhian palynofloras and palaeoclimatic properties of the Mugla-Milas (Kultak). *Geological Bulletin of Turkey*, *53*(1), 1–44.

Kayseri-Özer, M. S., Akgün, F., Mayda, S., & Kaya, T. (2014). Palynofloras and vertebrates from Mugla-Oren region (SW Turkey) and palaeoclimate of the Middle Burdigalian-Langhian period in Turkey. *Bulletin of Geosciences*, *89*(1), 137–167.

Kayseri-Özer, M. S., & Emre, T. (2022). Palaeovegetation and paleoclimate in the SW Turkey—A study based on the early-middle Miocene coal-bearing sediments from the Büyük Menderes Graben. *Review of Palaeobotany and Palynology*, *297*, 104560. https://doi.org/10.1016/j.revpalbo.2021.104560

Kayseri-Özer, M. S., Sözbilir, H., & Akgün, F. (2014). Miocene palynoflora of the Kocaçay and Cumaovası basins: A contribution to the synthesis of Miocene palynology, palaeoclimate, and palaeovegetation in western Turkey. *Turkish Journal of Earth Sciences*, *23*(3), 233–259. https://doi.org/10.3906/yer-1301-9

Kern, A., Harzhauser, M., Mandic, O., Roetzel, R., Ćorić, S., Bruch, A. A., & Zuschin, M. (2011). Millennial-scale vegetation dynamics in an estuary at the onset of the Miocene Climate Optimum. *Palaeogeography, Palaeoclimatology, Palaeoecology*, *304*(3–4), 247–261. https://doi.org/10.1016/j.palaeo.2010.07.014

Kershaw, A. P. (1997). A bioclimatic analysis of early to middle Miocene brown coal floras, Latrobe Valley, South-Eastern Australia. *Australian Journal of Botany*, *45*(3), 373–387. https://doi.org/10.1071/bt96033

Kezina, T. V., & Ol'kin, G. F. (2000). Palynological characteristics of Cenozoic coal-bearing deposits, the Snezhnogorskii locality in the Verkhnyaya Zeya Basin. *Stratigraphy and Geological Correlation*, *8*(5), 482–490.

Klimova, R. S. (1988). Some representatives of thermophilic Miocene plants from the Primor'ye Region. *Paleontologicheskii Zhurnal*, *1*, 92–99.

Knorr, G., Butzin, M., Micheels, A., & Lohmann, G. (2011). A warm Miocene climate at low atmospheric CO_2 levels. *Geophysical Research Letters*, *38*(20), L20701. https://doi.org/10.1029/2011gl048873

Knowlton, F. H. (1926). *Flora of the latah formation of Spokane, Washington, and Coeur d'Alene, Idaho*. US Government Printing Office. Retrieved from https://ifpni.org/publication.htm?id=ED1D8244-DC05-05B7-B2CA-23C29C545D9B

Kong, W.-S. (2000). Vegetational history of the Korean Peninsula. *Global Ecology and Biogeography*, *9*(5), 391–402. https://doi.org/10.1046/j.1365-2699.2000.00203.x

Konzalova, M. (2005). Filinaceae and other selected plant microfossils from Neogene deposits of tropical area (Malaysia). *Zpravy o Geologickych Vyzkumech v Roce*, *2005*, 89–91.

Korasidis, V. A., Wing, S. L., Shields, C. A., & Kiehl, J. T. (2022). Global changes in terrestrial vegetation and continental climate during the Paleocene-Eocene thermal maximum. *Paleoceanography and Paleoclimatology*, *37*(4), e2021PA004325. https://doi.org/10.1029/2021pa004325

Kotthoff, U., Greenwood, D. R., McCarthy, F. M. G., Müller-Navarra, K., Prader, S., & Hesselbo, S. P. (2014). Late Eocene to middle Miocene (33 to 13 million years ago) vegetation and climate development on the North American Atlantic Coastal Plain (IODP Expedition 313, Site M0027). *Climate of the Past*, *10*(4), 1523–1539. https://doi.org/10.5194/cp-10-1523-2014

Kovar-Eder, J., Kvaček, Z., & Ströbitzer-Hermann, M. (2003). The Miocene flora of Parschlug (Styria, Austria)–revision and synthesis. *Annalen des Naturhistorischen Museums in Wien. Serie A für Mineralogie und Petrographie, Geologie und Paläontologie, Anthropologie und Prähistorie*, *105*, 45–159.

Kovar-Eder, J., Meller, B., & Zetter, R. (1998). Comparative investigations on the basal fossiliferous layers at the opencast mine Oberdorf (Köflach-Voitsberg lignite deposit, Styria, Austria; Early Miocene). *Review of Palaeobotany and Palynology*, *101*(1–4), 125–145. https://doi.org/10.1016/s0034-6667(97)00073-0

Kowalski, E. A., & Dilcher, D. L. (2003). Warmer paleotemperatures for terrestrial ecosystems. *Proceedings of the National Academy of Sciences*, *100*(1), 167–170. https://doi.org/10.1073/pnas.232693599

Kukla, T., Rugenstein, J. K. C., Ibarra, D. E., Winnick, M. J., Strömberg, C. A. E., & Chamberlain, C. P. (2022). Drier winters drove Cenozoic open habitat expansion in North America. *AGU Advances*, *3*(2), e2021AV000566. https://doi.org/10.1029/2021av000566

Kvaček, Z., Kováč, M., Kovar-Eder, J., Doláková, N., Jechorek, H., Parashiv, V., et al. (2006). Miocene evolution of landscape and vegetation in the Central Paratethys. *Geologica Carpathica*, *57*(4), 295–310.

Lakhanpal, R. N., & Guleria, J. S. (1986). Fossil leaves of Dipterocarpus from the lower Siwalik beds near Jawalamukhi, Himachal Pradesh. The Palaeobotanist 35, 258–262. Fossil leaves of Dipterocarpus from the lower Siwalik beds near Jawalamukhi, Himachal Pradesh. *Palaeobotanist*, *35*((1–3)), 258–262. https://doi.org/10.54991/jop.1986.1539

Lancucka-Srodoniowa, M., & Zastawniak, E. (1997). The Middle-Miocene flora of Wieliczka revision of Jan Zablocki's collection. *Acta Palaeobotanica*, *37*(1), 17–49.

Larsson, L. M., Dybkjær, K., Rasmussen, E. S., Piasecki, S., Utescher, T., & Vajda, V. (2011). Miocene climate evolution of northern Europe: A palynological investigation from Denmark. *Palaeogeography, Palaeoclimatology, Palaeoecology*, *309*(3–4), 161–175. https://doi.org/10.1016/j.palaeo.2011.05.003

Larsson, L. M., Vajda, V., & Rasmussen, E. S. (2006). Early Miocene pollen and spores from western Jylland, Denmark-environmental and climatic implications. *GFF*, *128*(3), 261–272. https://doi.org/10.1080/11035890601283261

Laukhin, S. A., & Rybakova, N. O. (1981). The Neogene in central parts of the Yana-Kolyma Plain. *Doklady of the Academy of Sciences of the USSR Earth Sciences Sections*, *258*, 73–76.

Lavrushin, Y. A., & Alekseev, M. N. (2005). The Arctic regions. *Geological Society of America Special Paper*, *382*, 13–29. https://doi.org/10.1130/0-8137-2382-5.13

Leathwick, J. R. (2001). New Zealand's potential forest pattern as predicted from current species-environment relationships. *New Zealand Journal of Botany*, *39*(3), 447–464. https://doi.org/10.1080/0028825x.2001.9512748

Lei, Z. Q. (1985). Tertiary sporo-pollen assemblage of Zhujiangkou (Pearl River North) basin and its stratigraphical significance. *Acta Botanica Sinica*, *27*, 94–105. (in Chinese with English abstract).

Lenhardt, N., Martinez-Hernandez, E., Götz, A. E., Hinderer, M., Hornung, J., Torres-Alvarado, I. S., et al. (2006). Palaeoenvironmental reconstruction of the Miocene Tepoztlán Formation (Central Mexico): Preliminary results of palynological investigations. In *Proceedings of the X, XI, and XII international symposia on volcanospeleology: AMCS (Association for Mexican Cave studies) bulletin* (Vol. 19, pp. 158–161).

Leopold, E. B., & Denton, M. F. (1987). Comparative age of grassland and steppe east and west of the northern rocky mountain. *Annals of the Missouri Botanical Garden*, *74*(4), 841–867. https://doi.org/10.2307/2399452

Leopold, E. B., & Liu, G. (1994). A long pollen sequence of neogene age, Alaska range. *Quaternary International*, *22/23*, 103–140. https://doi.org/10.1016/1040-6182(94)90009-4

Levy, R., Harwood, D., Florindo, F., Sangiorgi, F., Tripati, R., Von Eynatten, H., et al. (2016). Antarctic ice sheet sensitivity to atmospheric CO_2 variations in the early to mid-Miocene. *Proceedings of the National Academy of Sciences*, *113*(13), 3453–3458. https://doi.org/10.1073/pnas.1516030113

Lewis, A. R., Marchant, D. R., Ashworth, A. C., Hedenäs, L., Hemming, S. R., Johnson, J. V., et al. (2008). Mid-Miocene cooling and the extinction of tundra in continental Antarctica. *Proceedings of the National Academy of Sciences of the United States of America*, *105*(31), 10676–10680. https://doi.org/10.1073/pnas.0802501105

Li, H., & Guo, S. (1976). The Miocene flora from the Namling of Xizang. *Acta Palaeontologica Sinica*, *15*(1), 8–18.

Li, J.-G., & Zhang, Y.-Y. (1998). Neogene Palynofloras from East offshore Hainan Island. *Acta Micropalaeontologica Sinica*, *15*(3), 323–330.

Li, Y., Huang, L., Quan, C., Jin, J., & Oskolski, A. A. (2021). Fossil wood of Syzygium from the Miocene of Guangxi, South China: The earliest fossil evidence of the genus in eastern Asia. *IAWA Journal*, *42*(4), 435–441. https://doi.org/10.1163/22941932-bja10069

Ling, H.-Y. (1965). Palynological study on plant microfossils from the Shihti Formation, Miocene “middle coal-bearing bed”, Taiwan. *Proceedings of the Geological Society of China*, *8*, 19–23.

Liu, G., & Leopold, E. B. (1994). Climatic comparison of Miocene pollen floras from northern East-China and south-central Alaska, USA. *Palaeogeography, Palaeoclimatology, Palaeoecology*, *108*(3–4), 217–228. https://doi.org/10.1016/0031-0182(94)90235-6

Lockley, M. G. & Rice, A. (Eds.) (1990). *Volcanism and fossil biotas* (Vol. 244). Geological Society of America. https://doi.org/10.1130/SPE244

Lohmann, G., Butzin, M., & Bickert, T. (2015). Effect of vegetation on the Late Miocene ocean circulation. *Journal of Marine Sciencse and Engineering*, *3*(4), 1311–1333. https://doi.org/10.3390/jmse3041311

Lopatina, D. A. (2001). Palynological assemblages and macrofloras from Eocene - Miocene deposits of the Tatar Strait Coast (Eastern Sikhote Alin). *Stratigraphy and Geological Correlation*, *9*(4), 387–405.

Lopatina, D. A. (2003). Comparative analysis of the Eocene-Miocene micro- and macrofloras of the Eastern Sikhote Alin. *Stratigraphy and Geological Correlation*, *11*(1), 74–90.

Lopatina, D. A. (2004). Vegetation and climate of the Eocene-Miocene, Eastern Sikhote-Alin (from palaeobotanical analysis data). *Pacific Geology*, *23*(3), 98–112.

Lott, T. A., Manchester, S. R., & Corbett, S. L. (2019). The Miocene flora of Alum Bluff, Liberty County, Florida. *Acta Palaeobotanica*, *59*(1), 75–129. https://doi.org/10.2478/acpa-2019-0003

Loughney, K. M., Hren, M. T., Smith, S. Y., & Pappas, J. L. (2020). Vegetation and habitat change in southern California through the Middle Miocene Climatic Optimum: Paleoenvironmental records from the Barstow Formation, Mojave Desert, USA. *Geological Society of America Bulletin*, *132*(1–2), 113–129. https://doi.org/10.1130/b35061.1

Lunt, D. J., Bragg, F., Chan, W. L., Hutchinson, D. K., Ladant, J. B., Morozova, P., et al. (2021). DeepMIP: Model intercomparison of early Eocene climatic optimum (EECO) large-scale climate features and comparison with proxy data. *Climate of the Past*, *17*(1), 203–227. https://doi.org/10.5194/cp-17-203-2021

Ma, J. Q. (1993). The tertiary sporopollen assemblage in the Jiuquan basin and the palaeoenvironment. *Petroleum Geology Expeiment* (in Chinese with English abstract) 4.

Ma, Y.-Z. (1991). Tertiary palynomorph assemblage in the southern Dunhuang Basin, Gansu Province [In Chinese]. *Acta Micropalaeontologica Sinica*, *1991*(2), 207–225.

Ma, Y. Z., Li, J. J., & Fan, X. M. (1998). Pollen-based vegetational and climatic records during 30.6 to 5.0 my from Linxia area, Gansu. *Chinese Science Bulletin*, *43*, 301–304.

Macphail, M., & Cantrill, D. J. (2006). Age and implications of the Forest Bed, Falkland Islands, southwest Atlantic Ocean: Evidence from fossil pollen and spores. *Palaeogeography, Palaeoclimatology, Palaeoecology*, *240*(3–4), 602–629. https://doi.org/10.1016/j.palaeo.2006.03.010

Manchester, S. R., Crane, P. R., & Dilcher, D. L. (1991). Nordenskioldia and trochodendron (Trochodendraceae) from the Miocene of Northwestern North America. *Botanical Gazette*, *152*(3), 357–368. https://doi.org/10.1086/337898

Mao, X., & Retallack, G. (2019). Late Miocene drying of central Australia. *Palaeogeography, Palaeoclimatology, Palaeoecology*, *514*, 292–304. https://doi.org/10.1016/j.palaeo.2018.10.008

Martin, H. A. (1993). The palaeovegetation of the Murray Basin, late Eocene to MidMiocene. *Australian Systematic Botany*, *6*, 491–531. https://doi.org/10.1071/sb9930491

Martin, H. A. (1997). The stratigraphic palynology of bores along the Darling River, downstream from Bourke, New South Wales. *Proceedings of the Linnean Society of New South Wales*, *118*, 51–67.

Martin, P. S., & Gray, J. (1962). Pollen analysis and the Cenozoic: Ancient climate and vegetation can be studied by comparison of modern and fossil pollen rains. *Science*, *137*(3524), 103–111. https://doi.org/10.1126/science.137.3524.103

Martínez, C., Jaramillo, C., Correa-Metrío, A., Crepet, W., Moreno, J. E., Aliaga, A., et al. (2020). Neogene precipitation, vegetation, and elevation history of the Central Andean Plateau. *Science Advances*, *6*(35), eaaz4724. https://doi.org/10.1126/sciadv.aaz4724

Martínez-Hernández, E. (1992). *Caracterización ambiental del Terciario de la Región de Ixtapa, Estado de Chiapas—Un enfoque paleoestratigráfico* (Vol. 10, pp. 54–64). Universidad Nacional Autónoma de México, Instituto de Geologia, Revista.

Mather, B. R., Müller, R. D., Zahirovic, S., Cannon, J., Chin, M., Ilano, L., et al. (2023). Deep time spatio-temporal data analysis using pyGPlates with PlateTectonicTools and GPlately. *Geoscience Data Journal*, *11*, 1–8. https://doi.org/10.1002/gdj3.185

Mathews, W. H., & Rouse, G. E. (1984). The Gang Ranch—Big bar area, south-central British Columbia: Stratigraphy, geochronology, and palynology of the tertiary beds and their relationship to the Fraser Fault. *Canadian Journal of Earth Sciences*, *21*(10), 1132–1144. https://doi.org/10.1139/e84-118

Matsuoka, K. (1990). *The early Middle Miocene inland paleoclimate around Central Kinki, Southwest Japan. Pacific Neogene Events. R. Tsuchi* (pp. 15–22). University of Tokyo Press.

McCurry, M. R., Cantrill, D. J., Smith, P. M., Beattie, R., Dettmann, M., Baranov, V., et al. (2022). A Lagerstätte from Australia provides insight into the nature of Miocene mesic ecosystems. *Science Advances*, *8*(1), eabm1406. https://doi.org/10.1126/sciadv.abm1406

McLaughlin, P. P., Miller, K. G., Browning, J. V., Ramsey, K. W., Benson, R. N., Tomlinson, J. L., & Sugarman, P. J. (2008). *Stratigraphy and correlation of the Oligocene to Pleistocene section at Bethany Beach, Delaware*. Delaware Geological Survey, University of Delaware. Retrieved from http://udspace.udel.edu/handle/19716/3767

Meehl, G. A., Washington, W. M., Arblaster, J. M., Hu, A., Teng, H., Kay, J. E., et al. (2013). Climate change projections in CESM1 (CAM5) compared to CCSM4. *Journal of Climate*, *26*(17), 6287–6308. https://doi.org/10.1175/jcli-d-12-00572.1

Meon-Vilain, H. (1968). Analyses sporo-polliniques dans l'Helvétientype du Imihubel (Berne). *Eclogae Geologicae Helvetiae*, *61*, 435–457.

Micheels, A., Bruch, A. A., Uhl, D., Utescher, T., & Mosbrugger, V. (2007). A Late Miocene climate model simulation with ECHAM4/ML and its quantitative validation with terrestrial proxy data. *Palaeogeography, Palaeoclimatology, Palaeoecology*, *253*(1–2), 251–270. https://doi.org/10.1016/j.palaeo.2007.03.042

Mildenhall, D. C., & Pocknall, D. T. (1984). Palaeobotanical evidence for changes in Miocene and Pliocene climates in New Zealand. In *Late Cainozic palaeoclimates of the Southern Hemisphere. International symposium held by the South African Society for Quaternary Research; Swaziland* (pp. 159–171).

Mohr, B. A. R. (2001). The development of Antarctic fern floras during the tertiary, and palaeoclimatic and palaeobiogeographic implications. *Palaeontographica Abtellung B Palaeophytologie*, *259*(1–6), 167–208. https://doi.org/10.1127/palb/259/2001/167

Moktar, N. B., & Mannaï-Tayech, B. (2016). Climatic control on vegetation and sedimentary dynamics during the Miocene (Burdigalian to Langhian) in northeastern Tunisia. *Revue de Micropaleontologie*, *59*(1), 1–17.

Moore, P. R., & Wallace, R. (2000). Petrified wood from the Miocene volcanic sequence of Coromandel Peninsula, northern New Zealand. *Journal of the Royal Society of New Zealand*, *30*(2), 115–130. https://doi.org/10.1080/03014223.2000.9517612

Morley, R. J., & Morley, H. P. (2011). Neogene climate history of Makassar Straits, Indonesia. In R. Hall, M. A. Cottam, & M. E. J. Wilson (Eds.), *The SE Asian gateway: History and tectonics of the Australia—Asia collision* (pp. 319–332). The Geological Society of London.

Mosbrugger, V., Utescher, T., & Dilcher, D. L. (2005). Cenozoic continental climatic evolution of Central Europe. *Proceedings of the National Academy of Sciences*, *102*(42), 14964–14969. https://doi.org/10.1073/pnas.0505267102

Müller, R. D., Cannon, J., Qin, X., Watson, R. J., Gurnis, M., Williams, S., et al. (2018). GPlates: Building a virtual Earth through deep time. *Geochemistry, Geophysics, Geosystems*, *19*(7), 2243–2261. https://doi.org/10.1029/2018GC007584

Nachtergaele, F., van Velthuizen, H., Verelst, L., Wiberg, D., Henry, M., Chiozza, F., et al. (2023). *Harmonized world soil database version 2.0*. Food and Agriculture Organization of the United Nations.

Nikitin, V. P. (2007). Paleogene and Neogene strata in Northeastern Asia: Paleocarpological background. *Russian Geology and Geophysics*, *48*(8), 675–682. https://doi.org/10.1016/j.rgg.2006.06.002

Norris, G. (1997). Paleocene-Pliocene deltaic to inner shelf palynostratigraphic zonation, depositional environments and paleoclimates in the Imperial ADGO F-28 well, Beaufort-Mackenzie Basin. *Geological Survey of Canada Bulletin*, *523*, 1–71. https://books.google.com.pa/books/about/Paleocene_Pliocene_Deltaic_to_Inner_Shel.html?id=aAkeWAxQHUMC

Oboh, F. E. (1992). Middle Miocene palaeoenvironments of the Niger Delta. *Palaeogeography, Palaeoclimatology, Palaeoecology*, *92*(1–2), 55–84. https://doi.org/10.1016/0031-0182(92)90135-r

Oboh, F. E. (1995). Sedimentological and palynological characteristics of the E2.0 Reservoir (Middle Miocene) in the Kolo Creek Field, Niger Delta. In M. N. Oti & G. Postma (Eds.), *Geology of deltas* (pp. 243–256). A.A. Balkema.

Ochoa, D., Hoorn, C., Jaramillo, C., Bayona, G., Parra, M., & De la Parra, F. (2012). The final phase of tropical lowland conditions in the axial zone of the Eastern Cordillera of Colombia: Evidence from three palynological records. *Journal of South American Earth Sciences*, *39*, 157–169. https://doi.org/10.1016/j.jsames.2012.04.010

Oerter, E., Amundson, R., Heimsath, A., Jungers, M., Chong, G., & Renne, P. (2016). Early to middle Miocene climate in the Atacama Desert of northern Chile. *Palaeogeography, Palaeoclimatology, Palaeoecology*, *441*, 890–900. https://doi.org/10.1016/j.palaeo.2015.10.038

O'Keefe, J. M., Pound, M. J., Romero, I. C., Nuñez Otaño, N. B., Gibson, M. E., McCoy, J., et al. (2024). Summer-wet hydrologic cycle during the Middle Miocene of the United States: New evidence from fossil fungi. *Research*, *7*, 0481. https://doi.org/10.34133/research.0481

Oliver, E. S. (1936). A Miocene flora from the Blue Mountains of Oregon. *Contributions to Paleontology from the Carnegie Institution of Washington*, *455*, 1–27.

Ottone, E. G., Barreda, V., & Pérez, D. J. (1998). Basin evolution as reflected by Miocene palynomorphs from the Chinches Formation, Frontal Cordillera (32°S), San Juan Province, Argentina. *Revista Espanola de Micropaleontologia*, *30*, 35–47.

Owens, J. P. (1988). *Stratigraphy of the Tertiary sediments in a 945-foot-deep corehole near Mays Landing in the southeastern New Jersey Coastal Plain (No. 1484)*. US Government Printing Office. https://doi.org/10.3133/pp1484

Passchier, S., Browne, G., Field, B., Fielding, C. R., Krissek, L. A., Panter, K., et al. (2011). Early and middle Miocene Antarctic glacial history from the sedimentary facies distribution in the AND-2A drill hole, Ross Sea, Antarctica. *Bulletin*, *123*(11–12), 2352–2365. https://doi.org/10.1130/b30334.1

Pazzaglia, F. J., Robinson, R. A. J., & Traverse, A. (1997). Palynology of the Bryn Mawr Formation (Miocene): Insights on the age and genesis of Middle Atlantic margin fluvial deposits. *Sedimentary Geology*, *108*(1–4), 19–44. https://doi.org/10.1016/S0037-0738(96)00047-4

Peppe, D. J., Cote, S. M., Deino, A. L., Fox, D. L., Kingston, J. D., Kinyanjui, R. N., et al. (2023). Oldest evidence of significant C4 grasses and habitat heterogeneity in eastern Africa. *Science*, *380*(6641), 173–177. https://doi.org/10.1126/science.abq2834

Piel, K. M. (1977). Miocene palynological assemblages from central British Columbia. *AASP Contributions Series*, *5A*, 91–109.

Pillot, Q., Donnadieu, Y., Sarr, A. C., Ladant, J. B., & Suchéras-Marx, B. (2022). Evolution of ocean circulation in the North Atlantic Ocean during the Miocene: Impact of the Greenland ice sheet and the Eastern Tethys Seaway. *Paleoceanography and Paleoclimatology*, *37*(8), e2022PA004415. https://doi.org/10.1029/2022pa004415

Ping, S., Jianhua, J., Dejun, S., & Jian, M. (2001). Early Miocene flora from Pingzhuang basin of inner mongolia and its paleoenvironment. *Zhongshan da xue xue bao. Zi ran ke xue ban = Acta Scientiarum Naturalium Universitatis Sunyatseni*, *40*(5), 108–112.

Planderová, E. (1971). Contribution à l'étude palynologique des sédiments Tertiaires de la Tunisie. Geologické práce. *Zprávy*, *56*, 199–216.

Pole, M., & Douglas, B. (1998). A quantitative palynostratigraphy of the Miocene Manuherikia Group, New Zealand. *Journal of the Royal Society of New Zealand*, *28*(3), 405–442. https://doi.org/10.1080/03014223.1998.9517572

Pole, M. S. (2003). New Zealand climate in the Neogene and implications for global atmospheric circulation. *Palaeogeography, Palaeoclimatology, Palaeoecology*, *193*(2), 269–284. https://doi.org/10.1016/s0031-0182(03)00232-3

Pontes, G. M., Wainer, I., Taschetto, A. S., Sen Gupta, A., Abe-Ouchi, A., Brady, E. C., et al. (2020). Drier tropical and subtropical Southern Hemisphere in the mid-Pliocene Warm Period. *Science Report UK*, *10*(1), 13458. https://doi.org/10.1038/s41598-020-68884-5

Popova, S., Utescher, T., Gromyko, D., Bruch, A., & Mosbrugger, V. (2012). Palaeoclimate evolution in Siberia and the Russian Far East from the Oligocene to Pliocene–evidence from fruit and seed floras. *Turkish Journal of Earth Sciences*, *21*(2), 315–334. https://doi.org/10.3906/yer-1005-6

Pound, J., Haywood, A. M., Salzmann, U., & Riding, J. B. (2012). Global vegetation dynamics and latitudinal temperature gradients during the mid to late Miocene (15.97–5.33 Ma). *Earth-Science Reviews*, *112*(1–2), 1–22. https://doi.org/10.1016/j.earscirev.2012.02.005

Pound, M. J., Haywood, A. M., Salzmann, U., Riding, J. B., Lunt, D. J., & Hunter, S. J. (2011). A Tortonian (late Miocene, 11.61–7.25 Ma) global vegetation reconstruction. *Palaeogeography, Palaeoclimatology, Palaeoecology*, *300*(1–4), 29–45. https://doi.org/10.1016/j.palaeo.2010.11.029

Pound, M. J., & McCoy, J. (2021). Palaeoclimate reconstruction and age assessment of the Miocene flora from the Trwyn y Parc solution pipe complex of Anglesey, Wales, UK. *Palynology*, *45*(4), 697–703. https://doi.org/10.1080/01916122.2021.1916636

Pound, M. J., Tindall, J., Pickering, S. J., Haywood, A. M., Dowsett, H. J., & Salzmann, U. (2014). Late Pliocene lakes and soils: A global data set for the analysis of climate feedbacks in a warmer world. *Climate of the Past*, *10*(1), 167–180. https://doi.org/10.5194/cp-10-167-2014

Prasad, M. (1993). Siwalik (Middle Miocene) woods from the Kalagarh area in the Himalayan foot hills and their bearing on palaeoclimate and phytogeography. *Review of Palaeobotany and Palynology*, *76*(1), 49–82. https://doi.org/10.1016/0034-6667(93)90080-e

Prasad, M., Ghosh, R., & Tripathi, P. P. (2004). Floristics and climate during Siwalik (Middle Miocene) near Kathgodam in the Himalayan foothills of Uttranchal, India. *Journal of the Palaeontological Society of India*, *49*(1), 35–93. https://doi.org/10.1177/0971102320040103

Prentice, I. C., & Webb, T., III. (1998). Biome 6000: Reconstructing global mid-holocene vegetation patterns from palaeoecological records. *Journal of Biogeography*, *25*(6), 997–1005. https://doi.org/10.1046/j.1365-2699.1998.00235.x

Pujana, R. R., Fernández, D. A., Panti, C., & Caviglia, N. (2021). The micro- and megafossil record of Nothofagaceae from South America. *Botanical Journal of the Linnean Society*, *196*, 1–20. https://doi.org/10.1093/botlinnean/boaa097

Quattrocchio, M., Durango de Cabrera, J., & Gallp, C. (2003). Formación Anta (Mioceno Temprano/Medio), Subgrupo Metán (Grupo) en el río Piedras, Pcia. de Salta. Datos palinológicos. *Revista de la Asociación Geológica Argentina*, *58*, 117–127.

Quattrocchio, M., & Guerstein, G. R. (1989). Evaluacion paleoambiental y paleoclimatica del Terciario de la Cuenca del Colorado, Republica Argentina. Palinofloras. *Revista de la Asociación Geológica Argentina*, *43*, 375–387.

Raigemborn, M. S., Krapovickas, V., Beilinson, E., Peral, L. E. G., Zucol, A. F., Zapata, L., et al. (2018). Multiproxy studies of Early Miocene pedogenic calcretes in the Santa Cruz formation of southern Patagonia, Argentina indicate the existence of a temperate warm vegetation adapted to a fluctuating water table. *Palaeogeography, Palaeoclimatology, Palaeoecology*, *500*, 1–23. https://doi.org/10.1016/j.palaeo.2018.03.037

Raitzsch, M., Bijma, J., Bickert, T., Schulz, M., Holbourn, A., & Kučera, M. (2021). Atmospheric carbon dioxide variations across the middle Miocene climate transition. *Climate of the Past*, *17*(2), 703–719. https://doi.org/10.5194/cp-17-703-2021

Rasser, M. W., Bechly, G., Böttcher, R., Ebner, M., Heizmann, E. P. J., Höltke, O., et al. (2013). The Randeck Maar: Palaeoenvironment and habitat differentiation of a Miocene lacustrine system. *Palaeogeography, Palaeoclimatology, Palaeoecology*, *392*, 426–453. https://doi.org/10.1016/j.palaeo.2013.09.025

Read, P. B. (2000). Geology and industrial minerals of the Tertiary basins, south-Central British Columbia. In *British Columbia Geological Survey GeoFile 2000-3* (pp. 1–109).

Rech, J. A., Currie, B. S., Jordan, T. E., Riquelme, R., Lehmann, S. B., Kirk-Lawlor, N. E., et al. (2019). Massive middle Miocene gypsic paleosols in the Atacama Desert and the formation of the Central Andean rain-shadow. *Earth and Planetary Science Letters*, *506*, 184–194. https://doi.org/10.1016/j.epsl.2018.10.040

Regali, M. S., Uesugui, N., & Santos, A. S. (1974). Palinologia dos sedimentos Meso-Cenozoicos do Brasil (1). *Boletim Tecnico da Petrobras*, *17*, 177–191.

Reichgelt, T., Baumgartner, A., Feng, R., & Willard, D. A. (2023). Poleward amplification, seasonal rainfall and forest heterogeneity in the Miocene of the eastern USA. *Global and Planetary Change*, *222*, 104073. https://doi.org/10.1016/j.gloplacha.2023.104073

Reichgelt, T., Kennedy, E. M., Conran, J. G., Lee, W. G., & Lee, D. E. (2019). The presence of moisture deficits in Miocene New Zealand. *Global and Planetary Change*, *172*, 268–277.

Reichgelt, T., Kennedy, E. M., Conran, J. G., Mildenhall, D. C., & Lee, D. E. (2015). The early Miocene paleolake Manuherikia: Vegetation heterogeneity and warm-temperate to subtropical climate in southern New Zealand. *Journal of Paleolimnology*, *53*(4), 349–365. https://doi.org/10.1007/s10933-015-9827-5

Reichgelt, T., Lee, W. G., & Lee, D. E. (2022). The extinction of Miocene broad-leaved deciduous nothofagaceae and loss of seasonal forest biomes in New Zealand. *Review of Palaeobotany and Palynology*, *307*, 104779. https://doi.org/10.1016/j.revpalbo.2022.104779

Reichgelt, T., & West, C. K. (2025). Insights into greener Miocene biomes and globally enhanced terrestrial productivity from fossil leaves. *Evolving Earth*, *3*, 100058. https://doi.org/10.1016/j.eve.2025.100058

Retallack, G. J. (2022). Soil carbon dioxide planetary thermostat. *Astrobiology*, *22*(1), 116–123. https://doi.org/10.1089/ast.2020.2415

Retallack, G. J., & Kirby, M. X. (2007). Middle Miocene global change and paleogeography of Panama. *PALAIOS*, *22*(6), 667–679. https://doi.org/10.2110/palo.2006.p06-130r

Salzmann, U., Haywood, A. M., Lunt, D. J., Valdes, P. J., & Hill, D. J. (2008). A new global biome reconstruction and data-model comparison for the Middle Pliocene. *Global Ecology and Biogeography*, *17*, 432–447. https://doi.org/10.1111/j.1466-8238.2007.00381.x

Sangiorgi, F., Bijl, P. K., Passchier, S., Salzmann, U., Schouten, S., McKay, R., et al. (2018). Southern Ocean warming and Wilkes Land ice sheet retreat during the mid-Miocene. *Nature Communications*, *9*(1), 317. https://doi.org/10.1038/s41467-017-02609-7

Scheiner, F., Havelcová, M., Holcová, K., Doláková, N., Nehyba, S., Ackerman, L., et al. (2023). Evolution of palaeoclimate, palaeoenvironment and vegetation in Central Europe during the Miocene Climate Optimum. *Palaeogeography, Palaeoclimatology, Palaeoecology*, *611*, 111364. https://doi.org/10.1016/j.palaeo.2022.111364

Şengör, A. C., & Canitez, N. (1982). The north anatolian fault. *Alpine-Mediterranean Geodynamics*, *7*, 205–216. https://doi.org/10.1029/gd007p0205

Shi, G. L., Jacques, F. M., & Li, H. (2014). Winged fruits of Shorea (Dipterocarpaceae) from the Miocene of Southeast China: Evidence for the northward extension of dipterocarps during the Mid-Miocene Climatic Optimum. *Review of Palaeobotany and Palynology*, *200*, 97–107. https://doi.org/10.1016/j.revpalbo.2013.09.003

Shi, G. L., & Li, H. (2010). A fossil fruit wing of Dipterocarpus from the middle Miocene of Fujian, China and its palaeoclimatic significance. *Review of Palaeobotany and Palynology*, *162*(4), 599–606. https://doi.org/10.1016/j.revpalbo.2010.08.001

Simon, P., Caratini, C., Charpy, N., & Tissot, C. (1984). Sédimentologie et palynologie du Cétacé terminal et du Tertiaire de la région de Bonoua (Côte d'Ivoire). *Geologie Mediterraneenne*, *11*(1), 77–85. https://doi.org/10.3406/geolm.1984.1291

Sittler, C. (1958). Palynological stratigraphy of the Miocene in France. In *Pollen analysis of various layers. [Stratigraphie palynologique du Miocene en France. Analyse Pollinique de Differents gisements.] Congres National des Societes Savantes, Comptes Rendu, Section de Geologie* (pp. 279–293).

Skopintsev, V. G., & Tregub, T. F. (2017). On the age of the Eastern sayan basalt covers. *Bulletin of Voronzh State University*, *2*, 53–58.

Smiley, C. J., Gray, J., & Huggins, L. M. (1975). Preservation of Miocene fossils in unoxidized lake deposits, Clarkia, Idaho; with a section on fossil Insecta by WF Barr and JM Gillespie. *Journal of Paleontology*, 833–844. Retrieved from https://www.jstor.org/stable/pdf/1303276.pdf

Smiley, C. J., & Rember, W. C. (1985). Physical setting of the Miocene Clarkia fossil beds, northern Idaho. In *Late Cenozoic history of the Pacific Northwest* (pp. 11–36). American Association for the Advancement of Science. Retrieved from https://eurekamag.com/research/019/725/019725871.php

Smiley, T. M., Hyland, E. G., Cotton, J. M., & Reynolds, R. E. (2018). Evidence of early C4 grasses, habitat heterogeneity, and faunal response during the Miocene Climatic Optimum in the Mojave Region. *Palaeogeography, Palaeoclimatology, Palaeoecology*, *490*, 415–430. https://doi.org/10.1016/j.palaeo.2017.11.020

Sobczyk, A., Worobiec, E., Olkowicz, M., & Szczygieł, J. (2024). Mid-Miocene onset of the NE Bohemian Massif (SW Poland, Europe) growth, landscape evolution, and paleoenvironmental changes unraveled using paleokarst sediment palynology. *Palaeogeography, Palaeoclimatology, Palaeoecology*, *640*, 112107. https://doi.org/10.1016/j.palaeo.2024.112107

Song, H., Huang, L., Xiang, H., Quan, C., & Jin, J. (2023). First reliable Miocene fossil winged fruits record of Engelhardia in Asia through anatomical investigation. *iScience*, *26*(6), 106867. https://doi.org/10.1016/j.isci.2023.106867

Songtham, W., Ratanasthien, B., Mildenhall, D. C., Singharajwarapan, S., & Kandharosa, W. (2003). Oligocene-Miocene climatic changes in northern Thailand resulting from extrusion tectonics of Southeast Asian landmass. *ScienceAsia*, *29*(3), 221–233. https://doi.org/10.2306/scienceasia1513-1874.2003.29.221

Spicer, R. A., Harris, N. B., Widdowson, M., Herman, A. B., Guo, S. X., Valdes, P. J., et al. (2003). Constant elevation of southern Tibet over the past 15 million years. *Nature*, *421*(6923), 622–624. https://doi.org/10.1038/nature01356

Srivastava, R., & Awasthi, N. (1994). Carbonised woods of Sterculiaceae and Sapindaceae from Middle Miocene sediments of Kerala coast. *Palaeobotanist*, *42*(1–3), 178–182. https://doi.org/10.54991/jop.1993.1145

Srivastava, S. K. (1984). Palynology of the Monterey Formation (Miocene) phosphatic facies at Lions Head, Santa Maria area, California. *Palynology*, *8*(1), 33–49. https://doi.org/10.1080/01916122.1984.9989270

Stärz, M., Jokat, W., Knorr, G., & Lohmann, G. (2017). Threshold in North Atlantic-Arctic Ocean circulation controlled by the subsidence of the Greenland-Scotland Ridge. *Nature Communications*, *8*(1), 15681. https://doi.org/10.1038/ncomms15681

Staver, A. C., Archibald, S., & Levin, S. A. (2011). The global extent and determinants of savanna and forest as alternative biome states. *Science*, *334*(6053), 230–232. https://doi.org/10.1126/science.1210465

Steinthorsdottir, M., Coxall, H. K., De Boer, A. M., Huber, M., Barbolini, N., Bradshaw, C. D., et al. (2021). The Miocene: The future of the past. *Paleoceanography and Paleoclimatology*, *36*(4), e2020PA004037. https://doi.org/10.1029/2020pa004037

Stott, D. F., & Aitken, J. D. (1993). *Tertiary; Subchapter 4J in sedimentary cover of the craton in Canada* (Vol. 5, pp. 439–465). Geological Survey of Canada, Geology of Canada.

Stromberg, C., & Smith, F. (2007). Towards calibrating the late Miocene C-3/C-4 shift in the Great Plains, North America: A combined record of phytolith assemblage composition and stable carbon isotopes. *Journal of Vertebrate Paleontology*, *27*(3), 154A.

Strömberg, C. A., Dunn, R. E., Crifò, C., & Harris, E. B. (2018). Phytoliths in paleoecology: Analytical considerations, current use, and future directions. In *Methods in paleoecology: Reconstructing Cenozoic terrestrial environments and ecological communities* (pp. 235–287). Springer International Publishing.

Strömberg, C. A., Saylor, B. Z., Engelman, R. K., Catena, A. M., Hembree, D. I., Anaya, F., & Croft, D. A. (2024). The flora, fauna, and paleoenvironment of the late Middle Miocene Quebrada Honda Basin, Bolivia (Eastern Cordillera, Central Andes). *Palaeogeography, Palaeoclimatology, Palaeoecology*, *656*, 112518. https://doi.org/10.1016/j.palaeo.2024.112518

Strömberg, C. A. E. (2005). Decoupled taxonomic radiation and ecological expansion of open-habitat grasses in the Cenozoic of North America. *Proceedings of the National Academy of Science102*, *102*(34), 11980–11984. https://doi.org/10.1073/pnas.0505700102

Strömberg, C. A. E. (2011). Evolution of grasses and grassland ecosystems. *Annual Review of Earth and Planetary Sciences*, *39*(1), 517–544. https://doi.org/10.1146/annurev-earth-040809-152402

Sun, J. M., & Zhang, Z. Q. (2008). Palynological evidence for the mid-Miocene climatic optimum recorded in Cenozoic sediments of the Tian Shan Range, northwestern China. *Global and Planetary Change*, *64*(1–2), 53–68. https://doi.org/10.1016/j.gloplacha.2008.09.001

Sun, M. R., Sun, X., Zhao, Y., Wang, D., Li, Z., Hu, Z., et al. (1989). *Cenozoic paleobiota of the continental shelf of the East China Sea (Donghai), micropaleobotanical volume* (pp. 6–111). Geological Publishing House. (in Chinese).

Sun, Q. G., Collinson, M. E., Li, C. S., Wang, Y. F., & Beerling, D. J. (2002). Quantitative reconstruction of palaeoclimate from the Middle Miocene Shanwang flora, eastern China. *Palaeogeography, Palaeoclimatology, Palaeoecology*, *180*(4), 315–329. https://doi.org/10.1016/s0031-0182(01)00433-3

Sun, X., Li, M., Zhang, Y., Lei, Z., Sun, Z., Li, P., et al. (1981). See: Nanhai Branch of Petroleum Exploration Company of the People's Republic of China, Guangzhou Branch of Geological Exploration Company of the People's Republic of China, Nanjing Institute of Geology and Paleontology, Chinese Academy of Sciences et al. (Eds.). In *Tertiary paleontological Atlas of the Northern Continental Shelf of the South China Sea* (pp. 1–30). Guangdong Science and Technology Press.

Sun, X., & Wang, P. (2005). How old is the Asian monsoon system? Palaeobotanical records from China. *Palaeogeography, Palaeoclimatology, Palaeoecology*, *222*(3–4), 181–222. https://doi.org/10.1016/j.palaeo.2005.03.005

Sun, X. J., & He, Y. M. (1987). Neogene sporo-pollen assemblages from Jiangxi Province, China. *Botanical Research*, *3*, 83–108. In Chinese with English abstract.
Sun, X.-Y. (1984). The Oligocene-Miocene palynological assemblages from the Xining-Minghe Basin, Qinghai Province. *Geological Review*, *30*, 207–216. (in Chinese with English abstract).
Syabryaj, S., Utescher, T., Molchanoff, S., & Bruch, A. A. (2007). Vegetation and palaeoclimate in the Miocene of Ukraine. *Palaeogeography, Palaeoclimatology, Palaeoecology*, *253*(1–2), 153–168. https://doi.org/10.1016/j.palaeo.2007.03.038
Tang, Z., Ding, Z., White, P. D., Dong, X., Ji, J., Jiang, H., et al. (2011). Late Cenozoic central Asian drying inferred from a palynological record from the northern Tian Shan. *Earth and Planetary Science Letters*, *302*(3–4), 439–447. https://doi.org/10.1016/j.epsl.2010.12.042
Tao, J.-J. (1997). The paleofloristic and paleoclimatic changes during the Mid-Miocene in China. In N. G. Jablonski (Ed.), *The changing face of East Asia during the Tertiary and Quaternary*. The University of Hong Kong.
Tao, J. R., Zhou, Z. K., & Liu, Y. S. (2000). *The evolution of the late Cretaceous-Cenozoic floras in China* (p. 703007520). Science Press.
Tardif, D., Sarr, A.-C., Fluteau, F., Licht, A., Kaya, M., Ladant, J.-B., et al. (2023). The role of paleogeography in Asian monsoon evolution: Associated a review and new insights from climate modelling. *Earth-Science Reviews*, *243*, 104464. https://doi.org/10.1016/j.earscirev.2023.104464
Terauds, A., & Lee, J. R. (2016). Antarctic biogeography revisited: Updating the antarctic Conservation Biogeographic Regions. *Diversity and Distributions*, *22*(8), 836–840. https://doi.org/10.1111/ddi.12453
Tiffney, B. H. (1994). Re-evaluation of the age of the Brandon Lignite (Vermont, USA) based on plant megafossils. *Review of Palaeobotany and Palynology*, *82*(3–4), 299–315. https://doi.org/10.1016/0034-6667(94)90081-7
Tindall, J., Haywood, A., Salzmann, U., Dolan, A., & Fletcher, T. (2022). The warm winter paradox in the Pliocene Northern high latitudes. *Climate of the Past*, *18*(6), 1385–1405. https://doi.org/10.5194/cp-18-1385-2022
Tipple, B. J., & Pagani, M. (2010). A 35 Myr North American leaf-wax compound-specific carbon and hydrogen isotope record: Implications for C4 grasslands and hydrologic cycle dynamics. *Earth and Planetary Science Letters*, *299*(1–2), 250–262. https://doi.org/10.1016/j.epsl.2010.09.006
Tong, J. A., You, Y., Müller, R. D., & Seton, M. (2009). Climate model sensitivity to atmospheric CO_2 concentrations for the middle Miocene. *Global and Planetary Change*, *67*, 129–140.
Traverse, A. (1988). *Paleopalynology*. Unwin Hyman.
Traverse, A. (1994). Palynofloral geochronology of the Brandon Lignite of Vermont, USA. *Review of Palaeobotany and Palynology*, *82*(3–4), 265–297. https://doi.org/10.1016/0034-6667(94)90080-9
Truswell, E. M., & Macphail, M. K. (2009). Polar forests on the edge of extinction: What does the fossil spore and pollen evidence from East Antarctica say? *Australian Systematic Botany*, *22*(2), 57–106. https://doi.org/10.1071/sb08046
Truswell, E. M., Sluiter, I. R., & Harris, W. K. (1984). Palynology of the Oligocene-Miocene sequence in the Oakvale-1 corehole, western Murray Basin, South Australia. *BMR Journal of Australian Geology and Geophysics*, *9*(4), 267–295.
Urban, M. A., Nelson, D. M., Jiménez-Moreno, G., Châteauneuf, J. J., Pearson, A., & Hu, F. S. (2010). Isotopic evidence of C4 grasses in southwestern Europe during the Early Oligocene–Middle Miocene. *Geology*, *38*(12), 1091–1094. https://doi.org/10.1130/g31117.1
Utescher, T., Ashraf, A. R., Kern, A. K., & Mosbrugger, V. (2021). Diversity patterns in microfloras recovered from Miocene brown coals of the lower Rhine Basin reveal distinct coupling of the structure of the peat-forming vegetation and continental climate variability. *Geological Journal*, *56*(2), 768–785. https://doi.org/10.1002/gj.3801
Utescher, T., Bruch, A. A., Micheels, A., Mosbrugger, V., & Popova, S. (2011). Cenozoic climate gradients in Eurasia—A palaeo-perspective on future climate change? *Palaeogeography, Palaeoclimatology, Palaeoecology*, *304*(3–4), 351–358. https://doi.org/10.1016/j.palaeo.2010.09.031
Utescher, T., Djordjevic-Milutinovic, D., Bruch, A., & Mosbrugger, V. (2007). Palaeoclimate and vegetation change in Serbia during the last 30 Ma. *Palaeogeography, Palaeoclimatology, Palaeoecology*, *253*(1–2), 141–152. https://doi.org/10.1016/j.palaeo.2007.03.037
Utescher, T., Erdei, B., François, L., & Mosbrugger, V. (2007). Tree diversity in the Miocene forests of Western Eurasia. *Palaeogeography, Palaeoclimatology, Palaeoecology*, *253*(1–2), 226–250. https://doi.org/10.1016/j.palaeo.2007.03.041
Van Vuuren, D. P., Edmonds, J., Kainuma, M., Riahi, K., Thomson, A., Hibbard, K., et al. (2011). The representative concentration pathways: An overview. *Climate Change*, *109*(1–2), 5–31. https://doi.org/10.1007/s10584-011-0148-z
Varma, Y. N. R., Ramanujam, C. G. K., & Patil, R. S. (1986). Palynoflora of tertiary sediments of Tonakkal Area, Kerala. *Journal of Palynology*, *22*, 39–53.
Veblen, T. T., Hill, R. S., & Read, J. (1996). *The ecology and biogeography of Nothofagus forests*. Yale Unsiversity Press.
Verkhovskaya, N. B., & Kundyshev, A. S. (1991). Palynological characteristics of Cenozoic deposits in Vankarem Depression. *Soviet Geology and Geophysics*, *32*, 93–99.
Vernyhorova, Y. V., Holcová, K., Doláková, N., Reichenbacher, B., Scheiner, F., Ackerman, L., et al. (2023). The Miocene Climatic Optimum at the interface of epicontinental sea and large continent: A case study from the Middle Miocene of the Eastern Paratethys. *Marine Micropaleontology*, *181*, 102231. https://doi.org/10.1016/j.marmicro.2023.102231
Vicente-Serrano, S. M., Miralles, D. G., McDowell, N., Brodribb, T., Domínguez-Castro, F., Leung, R., & Koppa, A. (2022). The uncertain role of rising atmospheric CO_2 on global plant transpiration. *Earth-Science Reviews*, *230*, 104055. https://doi.org/10.1016/j.earscirev.2022.104055
Vozenin-Serra, C., Privé-Gill, C., & Ginsburg, L. (1989). Bois miocenes du gisement de pong, Nord Ouest de la Thailande. *Review of Palaeobotany and Palynology*, *58*(2–4), 333–355. https://doi.org/10.1016/0034-6667(89)90091-2
Wahrhaftig, C. (1969). *The coal-bearing group in the Nenana coal field, Alaska (no. 1274)*. US Department of the Interior, Geological Survey. https://doi.org/10.3133/b1274D
Wan, C., Sun, Y., Xue, Y., Qiao, X., Jin, Y., & Zhang, Y. (2014). Neogene palynological assemblages in the west slope of Songliao Basin and their geological implications. *Science China Earth Sciences*, *57*(10), 2486–2497. https://doi.org/10.1007/s11430-014-4846-z
Wang, B., Shi, G., Xu, C., Spicer, R. A., Perrichot, V., Schmidt, A. R., et al. (2021). The mid-Miocene Zhangpu biota reveals an outstandingly rich rainforest biome in East Asia. *Science Advances*, *7*(18), eabg0625. https://doi.org/10.1126/sciadv.abg0625
Wang, W. (1988). Spore and pollen grains from Miocene lignite deposit of Yalong village, Yao Autonomous County, Guangxi, China. *Acta Palaeontologica Sinica*, *28*, 786–802.
Wang, Z., Sun, F., Wang, J., Yan, D., Dong, J., Sun, M., & Sun, B. (2019). New fossil leaves and fruits of Lauraceae from the Middle Miocene of Fujian, southeastern China differentiated using a cluster analysis. *Historical Biology*, *31*(5), 581–599. https://doi.org/10.1080/08912963.2017.1379517
Warny, S., Askin, R. A., Hannah, M. J., Mohr, B. A. R., Raine, J. I., Harwood, D. M., et al. (2009). Palynomorphs from a sediment core reveal a sudden remarkably warm Antarctica during the middle Miocene. *Geology*, *37*(10), 955–958. https://doi.org/10.1130/g30139a.1

Watanasak, M., Songtham, W., & Mildenhall, D. C. (1995). Age of the SUSAn Hoi (Shell Fossil Cemetary) Krabi Basin, Southern Thailand. In *International Conference on Geology, Geotechnology and Mineral Resources of IndoChina (Geo-Indo)* (Vol. 95, pp. 163–168).

Wheeler, E. A., & Dillhoff, T. A. (2009). The Middle Miocene wood flora of Vantage, Washington, USA. *IAWA Journal*, *30*, 1–101.

Wheeler, E. A., Wiemann, M. C., & Fleagle, J. G. (2007). Woods from the Miocene Bakate Formation, Ethiopia: Anatomical characteristics, estimates of original specific gravity and ecological inferences. *Review of Palaeobotany and Palynology*, *146*(1–4), 193–207. https://doi.org/10.1016/j.revpalbo.2007.04.002

White, J. M., & Ager, T. A. (1994). Palynology, paleoclimatology and correlation of middle Miocene beds from Porcupine River (locality 90-1), Alaska. *Quaternary International*, *22–23*, 43–77. https://doi.org/10.1016/1040-6182(94)90006-X

White, J. M., Ager, T. A., Adam, D. P., Leopold, E. B., Liu, G., Jetté, H., & Schweger, C. E. (1997). An 18 million year record of vegetation and climate change in northwestern Canada and Alaska: Tectonic and global climatic correlates. *Palaeogeography, Palaeoclimatology, Palaeoecology*, *130*(1–4), 293–306. https://doi.org/10.1016/S0031-0182(96)00146-0

White, L. D., Garrison, R. E., & Barron, J. A. (1992). Miocene intensification of upwelling along the California margin as recorded in siliceous facies of the Monterey Formation and offshore DSDP sites. *Geological Society, London, Special Publications*, *64*(1), 429–442. https://doi.org/10.1144/gsl.sp.1992.064.01.28

Whybrow, P. J., & McClure, H. A. (1980). Fossil mangrove roots and palaeoenvironments of the Miocene of the eastern Arabian Peninsula. *Palaeogeography, Palaeoclimatology, Palaeoecology*, *32*, 213–225. https://doi.org/10.1016/0031-0182(80)90041-3

Wijninga, V. M. (1996). Neogene ecology of the Salto de Tequendama site (2475 m altitude, Cordillera Oriental, Colombia): The paleobotanical record of montane and lowland forests. *Review of Palaeobotany and Palynology*, *92*(1–2), 97–156. https://doi.org/10.1016/0034-6667(94)00100-6

Williams, C. J., Mendell, E. K., Murphy, J., Court, W. M., Johnson, A. H., & Richter, S. L. (2008). Paleoenvironmental reconstruction of a Middle Miocene forest from the western Canadian Arctic. *Palaeogeography, Palaeoclimatology, Palaeoecology*, *261*(1–2), 160–176. https://doi.org/10.1016/j.palaeo.2008.01.014

Wing, S. L., DiMichele, W. A., Phillips, T. L., Taggart, R., Tiffney, B. H., & Mazer, S. J. (1992). Ecological characterization of fossil plants. In *Terrestrial ecosystems through time: Evolutionary paleoecology of terrestrial plants and animals* (pp. 139–180). University of Chicago Press.

Wolfe, J. A. (1966). *Tertiary plants from the Cook Inlet region, Alaska (No. 398-B)* (pp. 1–32). US Government Printing Office. https://doi.org/10.3133/pp398B

Wolfe, J. A. (1985). Distribution of major vegetational types during the Tertiary. In *The carbon cycle and atmospheric CO_2: natural variations Archean to present* (Vol. 32, pp. 357–375). https://doi.org/10.1029/gm032p0357

Wolfe, J. A., & Leopold, E. B. (1967). Neogene and early Quaternary vegetation of Northwestern North America and Northeastern Asia. In D. M. Hopkins (Ed.), *The bering land bridge* (pp. 193–206). Stanford University Press.

Wolfe, J. A., & Tanai, T. (1980). *The Miocene Seldovia point flora from the Kenai group, Alaska (No. 1105)*. US Government Printing Office. Retrieved from https://books.google.com.pa/books?hl=en&lr=&id=IjNSAQAAIAAJ

Worobiec, E. (2009). Middle Miocene palynoflora of the Legnica lignite deposit complex, Lower Silesia, Poland. *Acta Palaeobotanica*, *49*(1), 5–133.

Worobiec, E., & Szulc, J. (2010). A Middle Miocene palynoflora from sinkhole deposits from Upper Silesia, Poland and its palaeoenvironmental context. *Review of Palaeobotany and Palynology*, *163*(1–2), 1–10. https://doi.org/10.1016/j.revpalbo.2010.06.007

Worobiec, E., Widera, M., & Worobiec, G. (2022). Palaeoenvironment of the middle Miocene wetlands at Drzewce, Konin region, central Poland. *Annales Societatis Geologorum Poloniae*, *92*, 201–218. https://doi.org/10.14241/asgp.2022.07

Worobiec, E., Widera, M., Worobiec, G., & Kurdziel, B. (2021). Middle Miocene palynoflora from the Adamów lignite deposit, central Poland. *Palynology*, *45*(1), 59–71. https://doi.org/10.1080/01916122.2019.1697388

Worobiec, E., Worobiec, G., & Kasiński, J. R. (2022). Decline of Neogene lignite formation as a result of vegetation and climate changes reflected in the middle Miocene palynoflora from the Ruja lignite deposit, SW Poland. *Review of Palaeobotany and Palynology*, *298*, 104593. https://doi.org/10.1016/j.revpalbo.2021.104593

Wu, X., Zhang, H., Kodrul, T. M., Maslova, N. P., Jiang, S., Yin, Q., et al. (2021). First fossil Fokienia (Cupressaceae) in South China and its palaeogeographic and palaeoecological implications. *Frontiers in Earth Science*, *9*, 709663. https://doi.org/10.3389/feart.2021.709663

Wu, Y., Deng, T., Hu, Y., Ma, J., Zhou, X., Mao, L., et al. (2018). A grazing gomphotherium in Middle Miocene Central Asia, 10 million years prior to the origin of the Elephantidae. *Scientific Reports*, *8*(1), 7640. https://doi.org/10.1038/s41598-018-25909-4

Wynn, J. G., & Retallack, G. J. (2001). Paleoenvironmental reconstruction of middle Miocene paleosols bearing Kenyapithecus and Victoriapithecus, Nyakach Formation, southwestern Kenya. *Journal of Human Evolution*, *40*(4), 263–288. https://doi.org/10.1006/jhev.2000.0453

Yabe, A., & Nakagawa, T. (2018). A new legume fruit species from the mid-Miocene Climatic Optimum in Japan. *Review of Palaeobotany and Palynology*, *257*, 35–42. https://doi.org/10.1016/j.revpalbo.2018.06.006

Yakubovskaya, T. A., & Iosifova, Y. I. (1968). Miocene flora of the oka-don plain. *Doklady Akademii Nauk SSSR*, *179*, 108–111.

Yamanoi, T. (1984). Presence of sonneratiaceous pollen in middle Miocene sediments, central Japan. *Review of Palaeobotany and Palynology*, *40*(4), 347–357. https://doi.org/10.1016/0034-6667(84)90015-0

Yang, Y., Wang, W.-M., Shu, J.-W., & Chen, W. (2018). Miocene palynoflora from Shengxian Formation, Zhejiang Province, southeast China and its palaeovegetational and palaeoenvironmental implications. *Review of Palaeobotany and Palynology*, *259*, 185–197. https://doi.org/10.1016/j.revpalbo.2018.10.001

Yao, Y. M., Lian, H. D., & Cai, Z. G. (1994). *Tertiary in petroliferous regions of China (IV): The bohai Gulf Basin* (pp. 55–57). Petroleum Industry Press. (in Chinese).

Yi, S. (1998). Palynofossils from the early-middle Miocene deposits of Kachi-1 well in block II, yellow Sea Basin, Korea. *Palaeobotanist*, *47*, 116–133. https://doi.org/10.54991/jop.1998.1279

Yi, S., Yi, S., Batten, D. J., Yun, H., & Park, S.-J. (2003). Cretaceous and Cenozoic non-marine deposits of the Northern South Yellow Sea Basin, offshore western Korea: Palynostratigraphy and palaeoenvironments. *Palaeogeography, Palaeoclimatology, Palaeoecology*, *191*(1), 15–44. https://doi.org/10.1016/s0031-0182(02)00637-5

Yi, Y. (2020). *Research on the Miocene palynoflora and its paleovegetation and paleoenvironment in Zhejiang and Fujian regions (Ph.D. thesis)*. University of Science and Technology of China.

You, Y., Huber, M., Müller, R. D., Poulsen, C. J., & Ribbe, J. (2009). Simulation of the middle Miocene climate optimum Geophysical. *Research Letters*, *36*(4). https://doi.org/10.1029/2008gl036571

Zamaloa, M. D. C. (2000). Palinoflora y ambiente en el Terciario del nordeste de Tierra del Fuego, Argentina. *Revista del Museo Argentino de Ciencias Naturales*, *2*(1), 43–51.

Zamaloa, M. D. C., & Romero, E. J. (2005). Neogene palynology of Tierra del Fuego, Argentina: Conifers. *Alcheringa: An Australasian Journal of Palaeontology*, *29*(1), 113–121. https://doi.org/10.1080/03115510508619563

Zhang, J., Hu, Y., Zhu, C., Flögel, S., Fang, X., & Sun, J. (2023). Modeling the effects of global cooling and the Tethyan Seaway closure on North African and South Asian climates during the Middle Miocene Climate Transition Palaeogeography. *Palaeoclimatology Palaeoecology*, *619*, 111541. https://doi.org/10.1016/j.palaeo.2023.111541

Zhang, L., Shu, Y., Cai, G., Long, Z., Liu, D., & Wang, F. (2019). Eocene-Oligocene sedimentary environment evolution and its impact on hydrocarbon source conditions in eastern Pearl River Mouth Basin. *Acta Petrolei Sinica*, *40*(s1), 153.

Zhang, Z. (1986). *Zhao, Inner Mongolia Tertiary plant fossils of Mengpingzhuang*. Published by Shenyang Institute of Geology and Mineral Resources, Chinese Academy of Geological Sciences.

Zhang, Z., Ramstein, G., Schuster, M., Li, C., Contoux, C., & Yan, Q. (2014). Aridification of the Sahara desert caused by Tethys Sea shrinkage during the Late Miocene. *Nature*, *513*(7518), 401–404. https://doi.org/10.1038/nature13705

Zhao, H. H., & Guo, S. Y. (1995). *Stratigraphic paleontology of zhoukou and nanyang areas, Henan province* (pp. pp1–424). Geological Publishing House. (in Chinese).

Zhao, L., Lu, H., & Tang, L. (2018). Cenozoic palynological records and vegetation evolution in the Weihe Basin, Central China. *Quaternary Sciences*, *38*(5), 1083–1093.

Zhao, L.-C., Wang, Y.-F., Liu, C.-J., & Li, C.-S. (2004). Climatic implications of fruit and seed assemblage from Miocene of Yunnan, southwestern China. *Quaternary International*, *117*(1), 81–89. https://doi.org/10.1016/s1040-6182(03)00118-6

Zheng, D., Shi, G., Hemming, S. R., Zhang, H., Wang, W., Wang, B., & Chang, S.-C. (2019). Age constraints on a Neogene tropical rainforest in China and its relation to the Middle Miocene Climatic Optimum. *Palaeogeography, Palaeoclimatology, Palaeoecology*, *518*, 82–88. https://doi.org/10.1016/j.palaeo.2019.01.019

Zheng, Y., Zhou, S.-F., Liu, X.-Q., Wang, L.-U., Xu, S.-J., & Wang, X.-Z. (1981). Neogene sporopollen grains from Northern Jiangsu and South Yellow Sea Basin. *Bulletin of Nanjing Institute of Geology and Palaeontology*, *3*, 29–77.

Zhenjiang, Y., Xiaohong, L., Yuping, Z., & Runhua, W. (2006). Neogene stratigraphic order and age in Nanjing area. *Journal of Stratigraphy*, *31*(2), 223–230.

Zixi, W. (2018). *Microstructure and paleoclimate reconstruction of Miocene plant fossils in Zhangzhou, Fujian*. Lanzhou University.

Zyryanov, E. V. (1992). Palynological investigations of Miocene deposits on the New Siberian Archipelago (U.S.S.R). *Arctic*, *45*(3), 285–294. https://doi.org/10.14430/arctic1403